DISPERSION RELATIONS FOR ELASTIC WAVES IN PLATES AND RODS

BY FERUZA ABDUKADIROVNA AMIRKULOVA

A thesis submitted to the

Graduate School—New Brunswick

Rutgers, The State University of New Jersey

in partial fulfillment of the requirements

for the degree of

Master of Science

Graduate Program in Mechanical and Aerospace Engineering

Written under the direction of

Professor Andrew Norris

and approved by

_____

_____

_____

_____

New Brunswick, New Jersey

January, 2011

ABSTRACT OF THE THESIS

Dispersion relations for elastic waves in plates and rods

by Feruza Abdukadirovna Amirkulova

Thesis Director: Professor Andrew Norris

Wave propagation in homogeneous elastic structures is studied. Dispersion relations are obtained for elastic waves in plates and rods, for symmetric and antisymmetric modes using different displacement potentials. Some engineering beam theories are considered. Dispersion relations are obtained for phase velocity. The comparison of results based on the fundamental beam theories is presented for the lowest flexural mode. The Rayleigh-Lamb frequency equations are derived for elastic plate using the Helmholtz displacement decomposition. The Rayleigh-Lamb equations are considered in a new way. A new series expansion of frequency to any order of wave number, in principle, is obtained for symmetric and antisymmetric modes using an iteration method. Dispersion relations are shown in graphs for frequency, phase speed and group speed versus wave number. The obtained results are in good agreement with exact solutions. The cutoff frequencies for axial-shear, radial-shear and flexural modes are calculated and taken as starting points in dispersion relations for frequencies versus wave number. Different displacement potential representations are presented and compared. The Pochhammer-Chree frequency equations are derived for elastic rods using two displacement potentials, such as the Helmholtz decomposition for vector fields and Buchwald's vector potentials. Buchwald's representation enables us to find an efficient formulation of dispersion relations in an isotropic as well as anisotropic rods. Analysis of the numerical results on

dispersion relations and cutoff frequencies for axial-shear, radial-shear and flexural modes is given.

Acknowledgements

First and foremost I want to express my gratitude to my advisor, Professor Norris, for directing me throughout this research. It has been a pleasure to work with him on what turned out to be a very interesting research effort. I will always be grateful for the learning opportunities he has provided, for his kindness and patience.

I wish to express appreciation to my teachers, Professors Ellis H. Dill, Haim Baruh, William J. Bottega, Alberto Cuitino, Haym Benaroya, and Mitsunori Denta. I have indeed learned more about engineering at Rutgers than at any other time in my life.

I wish to show my appreciation to The Graduate School and the Mechanical and Aerospace Engineering Department at Rutgers University for awarding me a Graduate School Fellowship, offering me a Teaching Assistant position and providing me support.

Additionally, I want to thank my parents who have always persuaded me to pursue my dreams and have made enormous sacrifices and efforts to make it possible. Last, but certainly not least, I want to thank my children Dilnoza, Parvina and Jahongir, who have endured my late night study sessions and days away from home with grace and maturity. I could not have done any of this without their boundless love and encouragement.

Dedication

I want to dedicate this work to my parents, Abdukadir Rabimov and Qambar Mirkamilova, who have been supportive of my efforts to get my degrees and without whom I would not have the time to complete my work.

Table of Contents

List of Tables

List of Figures

Chapter 1

Introduction

Wave propagation in solids is of interest in a number of engineering applications. The study of structures involving wave phenomena includes the response to impact loads and crack propagation. For typical transient loads, the response can be evaluated by elastic wave theory. For acute loading elastic wave theory can still predict the response far from the region of load application. Some other areas of application of wave phenomena are in the field of ultrasonics, seismology (waves in rocks), earthquakes (waves in earth).

The application of numerical methods have enabled the solution of challenging problems. For instance, before the invention of computer, finding the roots of the Rayleigh-Lamb frequency equation was considered to be intractable. The roots of a transcendental equation can be now evaluated easily on a computer. Consequently, the interest in the theory of wave propagation has increased over the last few decades.

This thesis studies wave propagation in elastic solids, especially in plates, thin rectangular rods, and cylindrical rods. The thesis consists of four chapters, references, and appendixes. The introduction is given in this chapter.

Chapter §2 presents a review of the elastic wave theory for waveguides and it illustrates the basic ideas of wave propagation in solids. The chapter begins with the literature review of elastic wave propagation in plates, shells and rods. The fundamental research conducted in the past as well as recent publications concerning wave propagation are described, such as some complex characteristics of material in anisiotropy, viscosity, initial stress, polarization, as well as composite structure. The governing equations for a linear homogeneous isotropic elastic solid are developed. The displacement vector is expressed in terms of scalar and vector potentials. The Rayleigh-Lamb frequency equations for the propagation of symmetric and

antisymmetric waves in an isotropic elastic plate are derived next. Lastly, some approximate beam theories are discussed which substantially simplify wave analysis in beams and rods. The comparison of results for phase velocity for the considered models is shown.

Chapter §3 is devoted to the study the Rayleigh-Lamb frequency equations in more detail, and it proposes a new expansion of the roots of the Rayleigh-Lamb frequency equations. Introducing the non-dimensional frequency and wavenumber, the Rayleigh-Lamb frequency equation in non-dimentional parameters is developed. The non-dimensional frequency is expanded into a series for the wavenumber for symmetric modes. Numerical evalution of the series coefficients are performed with Maple 12 using the iteration method. We next represent the frequency series expansion for antisymmetric modes on the basis of the approach used in the previous section. This followed by a discussion of numerical results of the dispersion relations for phase speed and group speed. The dispersion relations in a plate for the symmetric and antisymmetric modes are obtained from the Rayleigh-Lamb frequency equations. These relations are illustrated as plots of frequency versus wavenumber.

Chapter §4 is concerned with the investigation of wave propagation in a rod. The chapter begins with a review of wave propagation in rods. Next the statement of problem of wave propagation in an elastic isotropic rod is formulated. The three different representations of displacement potentials are introduced. Then, using these potential representations, the frequency equations in the rod for symmetric and antisymmetric modes are derived. Finally, the numerical results of the dispersion relations and cutoff frequencies for axial-shear, radial-shear and flexural modes in the rod are given in Section §4.5.

The Appendixes give sample computational program codes written with Matlab and Maple. The Maple codes given in Appendix 1 calculate the coefficients U_n and W_n of the series expansions of frequency Ω in terms of wave number ξ, where the U_n depend on the polynomials B_n for symmetric modes, and W_n depend on the polynomials D_n for antisymmetric modes in a plate. Appendix 2 gives the Matlab codes that solve and plot the dispersion relations for plates and rods, using nondimensional frequency, phase speed and group speed versus wave number.

A new way to study the low frequency behavior of the Rayleigh-Lamb frequency equations

is proposed in Chapter §3. The approach is built on a new series expansion of the roots of Rayleigh-Lamb equations using iteration method combined with symbolic algebra on Maple. The frequency and phase speed dependence on wave number shows good agreement between series expansion method and the exact theory for low frequency waves.

A new approach to derive the frequency equations for rods using Buchwald's potential representation is proposed in Chapter §4. Some unexpected interesting behavior of cutoffs for antisymmetric modes in rods is revealed.

Finally, some applications, conclusions and suggestions are given in Chapter §5.

Chapter 2

Review on Elastic Wave Theory for Waveguides

2.1 Review

This section presents a review of problems concerning the topic of the thesis. References include works on exact and approximate theories for plates, shells and rods. Fundamental approaches in the development of mathematical models of non-stationary processes in plates, shell structures and beams are attributed to Euler, Bernoulli, Rayleigh [1], Timoshenko [2], Kirchhoff, Love, Mindlin [3], Flugge [4], Naghdi [5], Markus [6], Hermann and Mirsky [7] etc. The simple theories, such as engineering theories for compressional waves in rods, or flexural waves in beams, are restricted to low frequencies as a consequence of kinematical assumptions, as is shown at the end of this chapter. Consequently, the exact and refined theories of plates, rods and shells are necessary for considering problems at high frequencies and for transient loadings.

Frequency equations for waves in nfinite plates were presented by Rayleigh [1] and Lamb [8] in 1889. The frequency equations for wave propagation in an infinite rod were proposed by Pochhammer [9] in 1876 and independently, Chree [10] in 1889. A brief review of wave propagation in rods is given in Section §4.1. Lamb [8] analyzed the lowest symmetric and antisymmetric modes of the Rayleigh-Lamb equations, classifying the cutoff modes, Lamé modes and specific features of the high frequency spectrum. Holden's approach [11] of composing a portion of the frequency spectrum of symmetric modes for real wave numbers was employed and expanded for antisymmetric modes by Onoe [12]. A similar approach was proposed by Mindlin [13] to construct the branches of the frequency equation, to examine complex behavior of the branches in the neighborhood of zero wavenumber, to ascertain the

modes at the cut-off frequencies which differ from the modes determined by Lamb [8], and to identify complex wave numbers and phase velocities associated with real frequencies including higher modes. The general solution for a shell was first treated by Gazis [14] in 1959. The application of numerical methods has assisted in solving a number of dificult problems including the frequency spectrum analysis of higher modes and complex branches. An extensive review of related problems on wave propagation in rods and plates is given by Graff [15]. The basic concepts of one dimensional wave propagation and discussion of formal aspects of 3D elastodynamic theory, and description of typical mechanical wave propagation phenomena, such as reflextion, refraction, diffraction, radiation, and propagation in waveguides was presented by Achenbach [16].

The broad research and results offered for Rayleigh-Lamb and Pochhammer-Chree frequency spectrum show that propagation of harmonic waves in infinite elastic media can be solved in general [11], [12], [13], [15], [16]. For instance, free vibrations of an elastic layer may produce an infinite number of modes whose frequencies can be obtained from the Rayleigh-Lamb equation. Conversely, for forced motion of a plate of finite dimensions each of these modes couples, leading to an intricate frequency spectrum [16]. As a consequence of the complexity of the governing equations and boundary conditions, the solution of the forced and free vibration problems using exact theory is generally difficult. These obstacles have motivated the development of approximate theories for plates, shells and rods. The 3D governing equations were reduced to 2D equations in most of these theories by making some kinematical assumptions, such as the Kirchhoff assumption.

An approximate plate theory for isotropic elastic plates, taking into account rotary inertia and transverse shear, was proposed by Mindlin [3]. The displacement components were expanded in power series in the thickness coordinate, then substituted into the equations of motion, and then subsequently integrated over the thickness. Then, by incorporating boundary conditions, 3D equations of elasticity are altered into an infinite series of 2D equations in the in-plane coordinates which is then truncated to form the approximate equations. A survey of the kinematical hypotheses and governing equations of refined theories of plates is presented by Jemielita [17], where it is shown that a kinematical hypothesis by Vlasov

[18] is a model for all cited works in the survey. In a review article, Reissner [19] discussed some aspects of plate modeling, including the sixth-order plate theories. Norris [20] brought together the beam and plate theories, established relationships between them and showed that four classical theories for plates and beams yielded quite dissimilar results, which were illustrated by comparison of the wave speeds for antisymmetric modes on narrow plates.

Kirchhoff - Love theory and Timoshenko type theories [4, 6, 21, 22] are based on different hypothesis, which simplify the form of the governing equation of vibrations and at the same time lead to essential disadvantages and errors. To avoid such errors, various refined vibration equations were proposed such as those of Boström [23], Kulikov [24], Khudoynazarov [25], Amirkulova [26]. These models are free from hypotheses and preconditions used in known classical and refined theories. They are more general than Timoshenko type equations and Hermann-Mirsky [7] equations and take into account the effect of transversal shear deformation and the rotary inertia, and admit various truncations of equations. Boström [23] derived a refined set of flexural equations of motion for an isotropic elastic plate by an antisymmetric expansion in the thickness coordinate of the displacement components. These equations can be truncated to any order in the thickness, thus making it possible to have numerical comparision of different truncations of the equation with each other, in particular, with the exact 3D solution and Mindlin's plate theory is possible. It is noted by Boström [23] that the corresponding dispersion relation seems to correspond to a power series expansion of the exact Rayleigh-Lamb dispertion relation to all orders. The refined equations of non-stationary symmetric vibrations of the cylindrical prestressed viscoelastic shells was proposed by Amirkulova [26]. The approach is based on exact mathematical formulation of the 3D problems of theory of elasticity and their general solutions using transformations. The displacements of intermediate surface of the shell are taken as the basic unknowns. The intermediate surface of the shell can alter into median (neutral), external or internal surface. It allows one to use these equations for thin shells, thick walled layers, as well as rods. The obtained equations are of hyperbolic type and describe the wave distribution caused by dispersion.

Recent publications include [27] by Stephen, [24] by Kulikov, [28] by Guz, [29] by Guz and

Rushchitsky, [30] by Thurston, [31] by Selezov, [32] by Shulga, [33] by Norris and Shuvalov. Hyperbolic equations of motions for rods, plates and shells are derived by Selezev [31] using a series expansion technique in the thickness coordinate and by retaining as many terms as appropriate. The deformation due to plane harmonic waves propagating along the fibres of nanocomposite and polarised perpendicular direction is considered by Guz and Rushchitsky [29]. Norris and Shuvalov [33] constructed the wave impedance matrix for cylindrically anisotropic radially inhomogeneous elastic solids using the Stroh-like system of six first order differential equations.

2.2 The Governing Equations for 3D Solids

The equations for a linear homogeneous isotropic elastic solid are:

I_a) the equations of motion of three-dimensional elasticity

$$\sigma_{ij,j} + \rho f_i = \rho \ddot{u}_i, \tag{2.1}$$

I_b) the stress-strain relations (Hooke's law)

$$\sigma_{ij} = \lambda \varepsilon_{kk} \delta_{ij} + 2\mu \varepsilon_{ij}, \tag{2.2}$$

I_c) the strain-displacement relations (Cauchy's relations)

$$\varepsilon_{ij} = \frac{1}{2}(u_{i,j} + u_{j,i}), \tag{2.3}$$

Here u_i are the displacement components, σ_{ij} are the stress tensor components, ε_{ij} are the deformation tensor components, ε_{kk} is the trace of deformation tensor, f_i are the volume force components, ρ is the density, λ and μ are Lamé coefficients, and the summation convention is taken for $i = 1, 2, 3$.

Introducing the strain-displacement relations (2.3) into the stress-strain relations (2.2), the stress tensor components can be expressed in terms of displacement vector components as following:

$$\sigma_{ij} = \lambda u_{i,i} \delta_{ij} + \mu \big[u_{i,j} + u_{j,i}\big]. \tag{2.4}$$

Substituting the stress-displacement relations (2.4) in the equation of motion (2.1) and simplifying, *the Navier's equation of motion* in terms of displacements can be obtained in the form:

$$(\lambda+\mu)u_{j,ji}+u_{i,jj}+\rho\, f_i=\rho\ddot{u}_i, \tag{2.5}$$

or in vector form as

$$(\lambda+\mu)\boldsymbol{\nabla\nabla}\cdot\boldsymbol{u}+\mu\nabla^2\boldsymbol{u}+\rho\,\boldsymbol{f}=\rho\ddot{\boldsymbol{u}}, \tag{2.6}$$

where ∇^2 is the Laplace operator.

In terms of rectangular Cartesian coordinates (2.6) can be written as

$$\begin{aligned}
(\lambda+\mu)\left(\frac{\partial^2 u}{\partial x^2}+\frac{\partial^2 v}{\partial x\partial y}+\frac{\partial^2 w}{\partial x\partial z}\right)+\mu\nabla^2 u+\rho\, f_x&=\rho\frac{\partial^2 u}{\partial t^2},\\
(\lambda+\mu)\left(\frac{\partial^2 u}{\partial x\partial y}+\frac{\partial^2 v}{\partial y^2}+\frac{\partial^2 w}{\partial y\partial z}\right)+\mu\nabla^2 v+\rho\, f_y&=\rho\frac{\partial^2 v}{\partial t^2},\\
(\lambda+\mu)\left(\frac{\partial^2 u}{\partial x\partial z}+\frac{\partial^2 v}{\partial y\partial z}+\frac{\partial^2 w}{\partial z^2}\right)+\mu\nabla^2 w+\rho\, f_z&=\rho\frac{\partial^2 w}{\partial t^2},
\end{aligned} \tag{2.7}$$

where

$$\nabla^2=\frac{\partial^2}{\partial x^2}+\frac{\partial^2}{\partial y^2}+\frac{\partial^2}{\partial z^2}. \tag{2.8}$$

In the absence of body forces the equation of motion in vector form reduces to

$$(\lambda+\mu)\boldsymbol{\nabla\nabla}\cdot\boldsymbol{u}+\mu\nabla^2\boldsymbol{u}=\rho\ddot{\boldsymbol{u}}. \tag{2.9}$$

2.3 Displacement Potentials

The system of equations (2.9) is coupled in the three displacement components u, v, w. These equations can be uncoupled by expressing the components of the displacement vector in terms of derivatives of scalar and vector potentials in the form [16] of the Helmholtz decomposition for vector fields,

$$\boldsymbol{u}=\boldsymbol{\nabla}\varphi+\boldsymbol{\nabla}\times\boldsymbol{\psi}, \tag{2.10}$$

where ϕ is a scalar potential function and $\boldsymbol{\psi}$ is a vector potential function. In Cartesian coordinates $\boldsymbol{\psi}=\psi_x\,\boldsymbol{e}_x+\psi_y\,\boldsymbol{e}_y+\psi_z\,\boldsymbol{e}_z$, and the Helmholtz displacement decomposition will

have form

$$u = \frac{\partial \varphi}{\partial x} + \frac{\partial \psi_z}{\partial y} - \frac{\partial \psi_y}{\partial z}, \quad v = \frac{\partial \varphi}{\partial y} - \frac{\partial \psi_z}{\partial x} + \frac{\partial \psi_x}{\partial z}, \quad w = \frac{\partial \varphi}{\partial z} + \frac{\partial \psi_z}{\partial x} - \frac{\partial \psi_x}{\partial y}. \tag{2.11}$$

where

Plugging the equation (2.10) into the equation of motion (2.9) and taking into account that $\boldsymbol{\nabla} \cdot \boldsymbol{\nabla}\varphi = \nabla^2\varphi$ and $\boldsymbol{\nabla} \cdot \boldsymbol{\nabla} \times \boldsymbol{\psi} = 0$, we obtain

$$\boldsymbol{\nabla}\big[(\lambda + 2\mu)\nabla^2\varphi - \rho\,\ddot{\varphi}\big] + \boldsymbol{\nabla} \times \big[\mu\nabla^2\boldsymbol{\psi} - \rho\,\ddot{\boldsymbol{\psi}}\big] = 0. \tag{2.12}$$

Equation (2.10) therefore satisfies the equation of motion if it satisfies the following uncoupled wave equations

$$\nabla^2\varphi = \frac{1}{c_1^2}\ddot{\varphi}, \tag{2.13}$$

$$\nabla^2\boldsymbol{\psi} = \frac{1}{c_2^2}\ddot{\boldsymbol{\psi}}, \tag{2.14}$$

where

$$c_1^2 = \frac{\lambda + 2\mu}{\rho}, \qquad c_2^2 = \frac{\mu}{\rho}. \tag{2.15}$$

Here c_1 is the longitudinal wave velocity and c_2 is the transverse wave velocity.

In the xyz coordinate system (2.13) remains the same while (2.14) can be written as

$$\nabla^2\psi_x = \frac{1}{c_2^2}\frac{\partial^2\psi_x}{\partial t^2}, \qquad \nabla^2\psi_y = \frac{1}{c_2^2}\frac{\partial^2\psi_y}{\partial t^2}, \qquad \nabla^2\psi_z = \frac{1}{c_2^2}\frac{\partial^2\psi_z}{\partial t^2}. \tag{2.16}$$

In cylindrical coordinates (r, θ, z) the relations between the displacement components and the potentials follow from (2.10) as:

$$u_r = \frac{\partial \varphi}{\partial r} + \frac{1}{r}\frac{\partial \psi_z}{\partial \theta} - \frac{\partial \psi_\theta}{\partial z}, \tag{2.17a}$$

$$u_\theta = \frac{1}{r}\frac{\partial \varphi}{\partial \theta} + \frac{\partial \psi_r}{\partial z} - \frac{\partial \psi_z}{\partial r}, \tag{2.17b}$$

$$u_z = \frac{\partial \varphi}{\partial z} + \frac{1}{r}\frac{\partial(\psi_\theta r)}{\partial r} - \frac{1}{r}\frac{\partial \psi_r}{\partial \theta}. \tag{2.17c}$$

In (r, θ, z) system the scalar potential φ is defined again by (2.13) whereas the component of

vector potential $\boldsymbol{\psi}$ satisfy the following equations

$$\nabla^2\psi_r - \frac{\psi_r}{r^2} - \frac{2}{r^2}\frac{\partial\psi_\theta}{\partial\theta} = \frac{1}{c_2^2}\frac{\partial^2\psi_r}{\partial t^2}, \tag{2.18a}$$

$$\nabla^2\psi_\theta - \frac{\psi_\theta}{r^2} + \frac{2}{r^2}\frac{\partial\psi_r}{\partial\theta} = \frac{1}{c_2^2}\frac{\partial^2\psi_\theta}{\partial t^2}, \tag{2.18b}$$

$$\nabla^2\psi_z = \frac{1}{c_2^2}\frac{\partial^2\psi_z}{\partial t^2}, \tag{2.18c}$$

where the Laplacian is of the form

$$\nabla^2 = \frac{\partial^2}{\partial r^2} + \frac{1}{r}\frac{\partial}{\partial r} + \frac{1}{r^2}\frac{\partial^2}{\partial\theta^2} + \frac{\partial^2}{\partial z^2}. \tag{2.19}$$

2.4 Waves in Plane Strain in Thin Plates

2.4.1 General Solution

Consider harmonic wave propagation in thin plate having thickness $2h$ shown in Figure 2.1. For plane strain motion in xy plane: $u = u(x, y, t)$, $v = v(x, y, t)$. Then in the absence of body forces the equation of motion (2.1) will reduce to the form

$$\frac{\partial\sigma_{xx}}{\partial x} + \frac{\partial\sigma_{xy}}{\partial y} = \rho\frac{\partial^2 u}{\partial t^2}, \tag{2.20a}$$

$$\frac{\partial\sigma_{xy}}{\partial x} + \frac{\partial\sigma_{yy}}{\partial y} = \rho\frac{\partial^2 v}{\partial t^2}, \tag{2.20b}$$

and Hooke's law is

$$\sigma_{xx} = \lambda\left(\frac{\partial u}{\partial x} + \frac{\partial v}{\partial y}\right) + 2\mu\frac{\partial u}{\partial x}, \tag{2.21a}$$

$$\sigma_{yy} = \lambda\left(\frac{\partial u}{\partial x} + \frac{\partial v}{\partial y}\right) + 2\mu\frac{\partial v}{\partial y}, \tag{2.21b}$$

$$\sigma_{xy} = \mu\left(\frac{\partial u}{\partial y} + \frac{\partial v}{\partial x}\right). \tag{2.21c}$$

Plugging (2.21a)-(2.21c) into (2.20a)-(2.20b) the following equations are obtained

$$\lambda\left(\frac{\partial^2 u}{\partial x^2} + \frac{\partial^2 v}{\partial x\partial y}\right) + 2\mu\frac{\partial^2 u}{\partial x^2} + \mu\left(\frac{\partial^2 u}{\partial y^2} + \frac{\partial^2 v}{\partial x\partial y}\right) = \rho\frac{\partial^2 u}{\partial t^2},$$

$$\mu\left(\frac{\partial^2 v}{\partial x^2} + \frac{\partial^2 u}{\partial x\partial y}\right) + \lambda\left(\frac{\partial^2 v}{\partial y^2} + \frac{\partial^2 u}{\partial x\partial y}\right) + 2\mu\frac{\partial^2 v}{\partial y^2} = \rho\frac{\partial^2 v}{\partial t^2},$$

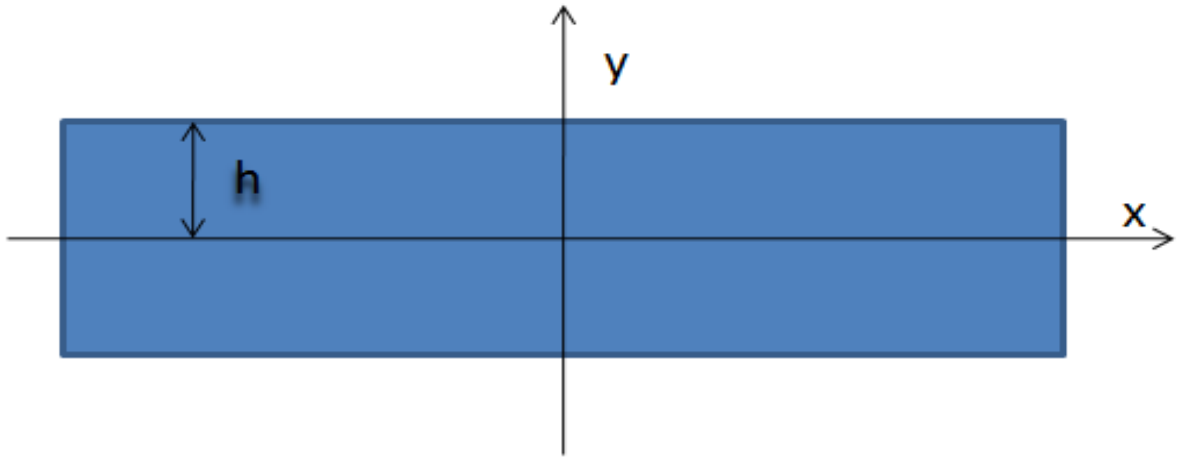

Figure 2.1: Plate in plane strain

which can be modified as

$$\frac{\partial^2 u}{\partial x^2} + \frac{\lambda+\mu}{\lambda+2\mu}\frac{\partial^2 v}{\partial x \partial y} + \frac{\mu}{\lambda+2\mu}\frac{\partial^2 u}{\partial y^2} = \frac{\rho}{\lambda+2\mu}\frac{\partial^2 u}{\partial t^2}, \tag{2.22a}$$

$$\frac{\partial^2 v}{\partial y^2} + \frac{\lambda+\mu}{\lambda+2\mu}\frac{\partial^2 u}{\partial x \partial y} + \frac{\mu}{\lambda+2\mu}\frac{\partial^2 v}{\partial x^2} = \frac{\rho}{\lambda+2\mu}\frac{\partial^2 v}{\partial t^2}. \tag{2.22b}$$

The Lamé coefficients are related to the Young modulus of elasticity E, the shear modulus G and Poisson's ratio ν as follows,

$$\mu = G = \frac{E}{2(1+\nu)}, \qquad \lambda = \frac{2G\nu}{1-2\nu}, \qquad \frac{\lambda}{\mu} = \frac{2\nu}{1-2\nu}. \tag{2.23}$$

Substitution of (2.23) into (2.22a) and (2.22b) yields

$$\frac{\partial^2 u}{\partial x^2} + \frac{1}{1-\nu}\frac{\partial^2 v}{\partial x \partial y} + \frac{1-2\nu}{2(1-\nu)}\frac{\partial^2 u}{\partial y^2} = \frac{1}{c_1^2}\frac{\partial^2 u}{\partial t^2}, \tag{2.24a}$$

$$\frac{\partial^2 v}{\partial y^2} + \frac{1}{1-\nu}\frac{\partial^2 u}{\partial x \partial y} + \frac{1-2\nu}{2(1-\nu)}\frac{\partial^2 v}{\partial x^2} = \frac{1}{c_1^2}\frac{\partial^2 v}{\partial t^2}. \tag{2.24b}$$

If conditions of plane strain hold in xy plane, equation (2.11) reduces to

$$u = \frac{\partial \varphi}{\partial x} + \frac{\partial \psi_z}{\partial y}, \qquad v = \frac{\partial \varphi}{\partial y} - \frac{\partial \psi_z}{\partial x}, \tag{2.25}$$

and the potentials φ and ψ_z satisfy 2D wave equations

$$\frac{\partial^2 \varphi}{\partial x^2} + \frac{\partial^2 \varphi}{\partial y^2} = \frac{1}{c_1^2}\frac{\partial^2 \varphi}{\partial t^2}, \tag{2.26a}$$

$$\frac{\partial^2 \psi_z}{\partial x^2} + \frac{\partial^2 \psi_z}{\partial y^2} = \frac{1}{c_2^2}\frac{\partial^2 \psi_z}{\partial t^2}. \tag{2.26b}$$

We seek solution of the wave equations (2.26a)-(2.26b) in the form

$$\varphi = \Phi(y)e^{i(kx-\omega t)}, \qquad \psi_z = i\Psi(y)e^{i(kx-\omega t)}, \tag{2.27}$$

where ω is the frequency and k is the wave number. These solutions represent traveling waves in the x direction and standing waves in the y direction. Having substituted the assumed solutions (2.27) back into displacement representation (2.25), we obtain

$$u = i\left(k\,\Phi + \frac{d\Psi}{dy}\right)e^{i(kx-\omega t)}, \tag{2.28a}$$

$$v = \left(\frac{d\Phi}{dy} - i\,k\,\Psi\right)e^{i(kx-\omega t)}. \tag{2.28b}$$

Substituting the solutions (2.27) into (2.26a)-(2.26b) results in the following Helmholtz equations for Φ and Ψ

$$\frac{d^2\Phi}{dy^2} + \alpha^2\Phi = 0, \qquad \frac{d^2\Psi}{dy^2} + \beta^2\Psi = 0. \tag{2.29}$$

where the longitudal and transverse wave numbers, α, β, are

$$\alpha^2 = \omega^2/c_1^2 - k^2, \qquad \beta^2 = \omega^2/c_2^2 - k^2.$$

The solutions of equations (2.29) are obtained as

$$\Phi(y) = A\,\sin\,\alpha y + B\,\cos\,\alpha y, \tag{2.30a}$$

$$\Psi(y) = C\,\sin\,\beta y + D\,\cos\,\beta y. \tag{2.30b}$$

Substitution of these solutions into the equations (2.27) and (2.28a)-(2.28b) results in the following potentials and displacements:

$$\varphi = (A\,\sin\,\alpha y + B\,\cos\,\alpha y)e^{i(kx-\omega t)}, \tag{2.31a}$$

$$\psi_z = i(C\,\sin\,\beta y + D\,\cos\,\beta y)e^{i(kx-\omega t)}, \tag{2.31b}$$

$$u = i\big[k(A\,\sin\,\alpha y + B\,\cos\,\alpha y) + \beta(C\,\cos\,\beta y - D\,\sin\,\beta y)\big]e^{i(kx-\omega t)}, \tag{2.31c}$$

$$v = \big[\alpha(A\,\cos\,\alpha y - B\,\sin\,\alpha y) - i\,k(C\,\sin\,\beta y + D\,\cos\,\beta y)\big]e^{i(kx-\omega t)}. \tag{2.31d}$$

The stress components can be obtained by rewriting (2.21a)-(2.21c) as

$$\sigma_{xx} = (\lambda + 2\mu)\left(\frac{\partial u}{\partial x} + \frac{\partial v}{\partial y}\right) - 2\mu\frac{\partial v}{\partial y}, \tag{2.32a}$$

$$\sigma_{yy} = (\lambda + 2\mu)\left(\frac{\partial u}{\partial x} + \frac{\partial v}{\partial y}\right) - 2\mu\frac{\partial u}{\partial x}, \tag{2.32b}$$

$$\sigma_{xy} = \mu\left(\frac{\partial u}{\partial y} + \frac{\partial v}{\partial x}\right). \tag{2.32c}$$

In terms of potentials φ and ψ_z the stresses are

$$\sigma_{xx} = (\lambda + 2\mu)\left(\frac{\partial^2\varphi}{\partial x^2} + \frac{\partial^2\varphi}{\partial y^2}\right) - 2\mu\left(\frac{\partial^2\varphi}{\partial y^2} - \frac{\partial^2\psi_z}{\partial x\partial y}\right), \tag{2.33a}$$

$$\sigma_{yy} = (\lambda + 2\mu)\left(\frac{\partial^2\varphi}{\partial x^2} + \frac{\partial^2\varphi}{\partial y^2}\right) - 2\mu\left(\frac{\partial^2\varphi}{\partial x^2} + \frac{\partial^2\psi_z}{\partial x\partial y}\right), \tag{2.33b}$$

$$\sigma_{xy} = \mu\left(2\frac{\partial^2\varphi}{\partial x\partial y} + \frac{\partial^2\psi_z}{\partial y^2} - \frac{\partial^2\psi_z}{\partial x^2}\right). \tag{2.33c}$$

Substituting the resulting potentials (2.31a)- (2.31b) into (2.33a)-(2.33c) yields the following

$$\sigma_{xx} = \mu\Big[[2\alpha^2 - \kappa^2(k^2 + \alpha^2)](A\,\sin\,\alpha y + B\,\cos\,\alpha y) - 2k\beta(C\,\cos\,\beta y - D\,\sin\,\beta y)\Big]e^{i(kx-\omega t)}, \tag{2.34a}$$

$$\sigma_{yy} = \mu\Big[[2k^2 - \kappa^2(k^2 + \alpha^2)](A\,\sin\,\alpha y + B\,\cos\,\alpha y) + 2k\beta(C\,\cos\,\beta y - D\,\sin\,\beta y)\Big]e^{i(kx-\omega t)}, \tag{2.34b}$$

$$\sigma_{xy} = i\mu\Big[2\alpha k(A\,\cos\,\alpha y - B\,\sin\,\alpha y) - 2(\beta^2 - k^2)(C\,\sin\,\beta y + D\,\cos\,\beta y)\Big]e^{i(kx-\omega t)}, \tag{2.34c}$$

where

$$\kappa^2 = \frac{c_1^2}{c_2^2} = \frac{\lambda + 2\mu}{\mu} = \frac{2(1-\nu)}{1-2\nu} > \frac{4}{3}.$$

We will omit the term $e^{i(kx-\omega t)}$ in the sequel because the exponential appears in all of the expressions and does not influence the determination of the frequency equation.

2.4.2 Symmetric and Antisymmetric Modes

Solution of the boundary-value problem for plates become simpler if we split the problem using symmetry. Thus, for u in the yz plane the motion is symmetric (antisymmetric) with

respect to $y = 0$ if u contains cosines(sines); for v it is vice versa. By inspection of equations (2.31a)- (2.31d), (2.34a)- (2.34c) we notice that the modes of wave propagation in a thin plate may be separated into two systems of symmetric and antisymmetric modes respectively:

SYMMETRIC MODES:

$$\Phi = B \cos \alpha y, \qquad \Psi = C \sin \beta y, \tag{2.35a}$$

$$u = i\big[kB \cos \alpha y + \beta C \cos \beta y\big], \tag{2.35b}$$

$$v = -B\alpha \sin \alpha y + Ck \sin \beta y, \tag{2.35c}$$

$$\sigma_{xx} = \mu\big[[2\alpha^2 - \kappa^2(k^2 + \alpha^2)]B \cos \alpha y - 2k\beta C \cos \beta y\big], \tag{2.35d}$$

$$\sigma_{yy} = \mu\big[[2k^2 - \kappa^2(k^2 + \alpha^2)]B \cos \alpha y + 2k\beta C \cos \beta y\big], \tag{2.35e}$$

$$\sigma_{xy} = -i\mu\big[2\alpha kB \sin \alpha y + (\beta^2 - k^2)C \sin \beta y\big], \tag{2.35f}$$

ANTISYMMETRIC MODES:

$$\Phi = A \sin \alpha y, \qquad \Psi = D \cos \beta y, \tag{2.36a}$$

$$u = i\big[kA \sin \alpha y - \beta D \sin \beta y\big], \tag{2.36b}$$

$$v = A\alpha \cos \alpha y + Dk \cos \beta y, \tag{2.36c}$$

$$\sigma_{xx} = \mu\big[[2\alpha^2 - \kappa^2(k^2 + \alpha^2)]A \sin \alpha y + 2k\beta D \sin \beta y\big], \tag{2.36d}$$

$$\sigma_{yy} = \mu\big[[2k^2 - \kappa^2(k^2 + \alpha^2)]A \sin \alpha y - 2k\beta D \sin \beta y\big], \tag{2.36e}$$

$$\sigma_{xy} = i\mu\big[2\alpha kA \cos \alpha y - (\beta^2 - k^2)D \cos \beta y\big]. \tag{2.36f}$$

The frequency equation can be obtained from the boundary conditions. If we consider the case of waves in a plate of thickness $2h$ having traction free boundaries, the boundary conditions are:

$$\sigma_{yy} = \sigma_{xy} = \sigma_{zy} = 0, \qquad \text{at } y = \pm h \tag{2.37}$$

where $\sigma_{zy} \equiv 0$ is satisfied identically.

Consider first the case of symmetric waves. Symmetric displacements and stresses are given by (2.35b)- (2.35f). Substitution of equations (2.35e)- (2.35f) into (2.37) yields the following system of two homogeneous equations for the constants B and C:

$$\begin{bmatrix} (k^2-\beta^2)\cos\alpha h & 2k\,\beta\cos\beta h \\ \mp 2ik\alpha\sin\alpha h & \mp(k^2-\beta^2)\sin\beta h \end{bmatrix} \cdot \begin{bmatrix} B \\ C \end{bmatrix} = \begin{bmatrix} 0 \\ 0 \end{bmatrix}. \tag{2.38}$$

Since the system of equations (2.38) is homogeneous, the determinant of the coefficients has to vanish, which results in the frequency equation. Thus

$$(k^2-\beta^2)^2\cos\alpha h\sin\alpha h + 4k^2\alpha\beta\sin\alpha h\cos\beta h = 0, \tag{2.39}$$

or the determinant can be written as

$$\boxed{\frac{\tan\beta h}{\tan\alpha h} = -\frac{4k^2\alpha\beta}{(k^2-\beta^2)^2}.} \tag{2.40}$$

Equation (2.40) is known as *the Rayleigh-Lamb frequency equation for symmetric waves in a plate.*

Similarly, for antisymmetric modes displacements and stresses are given by (2.36b)-(2.36f). Substituting (2.36d) and (2.36f) into (2.37) the following system for constants A and D is obtained:

$$\pm\left[(k^2-\beta^2)\,A\sin\alpha h - 2\beta k\,D\sin\beta h\right] = 0, \tag{2.41a}$$

$$2k\alpha\,A\cos\alpha h - (k^2-\beta^2)\,D\cos\beta h = 0. \tag{2.41b}$$

which gives *the Rayleigh-Lamb frequency equation for the propagation of antisymmetric waves in a plate*

$$\boxed{\frac{\tan\beta h}{\tan\alpha h} = -\frac{(k^2-\beta^2)^2}{4k^2\alpha\beta}.} \tag{2.42}$$

2.5 Engineering Theories for Beams and Rods

In this section, we discuss several fundamental beam theories used in engineering practice. The development and analysis of four beam models were presented by Han et al. in [34]. They are the Euler-Bernoulli, Rayleigh, shear, and Timoshenko models for transverse motion. In this paper beam models were obtained using Hamilton's variational principle, whereas here the theories are derived using force balance which will be presented below.

Consider a long elastic uniform beam (or thin rod) in Cartesian coordinates where coordinate x parallels the axis of the beam (rod). The thickness and width of the beam (rod) are small compared with the overall length of the beam. Let the beam (rod) of cross-sectional area A be comprised of material of mass density ρ and elastic modulus E. We assume that the arbitrary cross-sectional area of the beam (rod) remains plane after deformation.

2.5.1 Compressional Waves in Thin Rods

In compressional wave motions the longitudinal displacement is the dominant component. Let a thin rod be under a dynamically varying stress field $\sigma(x,t)$ and be subjected to the externally applied distributed axial force $f(x,t)$. For 1D stress σ and axial strain ϵ are related by Hooke's law

$$\sigma = E\,\epsilon, \tag{2.43}$$

where ϵ is defined by

$$\epsilon = \frac{\partial u}{\partial x}. \tag{2.44}$$

By writing the equation of motion for an element of rod, we obtain

$$\frac{\partial \sigma}{\partial x} + f = \rho\,\frac{\partial^2 u}{\partial t^2}. \tag{2.45}$$

Substitution of (2.43) and (2.44) into (2.45) yields

$$E\,\frac{\partial^2 u}{\partial x^2} + f = \rho\,\frac{\partial^2 u}{\partial t^2}. \tag{2.46}$$

In the absence of the distributed loads (f=0) (2.46) reduces to

$$\frac{\partial^2 u}{\partial x^2} = \frac{1}{c_b^2}\,\frac{\partial^2 u}{\partial t^2}, \tag{2.47}$$

where

$$c_b^2 = \frac{E}{\rho}, \tag{2.48}$$

c_b is referred to as bar velocity.

Seeking the solution of the form

$$u = Ce^{i(kx-\omega t)}, \tag{2.49}$$

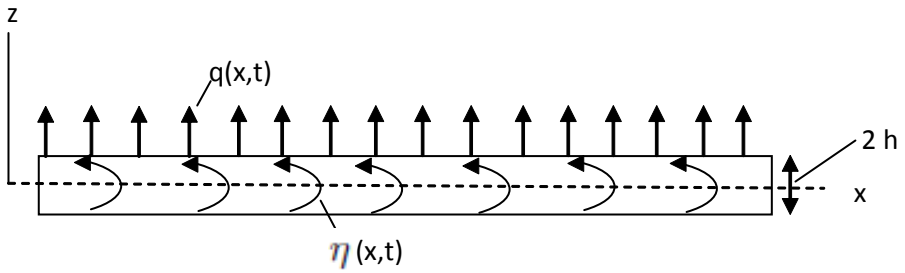

Figure 2.2: Beam with distributed transverse force and body couples

we obtain the following relation

$$\omega^2 = c_b^2 k^2, \tag{2.50}$$

or

$$\omega = \pm c_b k, \tag{2.51}$$

where ω is the frequency, k is the wave number.

Equation (2.51) predicts that compressional waves are not dispersive [16].

2.5.2 Bending and Flexural Waves in Elastic Beams

In this section we will examine how the alteration occurs between classical and refined beam theories, in particular, we will analyze the leading order correction to beam theory. The development is conducted in the context of the three fundamental beam theories used in engineering practice, beginning with the Euler-Bernoulli theory, then followed by Rayleigh and Timoshenko theories.

Consider a long beam that is loaded by normal and transverse shear stress over its upper and lower surfaces shown in Figure 2.2. The external forces may be expressed in terms of distributed transverse loads $q(x,t)$ and distributed body couples $\eta(x,t)$. Let the x-axis coincide with the centroid of the beam in the rest configuration. According to the Kirchhoff kinematic assumption, straight lines normal to the mid-surface remain straight after deformation; straight lines normal to the mid-surface remain normal to the mid-surface after deformation; the thickness of the beam does not change during a deformation. Using the

Kirchhoff assumption we have the following kinematical relations [35]:

$$u_x(x,z,t) = u(x,t) - z\,\varphi(x,t), \quad u_z(x,z,t) = w(x,t), \tag{2.52}$$

where φ is the in-plane rotation of the cross-section of the beam, $u_x(x,z,t)$ and $u_z(x,z,t)$ are the axial and transverse displacements of the particle originally located at the indicated coordinates, $u(x,t)$ and $w(x,t)$, respectively, corresponding to displacements of the particle on the neutral surface $z = 0$.

Utilizing the geometric relation

$$\epsilon_{xx} = \frac{\partial u_x}{\partial x}, \tag{2.53}$$

the strain distribution is found in the form

$$\epsilon_{xx}(x,z,t) = \epsilon(x,t) - z\,\kappa(x,t), \tag{2.54}$$

where

$$\epsilon(x,t) = \frac{\partial u}{\partial x}, \quad \kappa(x,t) = \frac{\partial \varphi}{\partial x}, \tag{2.55}$$

are correspondingly the axial strain of the neutral surface and the curvature of the neutral axis of the beam at x.

The stress-strain relation is

$$\sigma_{xx}(x,z,t) = E\,\epsilon_{xx}(x,z,t). \tag{2.56}$$

The bending moment acting on cross section x is

$$M(x,t) = \int_A \sigma_{xx}(x,z,t) z dA = -EI\kappa(x,t) = -EI\frac{d^2 w(x,t)}{dx^2}. \tag{2.57}$$

The shear force acting on cross-section is

$$V(x,t) = \int_A \tau(x,z,t) dA, \tag{2.58}$$

where $\tau(x,z,t)$ is the shear stress. Writing the equation of motion in the transverse direction, we obtain

$$-V(x,t) + \left(V(x,t) + \frac{\partial V}{\partial x}dx\right) + q(x,t)dx = \rho A dx \frac{\partial^2 w}{\partial t^2}, \tag{2.59}$$

where $q(x,t)$ is the distributed transverse force. This reduces to

$$\frac{\partial V}{\partial x} + q(x,t) = \rho A \frac{\partial^2 w}{\partial t^2}. \tag{2.60}$$

Summing moments about an axis perpendicular to the xz-plane and passing through the center of the beam element, we have

$$\eta(x,t)\,dx + M - \left(M + \frac{\partial M}{\partial x}dx\right) + \frac{1}{2}V dx + \frac{1}{2}\left(V + \frac{\partial V}{\partial x}dx\right)dx = J\frac{\partial^2 \varphi}{\partial t^2}, \tag{2.61}$$

where J is the polar inertia of the element, and η is the body couple. For an element of length dx and having a cross-sectional-area moment of inertia about the moment of neutral axis of I, we have that

$$J = \rho I dx = I_\rho dx, \tag{2.62}$$

where $I_\rho = \rho I$ is called *the rotary inertia of the beam.*

Substitution of (2.62) into (2.61) results in

$$V = \frac{\partial M}{\partial x} + I_\rho \frac{\partial^2 \varphi}{\partial t^2} - \eta(x,t). \tag{2.63}$$

Introducing (2.63) into (2.60) and incorporating equations (2.55) and (2.57) yields the following equation expressed in terms of the transverse displacement w and in-plane rotation φ

$$\frac{\partial^2}{\partial x^2}\left(EI\frac{\partial \varphi}{\partial x}\right) + \rho A \frac{\partial^2 w}{\partial t^2} - \frac{\partial}{\partial x} I_\rho \frac{\partial^2 \varphi}{\partial t^2} = q(x,t) - \frac{\partial \eta}{\partial x}. \tag{2.64}$$

Each term in equation (2.64) represents a different physical characteristic of beam behavior. If rotary effects are neglected, the third term on the right hand side of equation (2.64) is zero. This case is shown in detail in the following section.

Euler-Bernoulli Beam Theory

In this model, the effects of rotary inertia are neglected compared with those of the linear inertia. The deformations associated with transverse shear are also neglected. It is assumed that the dominant displacement component is parallel to the plane of symmetry so the displacement v in the y direction is zero, and that the deflections are small and $w = w(x,t)$.

Thus we have

$$\varphi(x,t) \cong \frac{\partial w}{\partial x}, \tag{2.65}$$

Substituting equation (2.65) into (2.64) and setting the rotation inertia $I_\rho = 0$, yields

$$\frac{\partial^2}{\partial x^2}\left(EI\frac{\partial^2 w}{\partial x^2}\right) + \rho A\frac{\partial^2 w}{\partial t^2} = q(x,t) - \frac{\partial \eta}{\partial x}. \tag{2.66}$$

Equation (2.66) is referred to as *the Euler-Bernoulli beam equation.* Equation (2.66) in the absence of body couples and external loadings can be modified into the form

$$\frac{\partial^4 w}{\partial x^4} + \frac{1}{b^2}\frac{\partial^2 w}{\partial t^2} = 0, \tag{2.67}$$

where

$$b^2 = \frac{EI}{\rho A}. \tag{2.68}$$

By considering a harmonic waves of the form:

$$w = C\, e^{i(kx-\omega t)}, \tag{2.69}$$

where k-wavenumber, ω-frequency, we find

$$k^4 - \frac{\omega^2}{b^2} = 0, \tag{2.70}$$

or

$$\omega^2 = b^2 k^4, \tag{2.71}$$

which yields

$$\omega = \pm b k^2. \tag{2.72}$$

Let us define the phase speed c:

$$c = \frac{\omega}{k}, \tag{2.73}$$

and the group speed c_g:

$$c_g = \frac{\partial \omega}{\partial k}. \tag{2.74}$$

Using relationship $\omega = k\, c$ and a propagating wave of the form (2.69), we obtain

$$c = \pm bk, \qquad c_g = 2c. \tag{2.75}$$

Thus the phase and the group velocity are proportional to the wavenumber which suggests that (2.75) cannot be correct for large wave numbers [16].

Let us introduce the non-dimensional parameters,

$$\Omega = \frac{\omega h}{c_2}, \qquad \xi = kh, \tag{2.76}$$

where Ω and ξ are non-dimensional frequency and wavenumber, respectively, $2h$ is the thickness of the beam, c_2 is transverse wave speed defined by (2.15). Introducing non-dimensional parameters (2.76) into (2.71) and incorporating (2.23), we obtain

$$\Omega^2 = \overline{a}\,\xi^4, \tag{2.77}$$

where

$$\overline{a} \;=\; \frac{2(1+\nu)}{k_2}, \tag{2.78}$$

k_2 is a non-dimensional parameter defined as:

$$k_2 = \frac{Ah^2}{I}. \tag{2.79}$$

Rayleigh Beam Theory

This model incorporates the rotary inertia into the model for Euler-Bernoulli beam theory. We derive the equation of motion for Rayleigh beams based on assumptions of Euler-Bernoulli theory but by including the effects of rotary inertia. Preserving the rotary inertia I_ρ in (2.64) and incorporating equation (2.65), we obtain the equation of motion for Rayleigh beams as [35], [1]

$$\frac{\partial^2}{\partial x^2}\left(EI\frac{\partial^2 w}{\partial x^2}\right) + \rho A\frac{\partial^2 w}{\partial t^2} - \frac{\partial}{\partial x}I_\rho\frac{\partial^3 w}{\partial x \partial t^2} = q(x,t) - \frac{\partial \eta}{\partial x}. \tag{2.80}$$

Considering free vibrations of Rayleigh beams we neglect terms on the right-hand side of equation (2.80)

$$\frac{\partial^4 w}{\partial x^4} + \frac{1}{b^2}\frac{\partial^2 w}{\partial t^2} - \frac{1}{c_b^2}\frac{\partial^4 w}{\partial x^2 \partial t^2} = 0, \tag{2.81}$$

where b is defined by (2.68) and c_b by (2.48).

We seek solutions of the form (2.69). Plugging (2.69) into (2.81) results in the following characteristic equation

$$k^4 - \frac{\omega^2}{b^2} - \frac{\omega^2 k^2}{c_b^2} = 0, \tag{2.82}$$

which gives following dispersion relation

$$\omega^2 = \frac{k^4 b^2}{1 + \frac{k^2 b^2}{c_b^2}}, \tag{2.83}$$

or

$$\omega = \pm \frac{k^2 b}{\sqrt{1 + \frac{k^2 b^2}{c_b^2}}}. \tag{2.84}$$

Introducing non-dimensional frequency and wavenumber parameters by (2.76) into (2.83) and incorporating (2.23), we obtain

$$\Omega^2 = \frac{\overline{a}\,\xi^4}{1 + \frac{\xi^2}{k_2}} \approx \overline{a}\,\xi^4 - \frac{\overline{a}}{k_2}\xi^6 + \frac{\overline{a}}{k_2^2}\xi^8 - \frac{\overline{a}}{k_2^3}\xi^{10} + ..., \tag{2.85}$$

where the non-dimensional parameters $\overline{a}$ and k_2 are defined by (2.78) and (2.79) and

$$c = \pm \frac{kb}{\sqrt{1 + \frac{k^2 b^2}{c_b^2}}}, \quad c_g = 2c - \frac{c^3}{c_b^2}. \tag{2.86}$$

Timoshenko Beam Theory

Beams whose description include both shear correction and rotary inertia are referred to as *Timoshenko Beams*. This model [2] includes shear deformation to the basic beam theories discussed above. Let's consider the transverse shear stress $\sigma_{xz} = \tau(x, z, t)$, acting on a cross section and associated shear strain $\epsilon_{xz}(x, z, t) = \frac{1}{2}\gamma_{xz}(x, z, t)$.

The stress-strain relation for shear is

$$\tau(x, z, t) = 2G\epsilon_{xz}(x, z, t) = G\gamma_{xz}(x, z, t), \tag{2.87}$$

where G is the shear modulus.

We define the shear angle for a beam as [35]:

$$\gamma(x, t) = \frac{1}{k_1 A}\int_A \gamma_{xz}(x, z, t)dA, \tag{2.88}$$

where k_1 is a "*shape factor*" and is known as *the Timoshenko Shear Coefficient.* Substitution of equation (2.87) and (2.88) into equation (2.58) yields

$$V(x,t) = k_s\gamma(x,t), \tag{2.89}$$

where

$$k_s = k_1 AG \tag{2.90}$$

is *the shear stiffness of the beam.*

The slope of the centroidal axis is considered to be made up of two contributions. The first is φ, due to bending. An additional contribution γ due to shear is included. Thus

$$\frac{\partial w}{\partial x} \cong \varphi(x,t) + \gamma(x,t), \tag{2.91}$$

substitution of which into (2.89) results in

$$\gamma(x,t) = \frac{\partial w}{\partial x} - \varphi(x,t) = \frac{V(x,t)}{k_s(x)}. \tag{2.92}$$

Substituting equations (2.91) and (2.92) into (2.57), yields

$$M(x,t) = -EI\frac{\partial}{\partial x}\left[\frac{\partial w}{\partial x} - \gamma(x,t)\right] = -EI\left[\frac{\partial^2 w}{\partial x^2} - \frac{\partial}{\partial x}\frac{V}{k_s}\right]. \tag{2.93}$$

Substitution of equations (2.89), (2.92), (2.93) into (2.60) and (2.63) results in the governing equations for the Timoshenko beams

$$\rho A\frac{\partial^2 w}{\partial t^2} + GAk_1\frac{\partial}{\partial x}\left[\varphi(x,t) - \frac{\partial w}{\partial x}\right] = q(x,t), \tag{2.94}$$

$$I_\rho\frac{\partial^2 \varphi}{\partial t^2} - GAk_1\left[\frac{\partial w}{\partial x} - \varphi(x,t)\right] - EI\frac{\partial^2 \varphi}{\partial t^2} = \eta(x,t). \tag{2.95}$$

Since there two degree of freedom this set of equations describes two wave modes. The equations of motion (2.94), (2.95) can be simplified to a single equation. From (2.95) it follows that

$$GAk_1\left[\frac{\partial w}{\partial x} - \varphi(x,t)\right] = \eta(x,t) + EI\frac{\partial^2 \varphi}{\partial x^2} - I_\rho\frac{\partial^2 \varphi}{\partial t^2}. \tag{2.96}$$

From (2.94) we have

$$\frac{\partial \varphi}{\partial x} = \frac{q(x,t)}{GAk_1} + \frac{\partial^2 w}{\partial x^2} - \frac{\rho}{Gk_1}\frac{\partial^2 w}{\partial t^2}. \tag{2.97}$$

Substituting equation (2.96) into (2.94) and incorporating equation (2.97) gives a single equation of motion in terms of flexural deflection w

$$\rho A\frac{\partial^2 w}{\partial t^2}+\frac{I_\rho \rho}{k_1 G}\frac{\partial^4 w}{\partial t^4}-\left(I_\rho+\frac{EI\rho}{k_1 G}\right)\frac{\partial^4 w}{\partial x^2\partial t^2}+EI\frac{\partial^4 w}{\partial x^4}=$$

$$=q(x,t)-\frac{\partial \eta}{\partial x}+\frac{I_\rho}{k_s}\frac{\partial^2 q}{\partial t^2}-\frac{EI}{k_s}\frac{\partial^2 q}{\partial x^2}, \tag{2.98}$$

where k_s is defined by (2.90). Equation (2.98) is known as *the Timoshenko Beam Equation.*

Let us study propagation of harmonic waves in infinite Timoshenko beams. There are two approaches. In the first approach, we consider the single equation (2.98). Assuming that beam has traction free boundaries, we neglect terms on the right-hand side of the equation (2.98), which is simplified as:

$$\frac{\partial^2 w}{\partial t^2}+\frac{I\rho}{kGA}\frac{\partial^4 w}{\partial t^4}-\frac{I}{A}\left(1+\frac{E}{kG}\right)\frac{\partial^4 w}{\partial x^2\partial t^2}+\frac{EI}{\rho A}\frac{\partial^4 w}{\partial x^4}=0. \tag{2.99}$$

Seeking a harmonic wave solution of the form (2.69) results

$$\frac{EI}{\rho A}k^4-\frac{I}{A}\left(1+\frac{E}{k_1 G}\right)k^2\omega^2-\omega^2+\frac{I\rho}{k_1 GA}\omega^4=0. \tag{2.100}$$

Using the identity $\omega = kc$ in above equation, the dispersion equation is obtained in the following form

$$\frac{EI}{\rho A}k^4-\frac{I}{A}\left(1+\frac{E}{k_1 G}\right)k^4c^2-k^2c^2+\frac{I\rho}{k_1 GA}k^4c^4=0. \tag{2.101}$$

In the second approach considering equations (2.94) and (2.95) directly, with $q(x,t)=0$ and $\eta(x,t)=0$, we assume solutions of the form

$$w=B_1\,e^{i(kx-\omega t)},\quad \varphi=B_2\,e^{i(kx-\omega t)}, \tag{2.102}$$

which leads to

$$(GAk_1k^2-\rho A\omega^2)B_1+iGAk_1kB_2=0, \tag{2.103a}$$

$$iGAk_1kB_1-(GAk_1+EIk^2-\rho I\omega^2)B_2=0. \tag{2.103b}$$

Equating the determinant of coefficients B_1, B_2 to zero in the above system yields the the frequency equation

$$(GAk_1k^2-\rho A\omega^2)(GAk_1+EIk^2-\rho I\omega^2)-G^2A^2k_1^2k^2=0, \tag{2.104}$$

which can be simplified to the form (2.100).

Let us modify the frequency equation (2.100) dividing it by $\frac{I\rho}{k_1GA}$, thus

$$\omega^4 - \omega^2\left(\frac{k_1GA}{I\rho} + \frac{k_1G+E}{\rho}k^2\right) + \frac{EGk_1}{\rho^2}k^4 = 0. \tag{2.105}$$

Introducing non-dimensional frequency and wavenumber parameters by (2.76) into (2.105) leads to

$$\frac{\Omega^4}{h^4}\frac{\mu^2}{\rho^2} - \frac{\Omega^2}{h^2}\frac{\mu}{\rho}\left(\frac{k_1\mu A}{I\rho} + \frac{k_1\mu+E}{\rho}\frac{\xi^2}{h^2}\right) + \frac{E\mu k_1}{\rho^2h^4}\xi^4 = 0. \tag{2.106}$$

Dividing the last equation by $\frac{\mu^2}{h^4\rho^2}$ and introducing the non-dimensional parameter k_2 by (2.79), we can write it as

$$\Omega^4 - \Omega^2\big(k_1k_2 + (k_1 + 2(1+\nu))\xi^2\big) + 2(1+\nu)k_1\xi^4 = 0, \tag{2.107}$$

which yields roots

$$\Omega^2 = \frac{k_1k_2 + (k_1+2(1+\nu))\xi^2}{2} \pm \sqrt{\left(\frac{k_1k_2 + (k_1+2(1+\nu))\xi^2}{2}\right)^2 - 2(1+\nu)k_1\xi^4}. \tag{2.108}$$

Let's consider now a smaller root, namely $(0,0)$ root which yields zero frequency $\Omega = 0$ when $\xi = 0$, and rewrite it as follows:

$$\begin{aligned}\Omega^2 =& \frac{k_1k_2}{2}\left[1 + \frac{(k_1+2(1+\nu))\xi^2}{k_1k_2}\right.\\ &\left.-\sqrt{\left(1 + \frac{(k_1+2(1+\nu))\xi^2}{k_1k_2}\right)^2 - \frac{4\cdot 2(1+\nu)k_1\xi^4}{k_1^2k_2^2}}\right]\\ =& \frac{k_1k_2}{2}\big[1 + a_1\xi^2 - \sqrt{(1-a_1\xi^2)^2 - a_2\xi^4}\big],\end{aligned} \tag{2.109}$$

where

$$a_1 = \frac{1}{k_2} + \frac{\overline{a}}{k_1}, \qquad a_2 = \frac{4\,\overline{a}}{k_1k_2}, \tag{2.110}$$

and $\overline{a}$ was introduced by (2.78). Assuming $\xi << 1$ and expanding the square root in expression (2.108) into a Taylor series about $\xi = 0$, we obtain

$$\begin{aligned}\Omega^2 =& \frac{k_1 k_2}{2}\left\{1 + a_1\xi^2 - \left[1 + a_1\xi^2 - \frac{a_2}{2}\xi^4 + \frac{a_1(a_1 - a_2) + a_1^3}{2}\xi^6 + \right.\right. \\ & \left.\left.\left(\frac{a_1^2(a_1 - a_2)}{4} - \frac{45a_1^4}{64}\right)\xi^8 + O(\xi^{10})\right]\right\} \qquad (2.111) \\ =& \frac{k_1 k_2}{2}\left\{\frac{a_2}{2}\xi^4 + \frac{a_1(a_1 - a_2) + a_1^3}{2}\xi^6 + \left(\frac{a_1^2(a_1 - a_2)}{4} - \frac{45a_1^4}{64}\right)\xi^8 + O(\xi^{10})\right]\right\} \\ =& \overline{a}\,\xi^4 + (k_1 + k_2\overline{a})\left\{\frac{(a_1 - a_2) + a_1^2}{2}\xi^6 + \left(\frac{(a_1 - a_2)a_1}{4} - \frac{45a_1^3}{64}\right)\xi^8 + O(\xi^{10})\right\}. \qquad (2.112)\end{aligned}$$

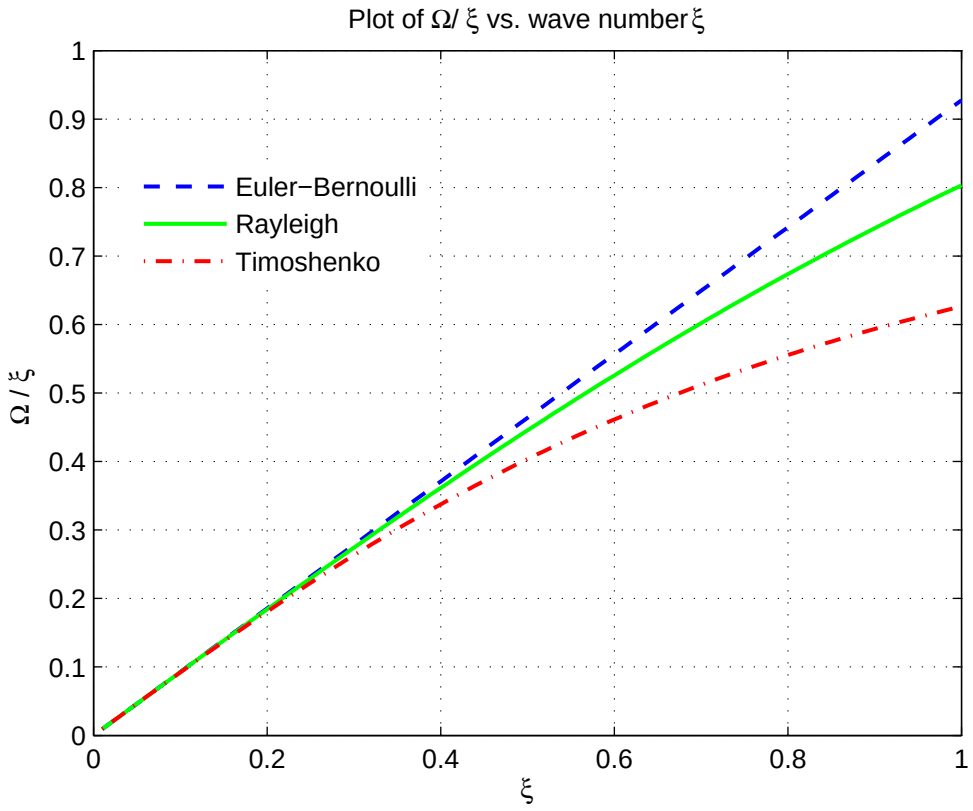

Figure 2.3: Plot of phase speed Ω/ξ vs. wave number ξ for $0 \leq \xi \leq 1$

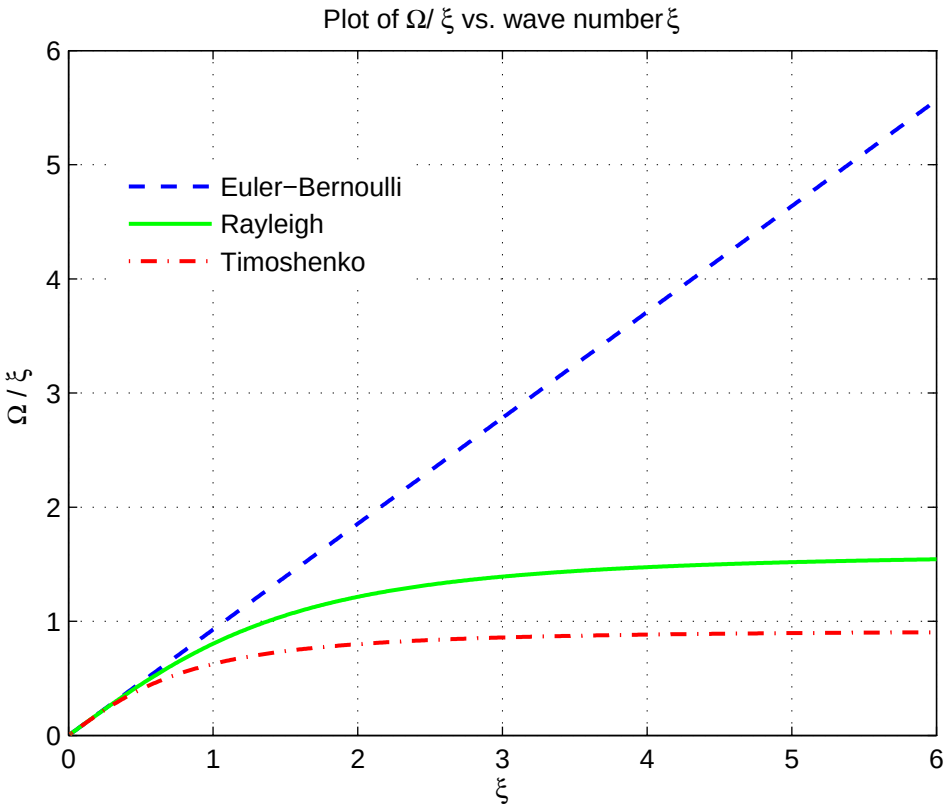

Figure 2.4: Plot of phase speed Ω/ξ vs. wave number ξ for $0 \leq \xi \leq 6$

Let us rewrite the dispersion relations for the above considered beam models in the form:

$$\Omega^2 = \overline{a}\,\xi^4, \quad \text{Euler-Bernoulli model,} \tag{2.113}$$

$$\Omega^2 = \overline{a}\left\{\xi^4 - k_2^{-1}\xi^6 + k_2^{-2}\xi^8 - k_2^{-3}\xi^{10} + O(\xi^{12})\right\}, \quad \text{Rayleigh model} \tag{2.114}$$

$$\Omega^2 = \overline{a}\left\{\xi^4 + \left(\frac{k_1}{\overline{a}} + k_2\right)\left[\frac{(a_1 - a_2) + a_1^2}{2}\xi^6 + \left(\frac{(a_1 - a_2)a_1}{4} - \frac{45a_1^3}{64}\right)\xi^8 + O(\xi^{10})\right]\right\}, \text{Timoshenko model.} \tag{2.115}$$

Comparing the results obtained for Euler-Bernoulli (2.77), Rayleigh (2.85) and Timoshenko beams (2.111), it can be noticed that the leading term $a\xi^4$ is the same for all considered models. Starting from the second term the results are different. Thus the second term in the Timoshenko model differs from the Rayleigh model by $-(k_1 + k_2\overline{a})(a_1 - a_2)/2$ times, the third term fluctuates $(k_1 + k_2\overline{a})\left(\frac{a_1(a_1-a_2)}{4} - \frac{45a_1^3}{64}\right)k_2^2$ times.

Dispersion relations in bar with rectangular cross section are shown in Figures 2.3-2.5 for phase velocity. For a solid rectangular cross section with thickness $2h$ the form factor k_1 is defined as [36]

$$k_1 = \frac{10(1+\nu)}{12+11\nu}. \tag{2.116}$$

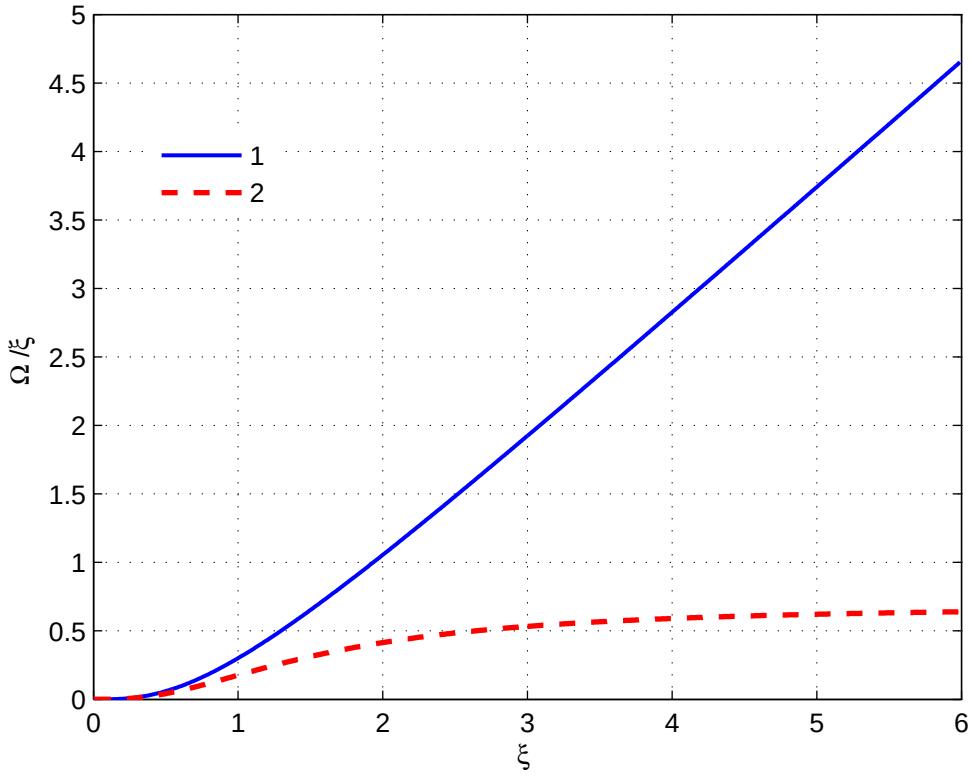

Figure 2.5: Plot of relative diffenrence between the models, $\nu = 0.29$, $k_2 = 3$. Curve '1' corresponds to the relative difference of phase velocities for Timoshenko and Euler-Bernoulli beams, curve '2' corresponds to the relative difference of phase velocities for Timoshenko and Rayleigh models

Calculations are performed on Matlab for Poisson's ratio $\nu = 0.29$ and the nondimentional parameter $k_2 = 3$. The program code is attached in Appendix 2. The dependence of phase speed Ω/ξ on wave number ξ for Euler-Bernoulli, Rayleigh and Timoshenko beams correspodingly for $0 \leq \xi \leq 1$ is given in Figure 2.3, for $0 \leq \xi \leq 6$ in Figure 2.4. As can be seen from the obtained results, the Euler-Bernoulli model gives accurate results only for small values of wave number ξ. For $0 \leq \xi \leq 0.2$ the results coincide and all three models

are in agreement. As ξ is increased the results become less accurate. It can be noticed from Figure 2.3 that for $\xi > 0.2$ the curve corresponding to Timoshenko beam starts deviating from the rest. For $\xi > 0.3$ the graph for Rayleigh beam also starts departing from one Euler-Bernoulli beam. However, the curves for the Timoshenko beam diverge from the plots for the Euler-Bernoulli beam much more than the ones for the Rayleigh beam. Figure 2.4 shows that Euler-Bernoulli theory gives unbounded phase velocity, whereas Timoshenko and Rayleigh models give a bounded phase speed. However the Rayleigh model gives a high phase speed.

Figure 2.5 compares the relative difference of phase velocities for the three models. It again shows that all three models yield accurate results for $0 \leq \xi \leq 0.2$. The difference for Timoshenko and Rayleigh models approaches some asymptote with increase of ξ. It can be noticed that the deviation between results for Timoshenko and Euler-Bernoulli beams is increasing as ξ is enlarging. This can be explained by looking at dispersion relations (2.113)-(2.115), the expansion of frequency to some order of wave number. Euler-Bernoulli model only gives one term in series expansion, whereas Timoshenko model gives more terms in series expansion, leading to more accurate results. When $\xi > 1$ the influence of coefficients of higher order wave numbers increases, leading to the deviation of results. As we expected the Euler-Bernoulli model works only for low frequency processes, for small wave numbers, whereas Timoshenko Theory can be applied for high frequency processes.

Chapter 3

The Rayleigh-Lamb Wave Equations

3.1 Introduction

Recall the frequency equations derived in the preceding chapter: the equation (2.40) for symmetric waves,

$$\frac{\tan(\beta h)}{\tan(\alpha h)} = -\frac{4\alpha\beta k^2}{(k^2-\beta^2)^2}, \tag{3.1}$$

and (2.42) for antisymmetric waves:

$$\frac{\tan(\beta h)}{\tan(\alpha h)} = -\frac{(k^2-\beta^2)^2}{4\alpha\beta k^2}, \tag{3.2}$$

where $\alpha^2 = \omega^2/c_1^2 - k^2$, $\beta^2 = \omega^2/c_2^2 - k^2$, ω is the frequency, k is the wavenumber, thickness is $2h$, speeds are c_1, c_2, with $\frac{c_1}{c_2} = \kappa$ where $\kappa^2 = \frac{2(1-\nu)}{1-2\nu} > \frac{4}{3}$.

The Rayleigh-Lamb wave equations state the dispersion relations between the frequencies and the wave numbers. They yield an infinite number of branches for an infinite number of symmetric and antisymmetric modes. The symmetric modes are referred to as *the longitudinal modes* because the average displacement over the thickness is in the longitudinal direction. The antisymmetric modes are generally termed *the flexural modes* since the average displacement is in the transverse direction.

Despite deceptively simple apperance of the Rayleigh-Lamb wave equations it is impossible to obtain analytical expressions for the branches. Even though these equations were derived at the end of 19^{th} century, a complete understanding of the frequency spectrum including higher modes and complex branches has been ascertained only comparatively recently, which became available with the development of computer software, and was shown in detail by Mindlin [13]. Nowadays, the root of the transcendental equations (3.1) and (3.2) can be obtained numerically using available software and programing codes.

Next, a new way to consider the Rayleigh-Lamb equations and find expansion to any order, in principle, is proposed.

3.2 Non Dimensional Equations

Let us introduce non-dimensional frequency and wavenumber parameters,

$$\Omega = \frac{\omega h}{c_2}, \qquad \xi = kh, \tag{3.3}$$

and let

$$x = \left(\Omega^2 - \xi^2\right)^{1/2}, \qquad y = \left(\Omega^2 \kappa^{-2} - \xi^2\right)^{1/2}, \tag{3.4}$$

then substitution of these non-dimensional parameters into the frequency equations (3.1) and (3.2) yields

$$\frac{4xy\xi^2}{(\xi^2 - x^2)^2} + \frac{\tan x}{\tan y} = 0, \quad \text{for symmetric waves,} \tag{3.5a}$$

$$\frac{4xy\xi^2}{(\xi^2 - x^2)^2} + \frac{\tan y}{\tan x} = 0, \quad \text{for antisymmetric waves.} \tag{3.5b}$$

Multiplying (3.38a) by $(\xi^2 - x^2)^2 \cos x \sin y$ and (3.5b) by $(\xi^2 - x^2)^2 \cos y \sin x$, we obtain the following equations

$$(\xi^2 - x^2)^2 \sin x \cos y + 4xy\xi^2 \cos x \sin y = 0, \tag{3.6}$$

$$(\xi^2 - x^2)^2 \sin y \cos x + 4xy\xi^2 \cos y \sin x = 0. \tag{3.7}$$

Let us now multiply last system of equations by $x^{-1}y^{-1}$, so that we have

$$(\xi^2 - x^2)^2 x^{-1} \sin x \cos y + 4y^2\xi^2 y^{-1} \sin y \cos x = 0, \tag{3.8}$$

$$(\xi^2 - x^2)^2 y^{-1} \sin y \cos x + 4x^2\xi^2 x^{-1} \sin x \cos y = 0, \tag{3.9}$$

which can be modified as

$$(\xi^2 - x^2)^2 f(x, y) + 4y^2\xi^2 f(y, x) = 0, \quad \text{for symmetric waves,} \tag{3.10}$$

$$(\xi^2 - x^2)^2 f(y, x) + 4x^2\xi^2 f(x, y) = 0, \quad \text{for antisymmetric waves.} \tag{3.11}$$

where

$$f(p,q) \equiv p^{-1} \sin p \cos q. \tag{3.12}$$

Expanding sin and cos in equation (3.12), we obtain

$$\begin{aligned} f(p,q) &= \big(1 - \frac{p^2}{6} + \frac{p^4}{120} + \dots\big)\big(1 - \frac{q^2}{2} + \frac{q^4}{24} + \dots\big) \\ &= 1 - \frac{p^2}{6} - \frac{q^2}{2} + \frac{p^4}{120} + \frac{q^4}{24} + \frac{p^2 q^2}{12} + \dots . \end{aligned} \tag{3.13}$$

Notice that f is even in p and q.

3.3 Symmetric Modes in Plates

Now let us assume that the non-dimensional frequency Ω can be expanded into series expansion though wavenumber ξ in the form

$$\Omega^2 = U_1\xi^2 + U_2\xi^4 + U_3\xi^6 + U_4\xi^8 + U_5\xi^{10} \dots . \tag{3.14}$$

Let us rewrite equation (3.10) in the following form:

$$F(\Omega, \xi, x, y) = 0, \tag{3.15}$$

where

$$F(\Omega, \xi, x, y) = (\xi^2 - x^2)^2 f(x,y) + 4y^2\xi^2 f(y,x). \tag{3.16}$$

Substitution of expansion (3.14) into (3.4) and then into (3.15) yields

$$\overline{F}(\Omega, \xi) = 0, \tag{3.17}$$

where

$$\overline{F}(\Omega, \xi) = S_1\xi^2 + S_2\xi^4 + S_3\xi^6 + S_4\xi^8 + S_5\xi^{10} + \dots, \tag{3.18}$$

$$S_1 = S_1(\nu, U_1), \quad S_2 = S_2(\nu, U_1, U_2),$$

$$S_3 = S_3(\nu, U_1, U_2, U_3), \dots, S_n = S_n(\nu, U_1, \dots U_n).$$

Equation (3.24) was solved numerically on Maple 12 using the iteration method by equating each of the coefficients $S_k,\ k = \overline{1,n}$ to zero in each step. It was noticed that S_1 is a linear

function of U_1, S_2 is a linear function of U_2 but nonlinear function of U_1 and so on, S_k is a linear function of U_k but is nonlinear in terms of $U_1, U_2, \dots U_{k-1}$, which leads us to find a unique solution $U_1, U_2, \dots U_{k-1}$. Thus first $U_1(\nu)$ was obtained from S_1=0, then U_1 was substituted into S_2 and $U_2(\nu)$ was calculated and so on. Continuing this procedure leads to the following solution:

$$U_1 = \frac{2}{1-\nu};\ U_2 = -\frac{2\cdot\nu^2}{3\cdot(1-\nu)^3};\ U_3 = \frac{2\cdot\nu^2\cdot(7\nu^2+10\nu-6)}{45\cdot(1-\nu)^5};$$
$$U_4 = -\frac{2\cdot\nu^2\cdot(62\nu^4+294\nu^3-27\nu^2-168\nu+51)}{945\cdot(1-\nu)^7};$$
$$U_5 = \frac{2\cdot\nu^2\cdot(381\nu^6+3852\nu^5+375\nu^4-5374\nu^3-554\nu^2+1524\nu-310)}{14175\cdot(1-\nu)^9};$$
$$U_6 = -\frac{2\nu^2}{467775\cdot(1-\nu)^{11}}\cdot(4146-27104\nu+23919\nu^2+145530\nu^3+253549\nu^4-$$
$$-107448\nu^5+238567\nu^6+89650\nu^7+5110\nu^8),$$

and so on.

Substituting the obtained solutions into (3.14) we obtain

$$\Omega^2 = \sum_{n=1}^{\infty}\xi^{2n}U_n, \tag{3.19}$$

where U_n has the form:

$$U_n = \frac{(-1)^{(2n-1)}\cdot 2^n\cdot(n-1)!\cdot\nu^2}{(2n-1)!(1-\nu)^{2n-1}}\cdot B_n, \tag{3.20}$$

and B_n are polynomials of order $(2n-4)$ in ν

$$B_1 = -1/\nu^2,\quad B_2 = 1,\quad B_3 = (-7\nu^2-10\nu+6)/3,$$
$$B_4 = (62\nu^4+294\nu^3-27\nu^2-168\nu+51)/9,$$
$$B_5 = (-381\nu^6-3852\nu^5-3750\nu^4+5374\nu^3+554\nu^2-1524\nu+310)/(3\cdot 5),$$
$$B_6 = (5110\nu^8+89650\nu^7+238567\nu^6-107448\nu^5$$
$$-253549\nu^4+145530\nu^3+23919\nu^2-27104\nu+4146)/(3^2\cdot 5),$$

and so on.

Calculations were performed on Maple 12. The program code is gived in Appendix 2.1.

3.4 Antisymmetric Modes in Plates

For the antisymmetric case we assume that the frequency is expressed by the expansion

$$\Omega^2 = W_1\xi^2 + W_2\xi^4 + W_3\xi^6 + W_4\xi^8 + W_5\xi^{10} + W_6\xi^{12} + W_7\xi^{14} + W_8\xi^{16} + W_9\xi^{18} + W_{10}\xi^{20} + \dots. \tag{3.21}$$

We then rewrite equation (3.11) in the following form:

$$F_1(\Omega, \xi, x, y) = 0, \tag{3.22}$$

where

$$F_1(\Omega, \xi, x, y) = (\xi^2 - x^2)^2 f(y, x) + 4x^2\xi^2 f(x, y). \tag{3.23}$$

After substituting series expansion (3.21) into equation (3.15) and incorporating equation (3.4), we obtain the following equation

$$\overline{F_1}(\Omega, \xi) = 0, \tag{3.24}$$

where

$$\overline{F_1}(\Omega, \xi) = G_1\xi^2 + G_2\xi^4 + G_3\xi^6 + G_4\xi^8 + G_5\xi^{10} + \dots, \tag{3.25}$$

$$G_1 = G_1(\nu, W_1), \quad G_2 = G_2(\nu, W_1, W_2),$$

$$G_3 = G_3(\nu, W_1, W_2, W_3), \dots, G_n = G_n(\nu, W_1, \dots W_n).$$

Equation (3.24) was solved numerically on Maple 12 by the iteration method described in detail in the previous section and the following solution was obtained:

$$\begin{aligned}
&W_1 = 0;\ \ W_2 = -\frac{2}{3(\nu-1)};\ \ W_3 = \frac{2\cdot(7\nu-17)}{45\cdot(\nu-1)^2};\ \ W_4 = -\frac{2\cdot(62\nu^2-418\nu+489)}{945\cdot(\nu-1)^3};\\
&W_5 = \frac{2\cdot(381\nu^3-4995\nu^2+14613\nu-11189)}{14175\cdot(\nu-1)^4};\\
&W_6 = -\frac{2\cdot(5110\nu^4-110090\nu^3+584257\nu^2-1059940\nu+602410)}{467775\cdot(\nu-1)^5};\\
&W_7 = \frac{2}{638512875\cdot(\nu-1)^6}\cdot(-1404361931+3109098177\nu-2386810276\nu^2\\
&\quad + 754982390\nu^3 - 90572134\nu^4 + 2828954\nu^5);
\end{aligned} \tag{3.26}$$

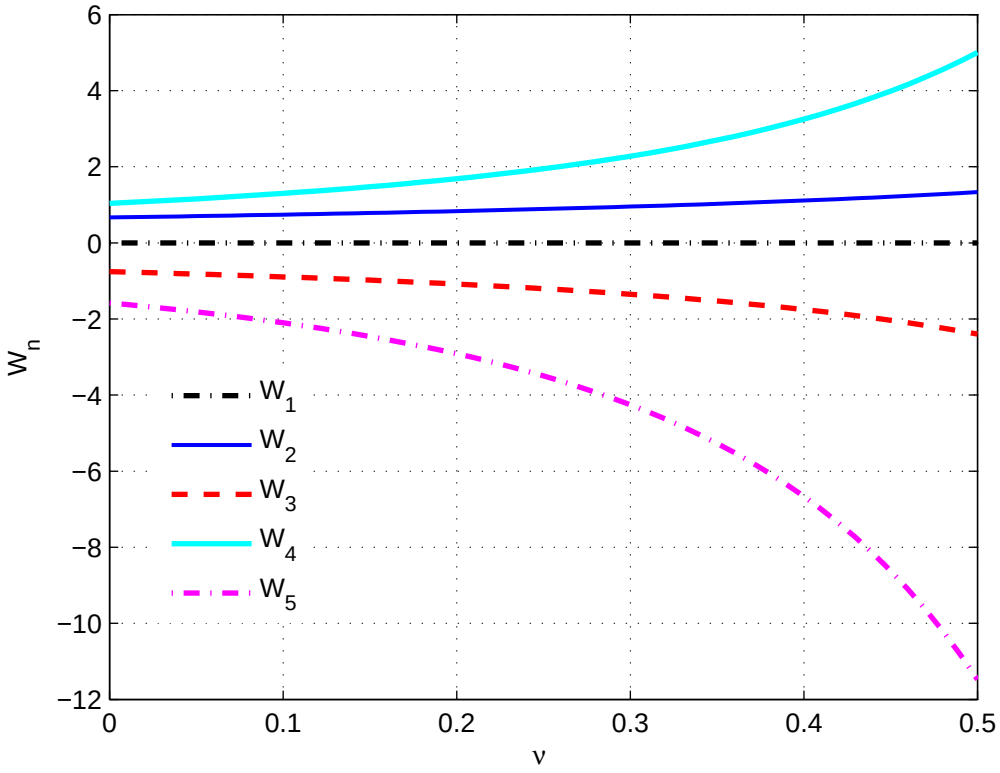

Figure 3.1: Plot of W_n vs Poisson's ratio ν for $n = 1, 2, 3, 4, 5$

$$W_8 = -\frac{2}{1915538625 \cdot (\nu-1)^7}(3440220\nu^6 - 153108900\nu^5 + 1840593186\nu^4$$
$$- 8868547040\nu^3 19607784669\nu^2 - 19849038802\nu + 7437643415);$$
$$W_9 = \frac{2}{488462349375 \cdot (\nu-1)^8}(355554717\nu^7 - 20978378363\nu^6 + 343393156317\nu^5$$
$$- 2332360918791\nu^4 + 7695401450679\nu^3 - 12978692736341\nu^2 + 10724754208055\nu$$
$$- 3433209020623),$$
$$W_{10} = -\frac{2}{194896477400625 \cdot (\nu-1)^9}(57496915570\nu^8 - 4341050683790\nu^7 + 92811983812139\nu^6$$
$$- 843435286359132\nu^5 + 3856675179582919\nu^4 - 9557544387771638\nu^3$$
$$+ 12977929665725313\nu^2 - 9051135401463140\nu + 2528890541707756)$$

and so on.

Figure 3.1 and Figure 3.2 show the dependence of W_n on Poisson's ratio ν. It can be

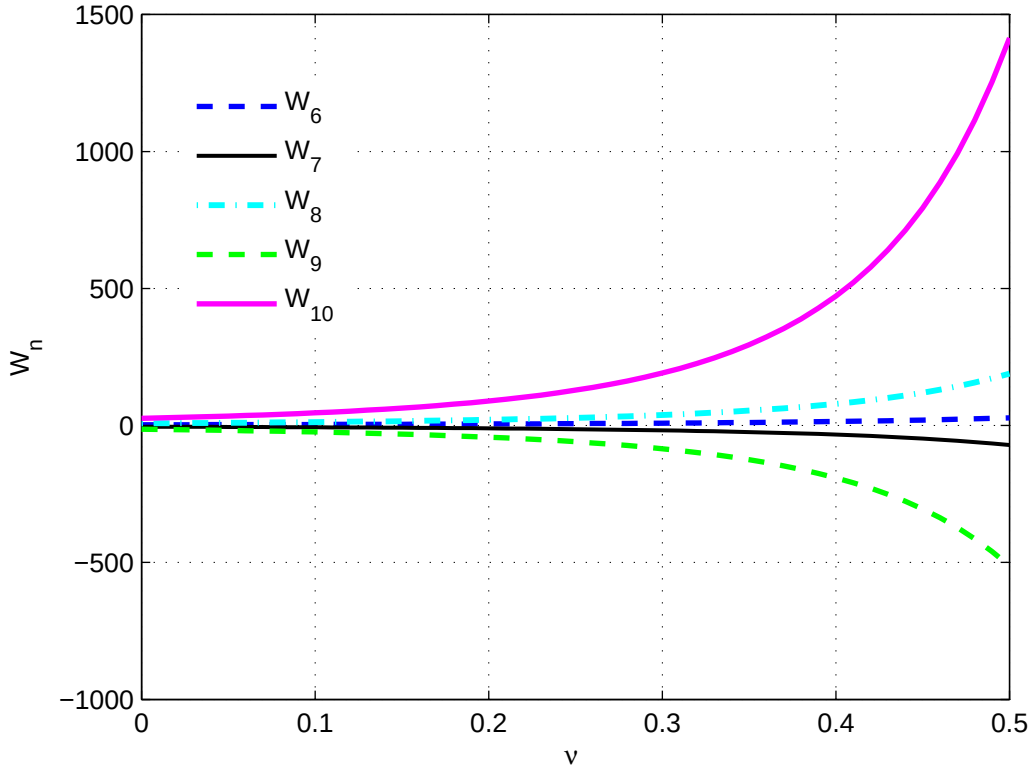

Figure 3.2: Plot of W_n vs Poisson's ratio ν for $n = 6, 7, 8, 9, 10$

noticed that plots of W_n for $n = 2k$, $k = 1, 2, 3...$ are monotonically increasing and for $n = 2k+1$, $k = 1, 2, 3...$ are monotonically decreasing as Poisson's ratio ν is enlarging, except W_1 which remains constant: $W_1 = 0$.

Plugging obtained above solutions (3.26) into equation (3.21) will result in following expression for Ω^2

$$\Omega^2 = \sum_{n=1}^{\infty} \xi^{2n} W_n, \tag{3.27}$$

where W_n has the form

$$W_n = \frac{(-1)^n \cdot 2^{n+5}}{(2n)!(1-\nu)^{n-1}} \cdot D_n = \frac{(-1)^n \cdot Z_n}{(1-\nu)^{n-1}} \cdot D_n, \tag{3.28}$$

Z_n has the form

$$Z_n = \frac{2^{n+5}}{(2n)!}, \tag{3.29}$$

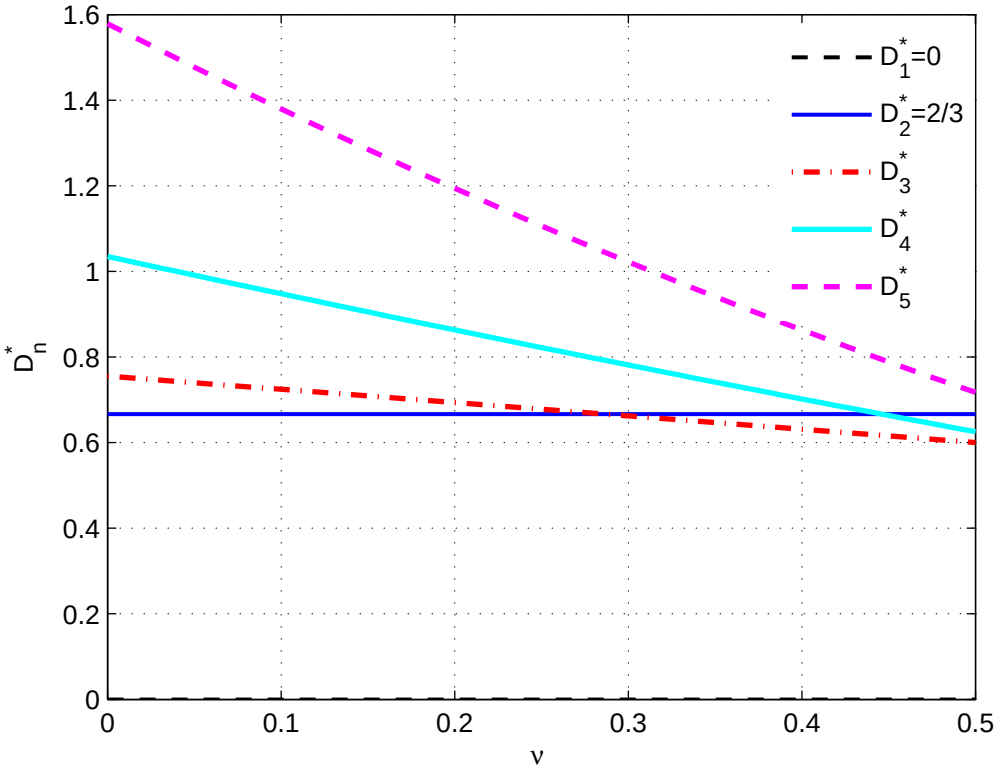

Figure 3.3: Plot of $D_n^* = D_n * Z_n$ versus Poisson's ratio ν for $6 \leq n \leq 10$

and D_n are polynomials of order $(n-2)$ in ν:

$$D_1 = 0; \quad D_2 = 1/8; \quad D_3 = (-7\nu + 17)/8; \quad D_4 = (62\nu^2 - 418\nu + 489)/6;$$

$$D_5 = (-381\nu^3 + 4995\nu^2 - 14613\nu + 11189)/2;$$

$$D_6 = 5110\nu^4 - 110090\nu^3 + 584257\nu^2 - 1059940\nu + 602410;$$

$$D_7 = (-2828954\nu^5 + 90572134\nu^4 - 754982390\nu^3 + 2386810276\nu^2 \tag{3.30}$$
$$- 3109098177\nu + 1404361931)/15;$$

$$D_8 = 9173920\nu^6 - 408290400\nu^5 + 4908248496\nu^4 - 70948376320\nu^3/3$$
$$+ 52287425784\nu^2 - 158792310416\nu/3 + 59501147320/3;$$

$$D_9 = (2844437736\nu^7 + 167827034904\nu^6 - 2747145250536\nu^5 + 18658887350328\nu^4$$
$$- 61563211605432\nu^3 + 103829541890728\nu^2 - 17159606732888 \cdot 5\nu$$
$$+ 27465672164984)/5,$$

$$D_{10} = (919950649120\nu^8 - 69456810940640\nu^7 + 1484991740994224\nu^6 - 4498321527248704$$
$$\cdot 3\nu^5 + 61706802873326704\nu^4 - 152920710204346208\nu^3 + 69215624883868336 \cdot \nu^2$$
$$- 144818166423410240\nu + 40462248667324096)/21.$$

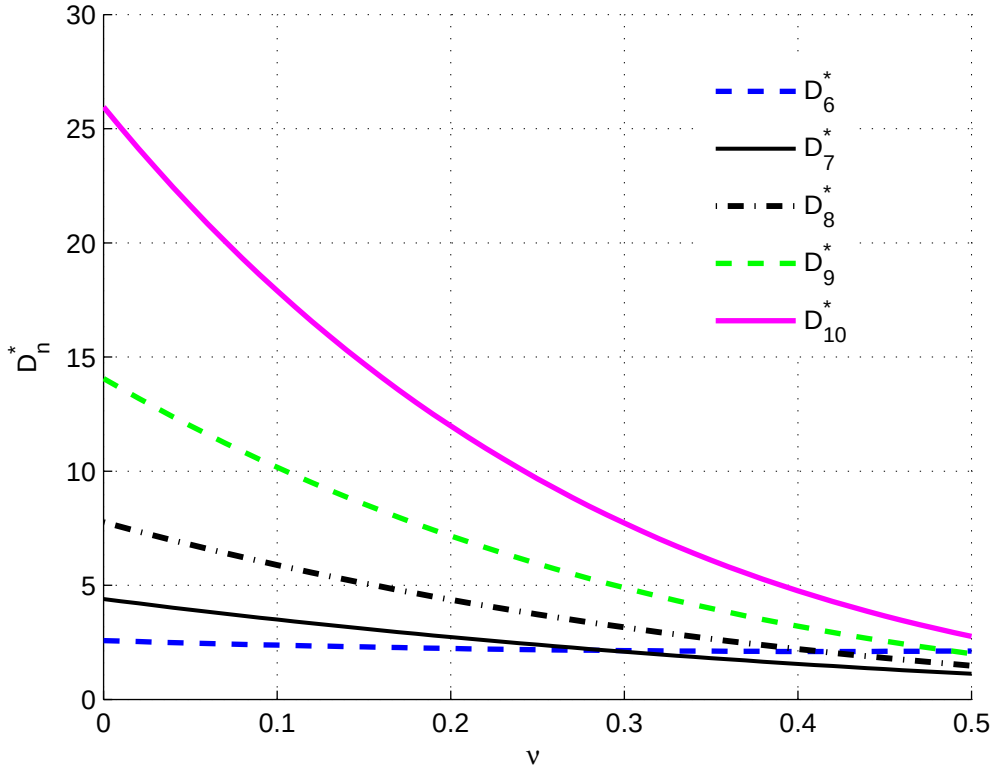

Figure 3.4: Plot of $D_n^* = D_n * Z_n$ versus Poisson's ratio ν for $6 \leq n \leq 10$

D_n can be expressed in terms of $(1-\nu)$ in the following form:

$$
\begin{aligned}
&D_1 = 0; \quad D_2 = 1/8; \quad D_3 = \frac{7}{8}(1-\nu) + \frac{5}{4}; \quad D_4 = \frac{31}{3}(1-\nu)^2 + 49(1-\nu) + \frac{133}{6};\\
&D_5 = \frac{381}{2}(1-\nu)^3 + 1926(1-\nu)^2 + 2883(1-\nu) + 595;\\
&D_6 = 5110(1-\nu)^4 + 89650(1-\nu)^3 + 284647(1-\nu)^2 + 201256(1-\nu) + 21747;\\
&D_7 = \frac{2828954}{15}(1-\nu)^5 + \frac{25475788}{5}(1-\nu)^4 + \frac{140327798}{5}(1-\nu)^3\\
&\quad + \frac{127401274}{3}(1-\nu)^2 + \frac{252281029}{15}(1-\nu) + 988988;\\
&D_8 = 9173920(1-\nu)^6 + 353246880(1-\nu)^5 + 3004405296(1-\nu)^4 \qquad (3.31)\\
&\quad + \frac{23747671168}{3}(1-\nu)^3 + 6843245240(1-\nu)^2 + \frac{4973128160}{3}(1-\nu) + \frac{150133984}{3};
\end{aligned}
$$

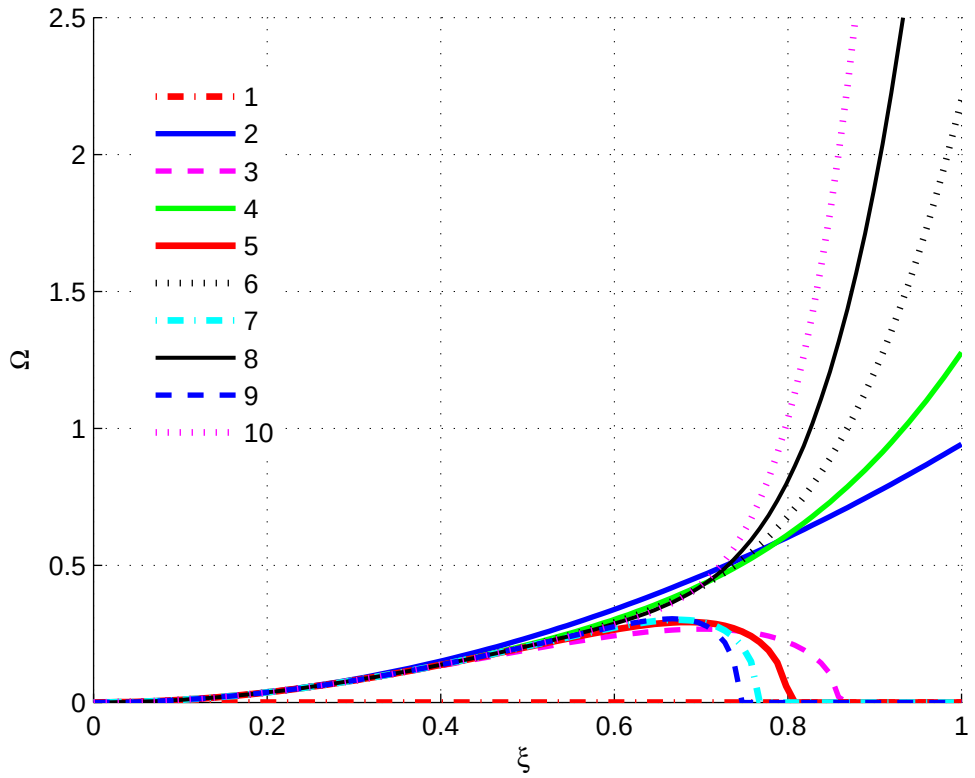

Figure 3.5: Plot of frequency Ω vs wave number ξ, $\nu = 0.25$. The Curve '1' corresponds to keeping the first term in series expansion (3.21), the curve '2' corresponds to keeping the first and the second terms, the curve '3' corresponds to keeping the first, the second and the third terms and so on, the curve '10' corresponds to keeping the first ten terms.

$$D_9 = \frac{2844437736}{5}(1-\nu)^7 + \frac{147915970752}{5}(1-\nu)^6 + \frac{1799916233568}{5}(1-\nu)^5 + \frac{7341011300448}{5}(1-\nu)^4 + 2228425866432(1-\nu)^3 + \frac{6079451002144}{5}(1-\nu)^2 + \frac{941710405376}{5}(1-\nu) + 2138696560,$$

$$D_{10} = (919950649120(1-\nu)^8 + 20699068582560 \cdot 3(1-\nu)^7 + 1024552682585104(1-\nu)^6 + 5992089929183488(1-\nu)^5 + 14140264242025504(1-\nu)^4 + 1960397265026816 \cdot 7(1-\nu)^3 + 716851023485824 \cdot 7(1-\nu)^2 + 71863824869824 \cdot 7(1-\nu) - 208590934864 \cdot 7)/21.$$

Evaluation of the coefficients W_n and D_n was performed on Maple 12, program code is attached in Appendix 1. As can be seen from last expressions for D_ns all coefficients of

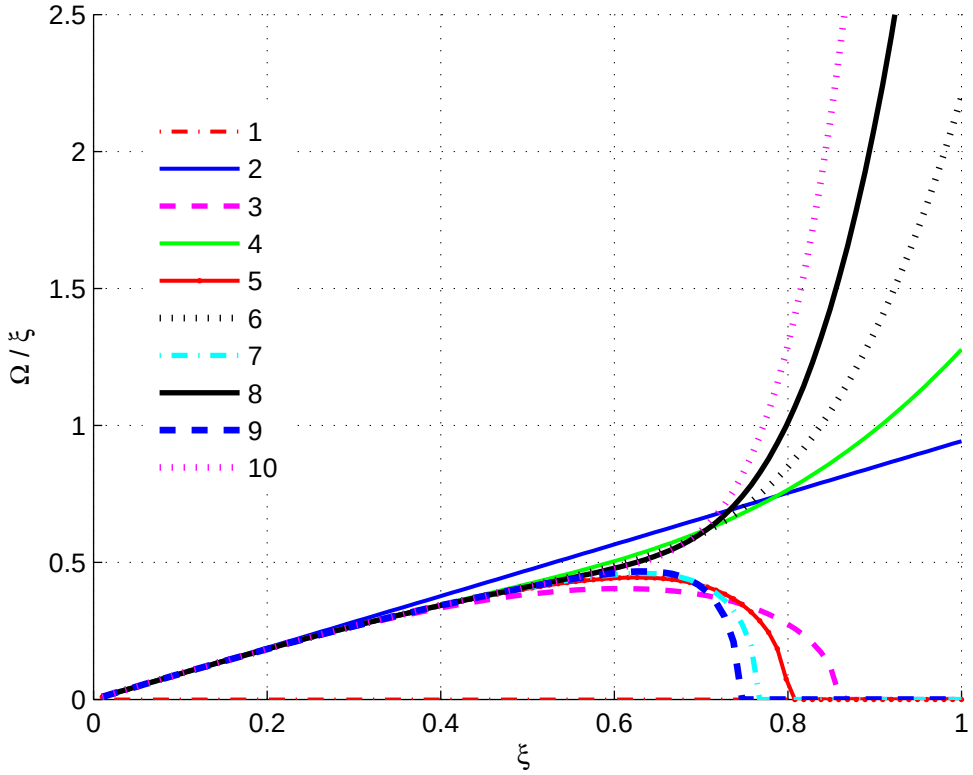

Figure 3.6: Plot of phase speed Ω/ξ versus wave number ξ, $\nu = 0.25$. Curve '1' corresponds to keeping the first term in series expansion (3.21), the curve '2' corresponds to keeping the first and the second term, the curve '3' corresponds to keeping the first, the second and the third terms and so on, the curve '10' corresponds to keeping the first ten terms.

$(1-\nu)^k$, $(k = 0, 1, 2, 3...)$ terms became positive except the expression for D_{10} for $k = 0$. The graphs of $D_n^* = D_n * Z_n$ versus Poisson's ratio ν are given correspondingly for $n = \overline{1,5}$ in Figure 3.3 and for $n = \overline{6,10}$ in Figure 3.4 , where Z_ns are defined by (3.28).

The plots of frequency Ω versus wave number ξ are calculated by (3.21) and given in Figures 3.5 for $\nu = 0.25$. The dependence of phase speed Ω/ξ on wave number ξ is shown in Figures 3.6 for $\nu = 0.25$. It can be noticed from plots given in Figures 3.5 and 3.6 that series expansion (3.21) gives accurate results only for small values of ξ. As ξ increases result become less accurate.

The group velocity c_g by definition is [15]:

$$c_g = \frac{\partial \Omega}{\partial \xi}. \tag{3.32}$$

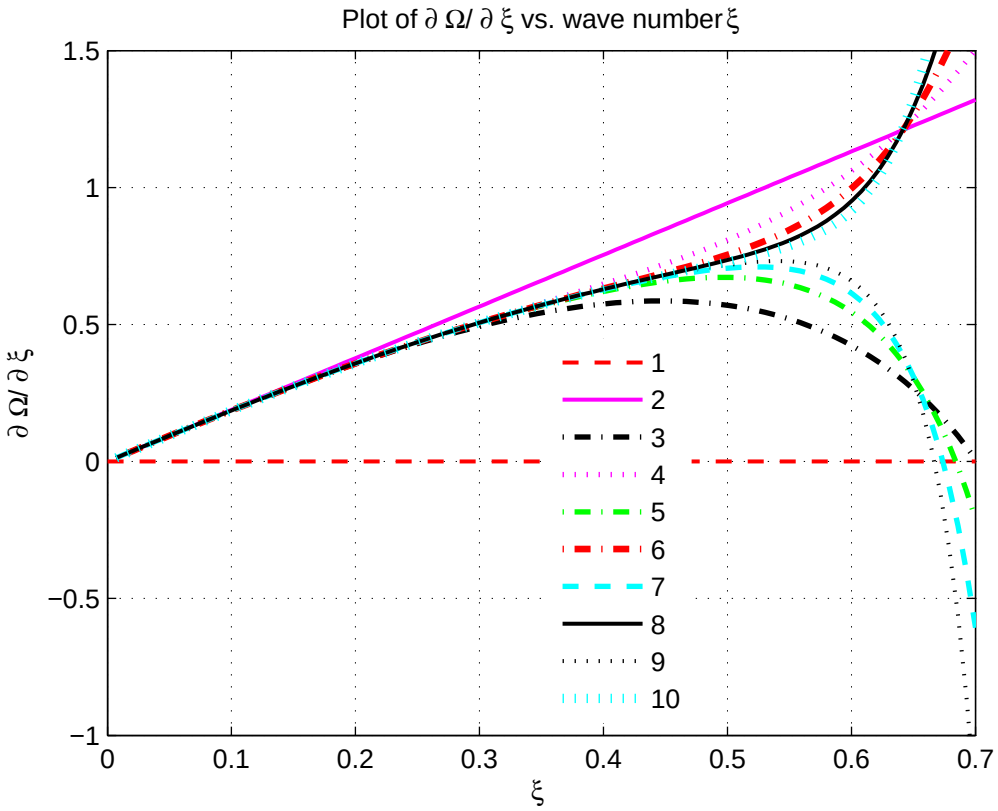

Figure 3.7: Plot of group speed $\partial\Omega/\partial\xi$ versus wave number ξ, $\nu = 0.25$. Curve '1' corresponds to keeping the first term in series expansion (3.21), the curve '2' corresponds to keeping the first and the second term, the curve '3' corresponds to keeping the first, the second and the third terms and so on, the curve '10' corresponds to keeping the first ten terms.

Using the chain rule, we have

$$\frac{\partial\Omega^2}{\partial\xi} = 2\Omega\frac{\partial\Omega}{\partial\xi} \tag{3.33}$$

and

$$\frac{\partial\Omega^2}{\partial\xi^2} = 2\Omega\frac{\partial\Omega}{\partial\xi}\frac{\partial\xi}{\partial\xi^2} = \frac{\Omega}{\xi}\frac{\partial\Omega}{\partial\xi}. \tag{3.34}$$

Thus the group velocity is obtained as:

$$c_g = \frac{\partial\Omega}{\partial\xi} = \frac{\frac{\partial\Omega^2}{\partial\xi}}{2\Omega} = \frac{\xi}{\Omega}\frac{\partial\Omega^2}{\partial\xi^2} \tag{3.35}$$

or

$$c_g = \frac{1}{c}\frac{\partial\Omega^2}{\partial\xi^2}, \tag{3.36}$$

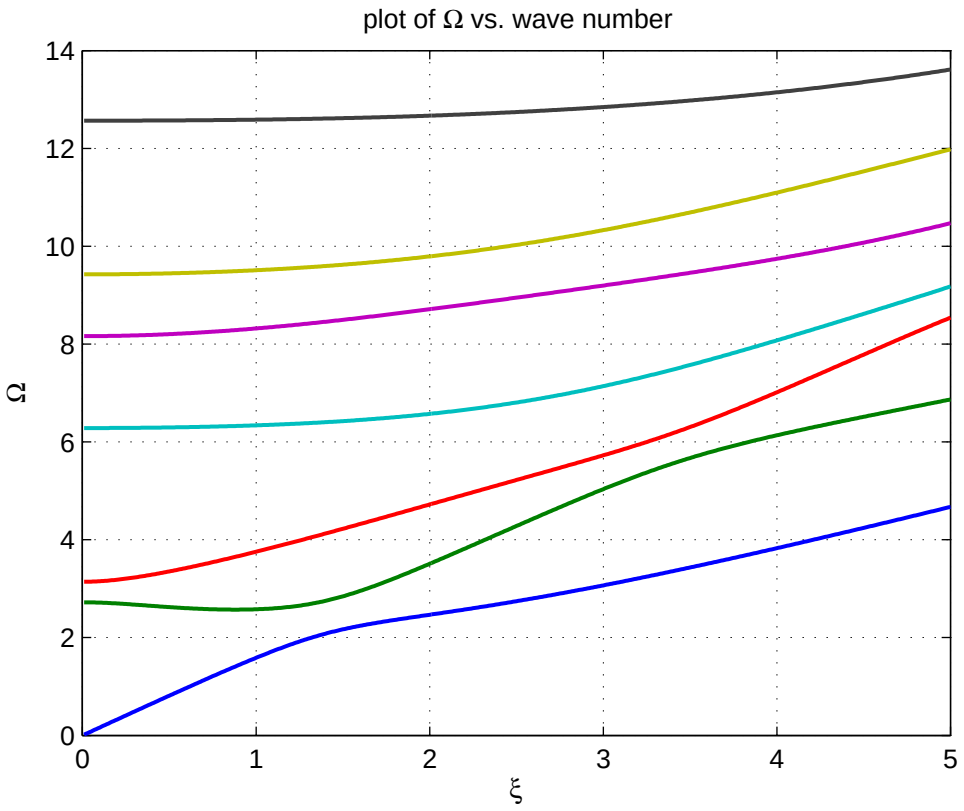

Figure 3.8: Plot of frequency Ω versus wave number ξ, symmetric modes, $\nu = 0.25$

where

$$\frac{\partial \Omega^2}{\partial \xi} = 2W_1\xi + 4W_2\xi^3 + 6W_3\xi^5 + 8W_4\xi^7 + 10W_5\xi^9 + 12W_6\xi^{11} + 14W_7\xi^{13} + 16W_8\xi^{15} + 18W_9\xi^{17} + 20W_{10}\xi^{19} + \dots. \tag{3.37}$$

Figure 3.7 illustrates the group speed $\partial\Omega/\partial\xi$ in plate as function of wave number ξ for $\nu = 0.25$. The plots illustrated in Figure 3.1-3.7 were produced on Matlab.

3.5 Numerical Evaluation of the Roots of the Rayleigh-Lamb Equations

Recall again the Rayleigh-Lamb wave equations for plates in non-dimentional parametrs:

$$(\xi^2 - x^2)^2 \sin x \cos y + 4xy\xi^2 \cos x \sin y = 0, \quad \text{for symmetric modes,} \tag{3.38a}$$

$$(\xi^2 - x^2)^2 \sin y \cos x + 4xy\xi^2 \cos y \sin x = 0, \quad \text{for antisymmetric modes.} \tag{3.38b}$$

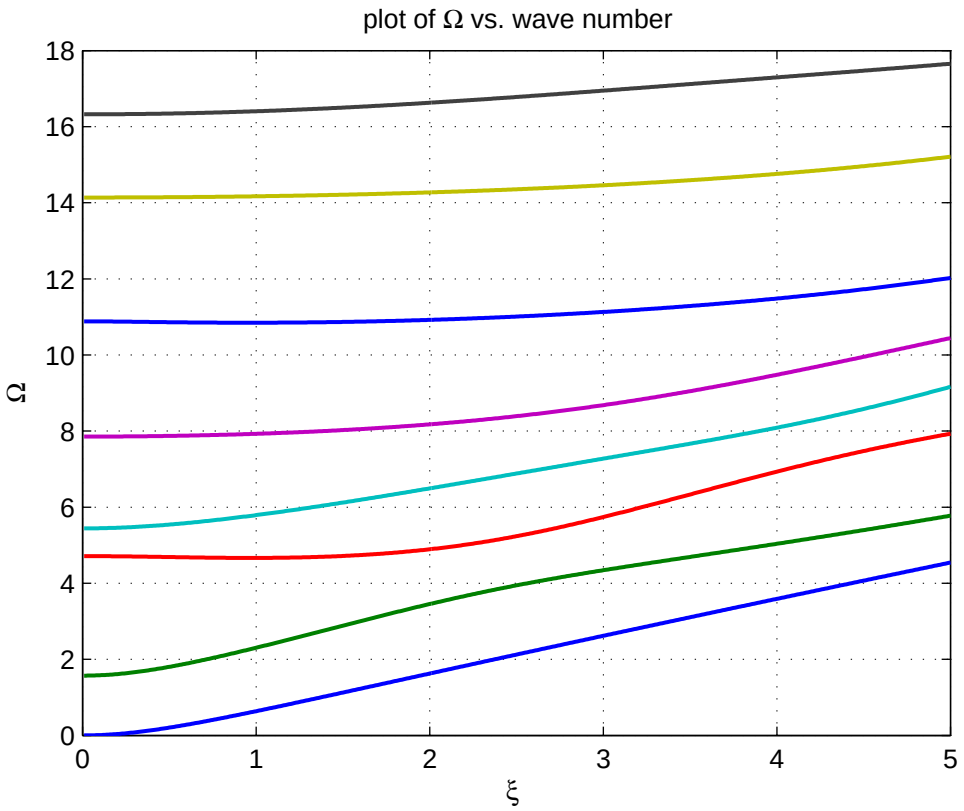

Figure 3.9: Plot of Frequency Ω versus wave number ξ, antisymmetric modes, $\nu = 0.25$

where

$$x = \left(\Omega^2 - \xi^2\right)^{1/2}, \qquad y = \left(\Omega^2\kappa^{-2} - \xi^2\right)^{1/2}, \qquad \Omega = \frac{\omega h}{c_2}, \qquad \xi = kh.$$

As it was mentioned above it is not possible to find the roots of the transcendental equations (3.38a)-(3.38b) analytically, therefore to solve these equations a numerical method is applied. The numerical evaluation of the roots of the transcendental equations (3.38a)-(3.38b) is performed on Matlab using the "fzero" routine. The codes are attached in Appendix 2. The plate is homogeneous, isotropic and elastic. Numerical analysis of real branches of frequency spectrum in plate for symmetric and antisymmetric modes was conducted by Mindlin [13]. Plots showing the frequency dependence on wave number are shown correspondingly for symmetric mode propagation in Figure 3.8 after Mindlin. Dispersion curves corresponding to real propagation constants for the antisymmetric mode are given in Figure 3.9, after Mindlin [13]. The cutoff frequencies are taken as starting points for each branch. The cutoff

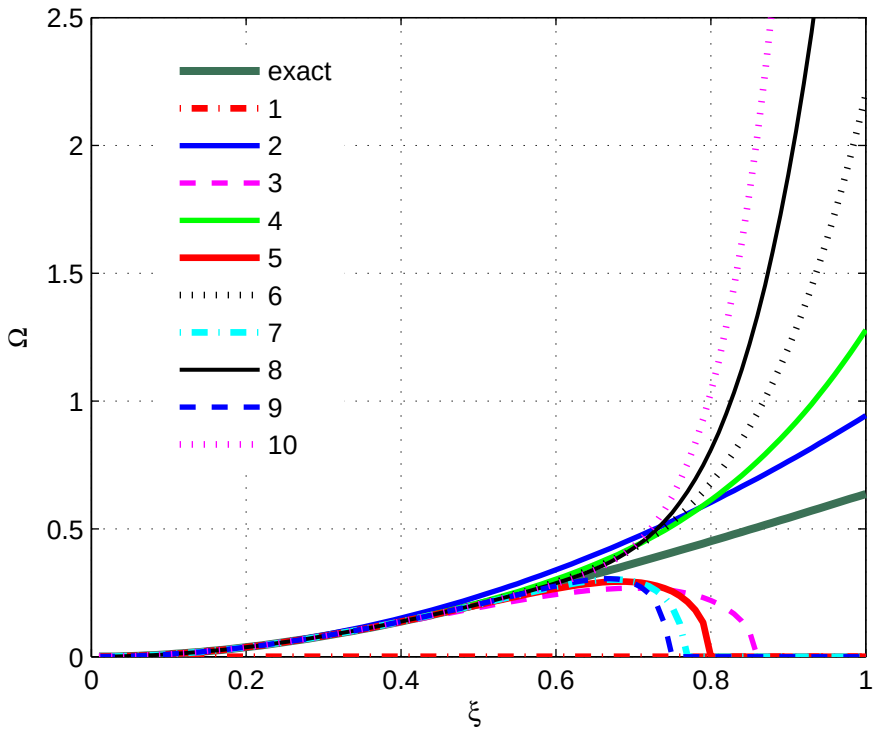

Figure 3.10: Plot of frequency Ω vs wave number ξ for the lowest mode. Comparison of results for series expansion method and exact theory, n=1

frequencies can be obtained setting $\xi = 0$ in the frequency equations (3.38a) - (3.38b). Thus, setting $\xi = 0$ in equation (3.38a), we have the following equation for symmetric modes

$$\Omega^4 \sin(\Omega) \cos(\kappa^{-1}\Omega) = 0, \tag{3.39}$$

which can be separated into two equations

$$\sin(\Omega) = 0, \tag{3.40}$$

and

$$\cos(\kappa^{-1}\Omega) = 0. \tag{3.41}$$

Equations (3.40) and (3.41) specify two independent sets of cutoff frequencies. The cutoff frequencies produced by equation (3.40) are independent of Poisson's ratio ν, some of them are given below:

$$0,\ \pi,\ 2\pi,\ 3\pi,\ 4\pi,\ 5\pi,\ 6\pi,\ 7\pi,\ 8\pi,\ 9\pi,\ 10\pi,\ 11\pi,\ \ldots \tag{3.42}$$

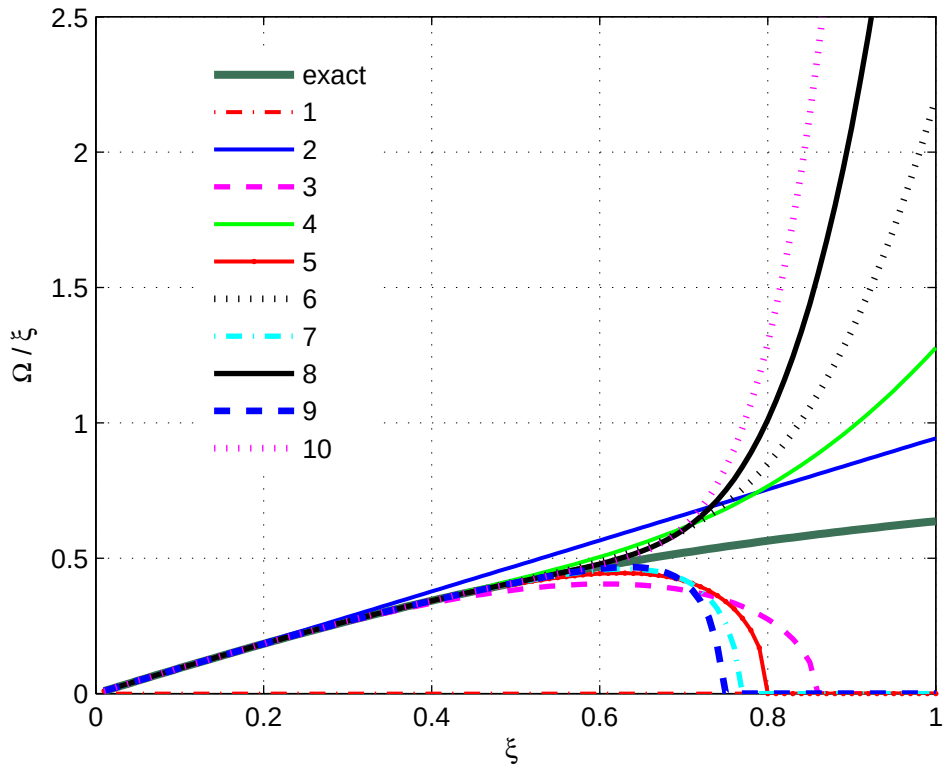

Figure 3.11: Plot of phase velocity Ω/ξ vs wave number ξ for the lowest mode. Comparison of results for series expansion method and exact theory, n=1

The cutoff frequencies determined by equation (3.41) depend on Poisson's ratio:

$$\kappa\frac{\pi}{2},\ \kappa\frac{3\pi}{2},\ \kappa\frac{5\pi}{2},\ \kappa\frac{7\pi}{2},\ \kappa\frac{9\pi}{2},\ \kappa\frac{11\pi}{2},\ \kappa\frac{13\pi}{2},\ \kappa\frac{15\pi}{2},\ldots \tag{3.43}$$

for $\nu = 0.25$ the cutoff frequencies become:

$$2.7207,\ 8.1621,\ 13.6035,\ 19.0449,\ 24.4863,\ 29.9277,\ 35.3691,\ 40.8105\ldots \tag{3.44}$$

For antisymmetric modes the cutoffs are found from the frequency equation (3.38b) setting $\xi = 0$,thus we have:

$$\Omega^4 \sin(\kappa^{-1}\Omega)\cos(\Omega) = 0, \tag{3.45}$$

Equation (3.45) can be separated into two equations

$$\cos(\Omega) = 0, \tag{3.46}$$

and

$$\sin(\kappa^{-1}\Omega) = 0, \tag{3.47}$$

Equation (3.45) specifies the following cutoffs:

$$\frac{\pi}{2}, \frac{3\pi}{2}, \frac{5\pi}{2}, \frac{7\pi}{2}, \frac{9\pi}{2}, \frac{11\pi}{2}, \frac{13\pi}{2}, \frac{15\pi}{2}, \ldots \tag{3.48}$$

Equation (3.45) yields the following cutoff frequencies which depend on Poisson's ratio ν:

$$0,\ \kappa\pi,\ 2\kappa\pi,\ 3\kappa\pi,\ 4\kappa\pi,\ 5\kappa\pi,\ 6\kappa\pi,\ 7\kappa\pi,\ 8\kappa\pi,\ 9\kappa\pi,\ 10\kappa\pi,\ 11\kappa\pi,\ \ldots \tag{3.49}$$

For $\nu = 0.25$ the cutoffs specified by (3.47) have the following values:

$$0,\ 5.4414,\ 10.8828,\ 16.3242,\ 21.7656,\ 27.2070,\ 32.6484,\ 38.0898,\ 43.5312,\ 48.9726,\ \ldots \tag{3.50}$$

It can be noticed from dispersion curves for frequency shown in Figure 3.10 and for phase velocity shown in Figure 3.11 that the series expansion method is in a good agrement with the exact theory and it gives accurate results for $0 \leq \xi \leq 0.6$. Keeping 10 terms in series expansion which corresponds to curve 10 in Figure 3.10-3.11, gives a more precise result for $0 \leq \xi \leq 0.6$.

To analyze the Rayleigh-Lamb frequency equations for high wave numbers, one can use the Pade approximant with obtained series expansion to expand the radius of convergence. The Padé approximant developed by Henri Padé which is the "best" approximation of a function by a rational function of given order. The approximant's power series agrees with the power series of the function it is approximating and it may still work where the Taylor series does not converge as in our case. Another approach is to use the effective equations of refined engineering theories [23] with specified boundary conditions. The refined equations are unclear sometimes, the specified boundary conditions should correspond to an order of PDE and a number of independent variables. The refined equations are high order PDEs. It is necessary to specify a large number of boundary conditions to relate the boundary conditions to the order of the PDE and the number of unknowns. Consequently, considered problem becomes complicated.

Chapter 4

Waves in Rods

This section is designed to study wave propagation in elastic isotropic circular cylindrical rods. We begin with a review of wave propagation in rods. In Section 4.2 the governing equation of elasticity in cylindrical coordinates and boundary conditions are derived. We present three different representations of displacement potentials, namely the Helmholtz decomposition (2.10) for vector fields given in [16], Buchwald's potential [37] and the scalar potential introduced by Morse and Feshbach [38]. Two of these representations, (2.10) and (4.47), are used to derive dispersion relations in rod for symmetric and antisymmetric modes in the succeding Section 4.4. Finally, this chapter ends with the discussion of the numerical results on dispersion relations and cutoff frequencies for axial-shear, radial-shear and flexural modes, which is given in Section 4.5.

4.1 Review of Elastic Waves in Rods

The frequency equations for waves in circular cylindrical rods, based on the solution of the boundary value problem of the theory of elasticity, were given by Pochhammer [9] and independently by Chree [10] in the 19th century. However, numerical solutions of the frequency equations were not attempted up to beginning of the computer era. In 1940, Shear et al. [39] tried to clarify obtained experimental results without referring to the Pochhammer-Chree theory. In 1941, Bancrof [40] first initiated the interpretation of wave propagation in rods on the basis of the Pochhammer-Chree theory.

The development of dispersion relations for an isotropic elastic bar has been studied by Green [41] who divided the development of approximate theories into two categories. In the

first category, where equations of motion were derived based on approximation, contributions by Rayleigh [1], Love, Timoshenko [2], Mindlin, Volterra [42] etc. were reviewed. In the second category, exact solutions of the theory of elasticity that only approximately satisfy the boundary conditions were studied and contributions by Chree [10], Morse [43], Green were cited. Thurston studied elastic waves in rods and clad rods of circular cross section in [30], with a broad review and descriptive material on typical waveguide dispersion, characteristic velocities of an isotropic elastic material, waves in homogeneous rods, and previous results on the clad rod were given. Investigation of elastic wave propagation in a cylinder has been conducted by Zemanek [44], both experimentally and theoretically. Dispersion of compressional waves in rods of rectangular cross section has been examined by Morse [43]. In most of the above mentioned references, [16], [15], [41], [44], etc., the exact solutions of the theory of elasticity were represented through potentials given by equation (2.10) in Section 2. However, there are alternative forms of the representation of displacement vector in terms of the scalar potentials such as one proposed by Morse and Feshbach [38], and Buchwald [37]. Chadwick [45] has applied Buchwald's approach [37] in the study of wave propagation in transversely isotropic heat conducting elastic materials. Honarvar and Sinclair [46] used the displacement decomposition proposed by Morse and Feshbach [38] in the analysis of wave scattering from transversely isotropic cylinders. Ahmad and Rahman [47] also studied the scattering of acoustic wave incident on a transversely isotropic cylinder. However, he showed that Buchwald's representation [37] yields much more simpler equations, and is much more efficient in application. Norris and Shuvalov [33] adopted Buchwald's approach to construct the solid-cylinder impedance matrix for transverse isotropic radially inhomogeneous elastic solids. We defer the discussion of this matter to Sections 4.3.2 and 4.4.2 where this approarch will be used in the development of frequency equations for rods.

4.2 Theory

In cylindrical coordinates (r, θ, z) consider an infinitely long solid circular rod of radius a, it's cross section shown in Figure 4.1. In (r, θ, z) system the equation of motion (2.9) can be

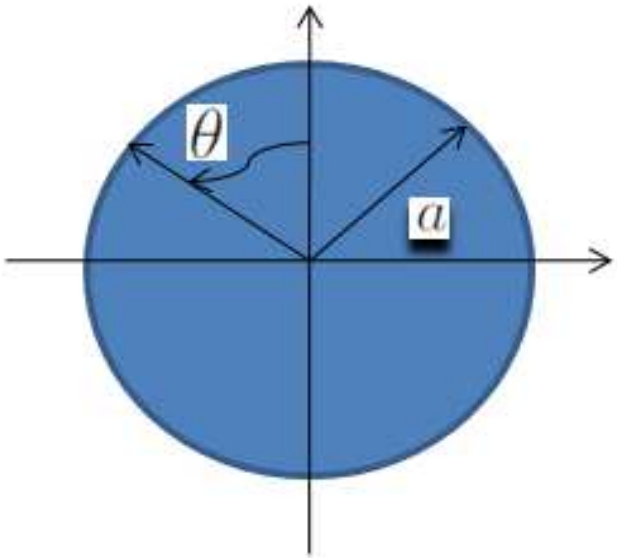

Figure 4.1: Cross section of circular rod in cylindrical coordinates

written as

$$\nabla^2 u_r - \frac{u_r}{r^2} - \frac{2}{r^2}\frac{\partial u_\theta}{\partial \theta} + \frac{1}{1-2\nu}\frac{\partial \epsilon}{\partial r} = \frac{1}{c_2^2}\frac{\partial^2 u_r}{\partial t^2}, \tag{4.1a}$$

$$\nabla^2 u_\theta - \frac{u_\theta}{r^2} + \frac{2}{r^2}\frac{\partial u_r}{\partial \theta} + \frac{1}{1-2\nu}\frac{1}{r}\frac{\partial \epsilon}{\partial \theta} = \frac{1}{c_2^2}\frac{\partial^2 u_\theta}{\partial t^2}, \tag{4.1b}$$

$$\nabla^2 u_z + \frac{1}{1-2\nu}\frac{\partial \epsilon}{\partial z} = \frac{1}{c_2^2}\frac{\partial^2 u_z}{\partial t^2}, \tag{4.1c}$$

where the Laplacian ∇^2 is defined by (2.19) and the dilatation ϵ is of the form

$$\epsilon = \frac{\partial u_r}{\partial r} + \frac{1}{r}\left(\frac{\partial u_\theta}{\partial \theta} + u_r\right) + \frac{\partial u_z}{\partial z}. \tag{4.2}$$

The displacement components are expressed in terms of the scalar potential φ and the vector potential $\boldsymbol{\psi}$ by the Helmholtz decomposion (2.17a)-(2.17c). The potentials φ and $\boldsymbol{\psi}$ satisfy equations (2.13), (2.18a)-(2.18c), where the component of vector potential ψ_r and ψ_θ are coupled in equations (2.18a) and (2.18b). The stress-strain relation is given by Hooke's law (2.2), where the strain-displacement relations (2.3) are defined as

$$\epsilon_{rr} = \frac{\partial u_r}{\partial r}; \qquad \epsilon_{\theta\theta} = \frac{1}{r}\frac{\partial u_\theta}{\partial \theta} + \frac{u_r}{r}; \qquad \epsilon_{\theta z} = \frac{1}{2}\left(\frac{\partial u_\theta}{\partial z} + \frac{1}{r}\frac{\partial u_z}{\partial \theta}\right) \tag{4.3a}$$

$$\epsilon_{zz} = \frac{\partial u_z}{\partial z}; \qquad \epsilon_{r\theta} = \frac{1}{2}\left(\frac{1}{r}\frac{\partial u_r}{\partial \theta} + \frac{\partial u_\theta}{\partial r} - \frac{u_\theta}{r}\right); \qquad \epsilon_{rz} = \frac{1}{2}\left(\frac{\partial u_z}{\partial r} + \frac{\partial u_r}{\partial z}\right). \tag{4.3b}$$

If the cylindrical surface is traction free the boundary conditions of the problem at $r = a$ will be given as

$$\tau_{rr} = \tau_{r\theta} = \tau_{rz} = 0. \tag{4.4}$$

4.3 Potentials

4.3.1 Displacement Potentials Using Helmholtz Decomposion

We seek solution of the wave equations in the general form

$$\varphi = \Phi(r)\Theta_\Phi(\theta)e^{i(kz-\omega t)}, \qquad \psi_r = \Psi_r(r)\Theta_r(\theta)e^{i(kz-\omega t)}, \tag{4.5a}$$

$$\psi_\theta = \Psi_\theta(r)\Theta_\theta(\theta)e^{i(kz-\omega t)}, \qquad \psi_z = \Psi_z(r)\Theta_z(\theta)e^{i(kz-\omega t)}, \tag{4.5b}$$

where ω is the frequency, and k is the wave number.

Plugging last solutions into (2.13), (2.18a)-(2.18c) yields sine and cosine solutions of argument $n\theta$. Thus, for $\Phi(r)$ and $\Theta_\Phi(\theta)$, we obtain

$$\frac{d^2\Phi}{dr^2} + \frac{1}{r}\frac{d\Phi}{dr} + \left(\beta_1{}^2 - \frac{n^2}{r^2}\right)\Phi = 0, \tag{4.6}$$

$$\frac{d^2\Theta_\Phi}{d\theta^2} + n^2\Theta_\Phi = 0, \tag{4.7}$$

where

$$\beta_1^2 = \omega^2/c_1^2 - k^2. \tag{4.8}$$

The solutions $\Theta_\Phi(\theta)$ are continuous 2π periodic functions of θ, with continuous derivatives, therefore, n is an integer, and

$$\Theta_\Phi = A_1 \sin n\theta + A_2 \cos n\theta.$$

Similar solutions have been obtained for Θ_r, Θ_θ, Θ_z. Considering the torsional, axial-radial and flexural modes separately, we will remove either sine or cosine terms in the results for Θ_Φ, Θ_r, Θ_θ, Θ_z. Thus the following set of resulting expressions for Φ, Ψ_r, Ψ_θ, Ψ_z may be considered

$$\varphi = \Phi(r)\cos n\theta e^{i(kz-\omega t)}, \qquad \psi_z = \Psi_z(r)\sin n\theta e^{i(kz-\omega t)}, \tag{4.9a}$$

$$\psi_\theta = \Psi_\theta(r)\cos n\theta e^{i(kz-\omega t)}, \qquad \psi_r = \Psi_r(r)\sin n\theta e^{i(kz-\omega t)}. \tag{4.9b}$$

Alternatively, the following set of potentials may be examined

$$\varphi = \Phi(r)\sin n\theta e^{i(kz-\omega t)}, \qquad \psi_z = \Psi_z(r)\cos n\theta e^{i(kz-\omega t)}, \tag{4.10a}$$

$$\psi_\theta = \Psi_\theta(r)\sin n\theta e^{i(kz-\omega t)}, \qquad \psi_r = \Psi_r(r)\cos n\theta e^{i(kz-\omega t)}. \tag{4.10b}$$

The solution of equation (4.6) for $\Phi(r)$ yields ordinary Bessel functions as solutions. Because of singular behavior of the solution at the origin only Bessel functions of first kind are used. Thus

$$\Phi = A_3\, J_n(\beta_1 r). \tag{4.11}$$

Similar solution is obtained for Ψ_z by replacing β_1^2 by β_2^2 in the resulting equation for Ψ_z :

$$\Psi_z = B_3\, J_n(\beta_2 r), \tag{4.12}$$

where

$$\beta_2^2 = \omega^2/c_2^2 - k^2. \tag{4.13}$$

Substitution of solutions (4.9b) into equations (4.1a)-(4.1b) results in the following equations for $\Psi_r(r)$ and $\Psi_\theta(r)$

$$\frac{d^2\Psi_r}{dr^2} + \frac{1}{r}\frac{d\Psi_r}{dr} + \frac{1}{r^2}\big[-n^2\Psi_r + 2n\Psi_\theta - \Psi_r\big] - \beta_2^2\Psi_r = 0,$$
$$\frac{d^2\Psi_\theta}{dr^2} + \frac{1}{r}\frac{d\Psi_\theta}{dr} + \frac{1}{r^2}\big[-n^2\Psi_\theta + 2n\Psi_r - \Psi_\theta\big] - \beta_2^2\Psi_\theta = 0.$$

These equations can be solved simultaneously. Thus, subtracting the first equation from the second one, we have

$$\left\{\frac{d^2}{dr^2} + \frac{1}{r}\frac{d}{dr} + \beta_2^2 - \frac{(n+1)^2}{r^2}\right\}\big(\Psi_r - \Psi_\theta\big) = 0, \tag{4.14}$$

which has a solution

$$\Psi_r - \Psi_\theta = 2B_2 J_{n+1}(\beta_2 r). \tag{4.15}$$

Similarly, upon adding the two equations, we obtain an equation for $\Psi_r + \Psi_\theta$, which yields

$$\Psi_r + \Psi_\theta = 2B_1 J_{n-1}(\beta_2 r). \tag{4.16}$$

Thus, we obtain

$$\Psi_r = B_1 J_{n-1}(\beta_2 r) + B_2 J_{n+1}(\beta_2 r), \tag{4.17}$$

$$\Psi_\theta = B_1 J_{n-1}(\beta_2 r) - B_2 J_{n+1}(\beta_2 r). \tag{4.18}$$

Potentials are determined in terms of four arbitrary constants whereas there are three displacement components and three boundary conditions. The additional condition $\nabla \cdot \boldsymbol{\psi} = 0$ can be used to eliminate one of the constants. This condition can be replaced by $\Psi_r = -\Psi_\theta$ which sets $B_1 = 0$. Therefore following the preceding analysis the following set of potentials may considered

$$\varphi = A J_n(\beta_1 r) \cos n\theta \, e^{i(kz-\omega t)}, \tag{4.19}$$

$$\psi_z = B J_n(\beta_2 r) \sin n\theta \, e^{i(kz-\omega t)}, \tag{4.20}$$

$$\psi_\theta = -C J_{n+1}(\beta_2 r) \cos n\theta \, e^{i(kz-\omega t)}, \tag{4.21}$$

$$\psi_r = C J_{n+1}(\beta_2 r) \sin n\theta \, e^{i(kz-\omega t)}, \tag{4.22}$$

or alternatively the following analogous set may be discussed

$$\varphi = A^* J_n(\beta_1 r) \sin n\theta \, e^{i(kz-\omega t)}, \tag{4.23}$$

$$\psi_z = B^* J_n(\beta_2 r) \cos n\theta \, e^{i(kz-\omega t)}, \tag{4.24}$$

$$\psi_\theta = -C^* J_{n+1}(\beta_2 r) \sin n\theta \, e^{i(kz-\omega t)}, \tag{4.25}$$

$$\psi_r = C^* J_{n+1}(\beta_2 r) \cos n\theta \, e^{i(kz-\omega t)}. \tag{4.26}$$

The first set of potentials (4.19)-(4.22) results in the following displacements

$$u_r = \left\{ \Phi' + \frac{n}{r}\Psi_z + i\,k\Psi_r \right\} \cos n\theta \, e^{i(kz-\omega t)}, \tag{4.27}$$

$$u_\theta = \left\{ -\frac{n}{r}\Phi + i\,k\Psi_r - \Psi_z' \right\} \sin n\theta \, e^{i(kz-\omega t)}, \tag{4.28}$$

$$u_z = \left\{ i\,k\Phi - \Psi_r' - \frac{n+1}{r}\Psi_r \right\} \cos n\theta \, e^{i(kz-\omega t)}. \tag{4.29}$$

Having substituted the resulting displacements into Hooke's law, we obtain

$$\sigma_{rr} = \bigg[-\lambda(\beta_1^2 + k^2)\Phi + 2\mu\bigg\{ \Phi'' + \frac{n}{r}\bigg(\Psi_z' - \frac{1}{r}\Psi_z \bigg) + i\,k\Psi_r' \bigg\}\bigg] \cos n\theta\, e^{i(kz-\omega t)}, \tag{4.30}$$

$$\sigma_{r\theta} = \mu\bigg[-\frac{2n}{r}\bigg(\Phi' - \frac{\Phi}{r} \bigg) - \big[2\Psi_z'' + \beta_2^2\Psi_z \big] + i\,k\bigg(\frac{n+1}{r}\Psi_r - \Psi_r' \bigg)\bigg] \sin n\theta\, e^{i(kz-\omega t)}, \tag{4.31}$$

$$\sigma_{rz} = \mu\bigg[2\,i\,k\Phi' - \frac{n}{r}\Psi_r' + \bigg(\frac{1+n-n^2}{r^2} + \beta_2^2 - k^2 \bigg)\Psi_r + \frac{i\,n\,k}{r}\Psi_z \bigg] \cos n\theta\, e^{i(kz-\omega t)}. \tag{4.32}$$

Incorporating (4.11), (4.12), (4.17) and (4.17), the displacements can be modified as

$$u_r = \bigg\{ A\beta_1 J_n'(\beta_1 r) + \frac{n}{r}BJ_n(\beta_2 r) + i\,k\,C\,J_{n+1}(\beta_2 r) \bigg\} \cos n\theta\, e^{i(kz-\omega t)}, \tag{4.33}$$

$$u_\theta = \bigg\{ -\frac{n}{r}AJ_n(\beta_1 r) + i\,k\,C\,J_{n+1}(\beta_2 r) - B\,\beta_2\,J_n'(\beta_2 r) \bigg\} \sin n\theta\, e^{i(kz-\omega t)}, \tag{4.34}$$

$$u_z = \bigg\{ i\,k\,AJ_n(\beta_1 r) - C\,\beta_2\,J_{n+1}'(\beta_2 r) - \frac{n+1}{r}C\,J_{n+1}(\beta_2 r) \bigg\} \cos n\theta\, e^{i(kz-\omega t)}, \tag{4.35}$$

yielding the stresses in the form

$$\begin{aligned} \sigma_{rr} = \bigg[& -\lambda(\beta_1^2 + k^2)AJ_n(\beta_1 r) + 2\mu\bigg\{ -A\bigg[\frac{\beta_1}{r}J_n'(\beta_1 r) + \bigg(\beta_1^2 - \frac{n^2}{r^2} \bigg) J_n(\beta_1 r) \bigg] \\ & + \frac{n}{r}B\bigg(\beta_2\,J_n'(\beta_2 r) - \frac{1}{r}J_n(\beta_2 r) \bigg) + i\,kC\beta_2\,J_{n+1}'(\beta_2 r) \bigg\}\bigg] \cos n\theta\, e^{i(kz-\omega t)}, \end{aligned} \tag{4.36}$$

$$\begin{aligned} \sigma_{r\theta} = \mu\bigg[& -\frac{2n}{r}A\bigg(\beta_1 J_n'(\beta_1 r) - \frac{1}{r}J_n(\beta_1 r) \bigg) - 2B\bigg[\frac{\beta_2}{r}J_n'(\beta_2 r) + \bigg(\beta_2^2 - \frac{n^2}{r^2} \bigg) J_n(\beta_2 r) \bigg] \\ & - \beta_2^2 BJ_n(\beta_2 r) - i\,k\bigg(\frac{n+1}{r}C\,J_{n+1}(\beta_2 r) - C\beta_2\,J_{n+1}'(\beta_2 r) \bigg)\bigg] \sin n\theta\, e^{i(kz-\omega t)}, \end{aligned} \tag{4.37}$$

$$\begin{aligned} \sigma_{rz} = \mu\bigg[& -2\,i\,k\,A\beta_1 J_n'(\beta_1 r) - \frac{n}{r}C\beta_2\,J_{n+1}'(\beta_2 r) + \bigg(\frac{1+n-n^2}{r^2} + \beta_2^2 - k^2 \bigg) C\,J_{n+1}(\beta_2 r) \\ & + \frac{i\,n\,k}{r}BJ_n(\beta_2 r) \bigg] \cos n\theta\, e^{i(kz-\omega t)}. \end{aligned} \tag{4.38}$$

Analogous results can be obtained by keeping on preceding procedure for the second set of potential given by (4.23)-(4.26). Thus the resulting displacements are [30]

$$u_r = U(r)\begin{bmatrix} \sin n\theta \\ \cos n\theta \end{bmatrix} e^{i(kz-\omega t)},\; u_\theta = V(r)\begin{bmatrix} \cos n\theta \\ -\sin n\theta \end{bmatrix} \theta e^{i(kz-\omega t)},\; u_z = W(r)\begin{bmatrix} \sin n\theta \\ \cos n\theta \end{bmatrix} e^{i(kz-\omega t)}, \tag{4.39}$$

where an integer n determines the type of mode, and either upper set $(\sin n\theta, \cos n\theta, \sin n\theta)$

or lower set $(\cos n\theta, -\sin n\theta, \cos n\theta)$ is used; the functions U, V, W are defined as:

$$U(r) = A\,\beta_1 J_n'(\beta_1 r) + \frac{n}{r} B J_n(\beta_2 r) + i\,k\,C\,J_{n+1}(\beta_2 r), \tag{4.40}$$

$$V(r) = -\frac{n}{r} A J_n(\beta_1 r) + i\,k\,C\,J_{n+1}(\beta_2 r) - B\beta_2\,J_n'(\beta_2 r), \tag{4.41}$$

$$W(r) = i\,k\,A J_n(\beta_1 r) - C\beta_2\,J_{n+1}'(\beta_2 r) - \frac{n+1}{r} C\,J_{n+1}(\beta_2 r). \tag{4.42}$$

The potential representation (2.10) was used in [15], [16], [12]. The alternative displacement representations proposed by Buchwald [37] and Morse and Feshbach [38] will be discussed next, and their advantages and disadvantages will be shown.

4.3.2 Alternative Representation Using Buchwald's Potentials

Recall that solutions (4.39)- (4.42) were obtained by decomposing the displacement vector in terms of vector and scalar potentials in the form (2.10). It can be noticed from the form of solutions that that it contains J_{n+1}, whereas it is possible to obtain a solution with the lower order Bessel functions J_n. Below we will show that an alternative decomposition of the displacement vector $\boldsymbol{u}$ through scalar potentials results in much simpler equations and consequently simpler solutions. The alternative representation was proposed by Buchwald [37] and was applied in [47], [48], [45], [33]. As it was mentioned above this representation is much simpler and its application is timesaving.

Let's consider transversely isotropic elastic cylinder of radius a. The equations of motion in the absence of body forces are

$$\sigma_{ij,j} = \rho \ddot{u}_i. \tag{4.43}$$

Hooke's Law for a transversely isotropic elastic material is

$$\begin{bmatrix} \sigma_{rr} \\ \sigma_{\theta\theta} \\ \sigma_{zz} \\ \sigma_{\theta z} \\ \sigma_{rz} \\ \sigma_{r\theta} \end{bmatrix} = \begin{bmatrix} c_{11} & c_{12} & c_{13} & 0 & 0 & 0 \\ c_{12} & c_{11} & c_{13} & 0 & 0 & 0 \\ c_{13} & c_{13} & c_{33} & 0 & 0 & 0 \\ 0 & 0 & 0 & c_{44} & 0 & 0 \\ 0 & 0 & 0 & 0 & c_{44} & 0 \\ 0 & 0 & 0 & 0 & 0 & (c_{11}-c_{12})/2 \end{bmatrix} \begin{bmatrix} \varepsilon_{rr} \\ \varepsilon_{\theta\theta} \\ \varepsilon_{zz} \\ 2\varepsilon_{\theta z} \\ 2\varepsilon_{rz} \\ 2\varepsilon_{r\theta} \end{bmatrix}. \tag{4.44}$$

Substituting the geometrical relations between displacement field and deformation tensor into (4.44) and then into equations of motion (4.43) yields [45]

$$\frac{1}{2}(c_{11}-c_{12})\nabla_1^2 u_r+\frac{1}{2}(c_{11}+c_{12})\left[\frac{\partial^2 u_r}{\partial r^2}+\frac{1}{r}\frac{\partial^2 u_\theta}{\partial r\partial\theta}\right]+c_{44}\frac{\partial^2 u_r}{\partial z^2}+(c_{13}+c_{44})\frac{\partial^2 u_z}{\partial r\partial z}=\rho\frac{\partial^2 u_r}{\partial t^2}, \tag{4.45a}$$

$$\frac{1}{2}(c_{11}-c_{12})\nabla_1^2 u_\theta+\frac{1}{2}(c_{11}+c_{12})\left[\frac{\partial^2 u_\theta}{\partial r^2}+\frac{1}{r}\frac{\partial^2 u_r}{\partial r\partial\theta}\right]+c_{44}\frac{\partial^2 u_\theta}{\partial z^2}+(c_{13}+c_{44})\frac{1}{r}\frac{\partial^2 u_z}{\partial\theta\partial z}=\rho\frac{\partial^2 u_\theta}{\partial t^2}, \tag{4.45b}$$

$$c_{44}\nabla_1^2 u_z+c_{33}\frac{\partial^2 u_z}{\partial z^2}+(c_{13}+c_{44})\left[\frac{\partial^2 u_r}{\partial r\partial z}+\frac{1}{r}\frac{\partial^2 u_\theta}{\partial z\partial\theta}\right]=\rho\frac{\partial^2 u_z}{\partial t^2}, \tag{4.45c}$$

where

$$\nabla_1^2=\nabla^2-\frac{\partial^2}{\partial z^2}=\frac{\partial^2}{\partial r^2}+\frac{1}{r}\frac{\partial}{\partial r}+\frac{1}{r^2}\frac{\partial^2}{\partial\theta^2}. \tag{4.46}$$

Let the displacement vector be decomposed in terms of scalar wave functions φ, χ and ψ [37]

$$\boldsymbol{u}=\boldsymbol{\nabla}\varphi+\boldsymbol{\nabla}\times(\chi\boldsymbol{e_z})+\left(\frac{\partial\psi}{\partial z}-\frac{\partial\varphi}{\partial z}\right)\boldsymbol{e_z} \tag{4.47}$$

or in component form in cylindrical coordinates as

$$u_r=\frac{\partial\varphi}{\partial r}+\frac{1}{r}\frac{\partial\chi}{\partial\theta},\quad u_\theta=\frac{1}{r}\frac{\partial\varphi}{\partial\theta}-\frac{\partial\chi}{\partial r},\quad u_z=\frac{\partial\psi}{\partial z}. \tag{4.48}$$

The wave function representation (4.47) was introduced into the theory of wave propagation by Buchwald [37]. Inserting equation (4.48) into (4.45a)- (4.45c) results in the following system of equations:

$$\left(c_{11}\nabla_1^2+c_{44}\frac{\partial^2}{\partial z^2}-\rho\frac{\partial^2}{\partial t^2}\right)\nabla_1^2\varphi+(c_{13}+c_{44})\nabla_1^2\frac{\partial^2\psi}{\partial z^2}=0, \tag{4.49a}$$

$$\left(c_{44}\nabla_1^2+c_{33}\frac{\partial^2}{\partial z^2}-\rho\frac{\partial^2}{\partial t^2}\right)\frac{\partial^2}{\partial z^2}\psi+(c_{13}+c_{44})\frac{\partial^2}{\partial z^2}\nabla_1^2\varphi=0, \tag{4.49b}$$

$$\left(\frac{1}{2}(c_{11}-c_{12})\nabla_1^2+c_{44}\frac{\partial^2}{\partial z^2}-\rho\frac{\partial^2}{\partial t^2}\right)\nabla_1^2\chi=0. \tag{4.49c}$$

Omitting ∇_1^2 in the first and the third equations and $\frac{\partial^2}{\partial z^2}$ in the second equation, the system

of equation (4.49a)- (4.49c) can be modified as

$$c_{11}\nabla_1^2\varphi + c_{44}\frac{\partial^2\varphi}{\partial z^2} + (c_{13}+c_{44})\frac{\partial^2\psi}{\partial z^2} - \rho\frac{\partial^2\varphi}{\partial t^2} = 0, \tag{4.50a}$$

$$(c_{13}+c_{44})\nabla_1^2\varphi + c_{44}\nabla_1^2\psi + c_{33}\frac{\partial^2\psi}{\partial z^2} - \rho\frac{\partial^2\psi}{\partial t^2} = 0, \tag{4.50b}$$

$$\frac{1}{2}(c_{11}-c_{12})\nabla_1^2\chi + c_{44}\frac{\partial^2\chi}{\partial z^2} - \rho\frac{\partial^2\chi}{\partial t^2} = 0. \tag{4.50c}$$

It can be noticed that the equation for χ is uncoupled, whereas φ and ψ functions are coupled by (4.50a) and (4.50b). The function χ is independent, it generates the separate pure SH-shear waves from the rest of displacements.

For an isotropic elastic material Hooke's Law has the form:

$$\begin{bmatrix} \sigma_{rr} \\ \sigma_{\theta\theta} \\ \sigma_{zz} \\ \sigma_{\theta z} \\ \sigma_{rz} \\ \sigma_{r\theta} \end{bmatrix} = \begin{bmatrix} \lambda+2\mu & \lambda & \lambda & 0 & 0 & 0 \\ \lambda & \lambda+2\mu & \lambda & 0 & 0 & 0 \\ \lambda & \lambda & \lambda+2\mu & 0 & 0 & 0 \\ 0 & 0 & 0 & \mu & 0 & 0 \\ 0 & 0 & 0 & 0 & \mu & 0 \\ 0 & 0 & 0 & 0 & 0 & \mu \end{bmatrix} \begin{bmatrix} \varepsilon_{rr} \\ \varepsilon_{\theta\theta} \\ \varepsilon_{zz} \\ 2\varepsilon_{\theta z} \\ 2\varepsilon_{rz} \\ 2\varepsilon_{r\theta} \end{bmatrix}. \tag{4.51}$$

Incorporating (4.44) and (4.51) for an isotropic material the system of equations (4.50a)-(4.50c) will reduce to:

$$(\lambda+2\mu)\nabla_1^2\varphi + \mu\frac{\partial^2\varphi}{\partial z^2} + (\lambda+\mu)\frac{\partial^2\psi}{\partial z^2} - \rho\frac{\partial^2\varphi}{\partial t^2} = 0, \tag{4.52a}$$

$$(\lambda+\mu)\nabla_1^2\varphi + \mu\nabla_1^2\psi + (\lambda+2\mu)\frac{\partial^2\psi}{\partial z^2} - \rho\frac{\partial^2\psi}{\partial t^2} = 0, \tag{4.52b}$$

$$\mu\nabla_1^2\chi + \mu\frac{\partial^2\chi}{\partial z^2} - \rho\frac{\partial^2\chi}{\partial t^2} = 0, \tag{4.52c}$$

or dividing by ρ, this system of equations can be modified as

$$c_1^2\nabla_1^2\varphi + c_2^2\frac{\partial^2\varphi}{\partial z^2} + (c_1^2-c_2^2)\frac{\partial^2\psi}{\partial z^2} - \frac{\partial^2\varphi}{\partial t^2} = 0, \tag{4.53a}$$

$$(c_1^2-c_2^2)\nabla_1^2\varphi + c_2^2\nabla_1^2\psi + c_1^2\frac{\partial^2\psi}{\partial z^2} - \frac{\partial^2\psi}{\partial t^2} = 0, \tag{4.53b}$$

$$c_2^2\nabla^2\chi - \frac{\partial^2\chi}{\partial t^2} = 0. \tag{4.53c}$$

We assume solutions of the form:

$$\begin{pmatrix}\varphi\\ \psi\end{pmatrix} = \begin{pmatrix}A\\ B\end{pmatrix} J_n(\beta r)\cos n\theta\, e^{i(kz-\omega t)}, \tag{4.54}$$

$$\chi = C J_n(\gamma r)\sin n\theta\, e^{i(kz-\omega t)}. \tag{4.55}$$

Inserting these solutions into equations (4.53a)-(4.53c), we obtain

$$\left[c_1^2\beta^2 - \omega^2 + c_2^2k^2\right] A + \left[(c_1^2 - c_2^2)k^2\right] B = 0, \tag{4.56a}$$

$$\left[(c_1^2 - c_2^2)\beta^2\right] A + \left[c_2^2\beta^2 - \omega^2 + c_1^2k^2\right] B = 0, \tag{4.56b}$$

$$\left[c_2^2\left(\gamma^2 + k^2\right) - \omega^2\right] C = 0. \tag{4.56c}$$

Thus for potential function χ equation (4.56c) yields

$$\gamma^2 = \frac{\omega^2}{c_2^2} - k^2. \tag{4.57}$$

Equating the determinant of coefficients of A and B to zero in equations (4.56a)-(4.56b) for potentials φ and ψ, we obtain the following characteristic equation:

$$c_1^2\, c_2^2\, \beta^4 + \beta^2\, E + F = 0, \tag{4.58}$$

where

$$F = \omega^4 - \omega^2(c_1^2 + c_2^2)\, k^2 + c_1^2\, c_2^2 k^4, \qquad E = 2c_1^2\, c_2^2\, k^2 - \omega^2(c_1^2 + c_2^2). \tag{4.59}$$

The roots of the characteristic equation (4.58) are

$$\beta_{1,\,2}^2 = \frac{-E \mp \sqrt{E^2 - 4c_1^2\, c_2^2\, F}}{2\, c_1^2\, c_2^2}. \tag{4.60}$$

Substitution of equation (4.59) into the above equation yields

$$\beta_1 = \sqrt{\frac{\omega^2}{c_1^2} - k^2}, \qquad \beta_2 = \sqrt{\frac{\omega^2}{c_2^2} - k^2}. \tag{4.61}$$

We can notice that $\gamma = \beta_2$, and the general solutions for Buchwald's potentials are of the form [47]:

$$\varphi = \left[A\, J_n(\beta_1 r) + q_2 B\, J_n(\beta_2 r)\right]\cos n\theta\, e^{i(kz-\omega t)}, \tag{4.62}$$

$$\psi = \left[q_1\, A\, J_n(\beta_1 r) + B\, J_n(\beta_2 r)\right]\cos n\theta\, e^{i(kz-\omega t)}, \tag{4.63}$$

$$\chi = C\, J_n(\beta_2 r)\sin n\theta\, e^{i(kz-\omega t)}, \tag{4.64}$$

where q_1 and q_2 are the amplitude ratios defined in [47]. They follow from (4.56a)-(4.56b) for an isotropic material as $q_1 = 1$ and $q_2 = -\frac{k^2}{\beta_2^2}$, and hence solutions become

$$\varphi = \left[A\, J_n(\beta_1 r) - \frac{k^2}{\beta_2^2} B\, J_n(\beta_2 r)\right] \cos n\theta\, e^{i(kz-\omega t)}, \tag{4.65}$$

$$\psi = \left[A\, J_n(\beta_1 r) + B\, J_n(\beta_2 r)\right] \cos n\theta\, e^{i(kz-\omega t)}, \tag{4.66}$$

$$\chi = C\, J_n(\beta_2 r) \sin n\theta\, e^{i(kz-\omega t)}. \tag{4.67}$$

As it was anticipated at the beginning, the results obtained contain only $J_n(\beta_1 r)$ and $J_n(\beta_2 r)$ terms, which are Bessel functions of the first kind of order n. The results obtained earlier using displacement decomposition (2.10) involved higher order Bessel functions, namely $J_n(\alpha r)$, $J_n(\beta r)$ and $J_{n+1}(\beta r)$ - Bessel functions of order n and $(n+1)$ respectively, which leads to extraneous terms and cumbersome expressions. The evaluation of the result shows that Buchwald's representation [37] yields a simplier solution, involving lower order Bessel functions, J_n instead of J_{n+1}. We observe that Buchwald's representation produces simplified expressions.

It should be noted that introducing the roots (4.57) and (4.61) into (4.54)-(4.55) yields

$$\varphi = A\, J_n(\beta_1 r) \cos n\theta\, e^{i(kz-\omega t)}, \tag{4.68}$$

$$\psi = B\, J_n(\beta_2 r) \cos n\theta\, e^{i(kz-\omega t)}, \tag{4.69}$$

$$\chi = C\, J_n(\beta_2 r) \sin n\theta\, e^{i(kz-\omega t)}. \tag{4.70}$$

However, this set of solutions for $n = 0$ does not lead to the Pochhammer-Chree frequency equations (4.109) given in the subsequent section because the general solutions for Buchwald's potentials φ and ψ depend on both $J_n(\beta_1 r)$ and $J_n(\beta_2 r)$ functions as shown in equations (4.62)-(4.63). The set of potentials (4.68)- (4.70) instead of the frequency equation yields the following relation for $n = 0$:

$$(\beta_2^2 + k^2)\beta_1\beta_2\, J_0(\beta_1 a)J_1(\beta_1 a) - k^2(\beta_2^2 - 2\beta_1^2 - k^2)J_1(\beta_1 a)J_0(\beta_2 a) \\ -2(\beta_1^2 + k^2)\beta_2/a J_1(\beta_1 a)J_1(\beta_2 a) = 0. \tag{4.71}$$

As it will be shown in the next section, the general solutions (4.65)- (4.67) lead to the Pochhammer-Chree frequency equations.

The set of potentials (4.65)- (4.67) yields the following displacement field

$$u_r = \left\{ A\beta_1 J_n'(\beta_1 r) - \frac{k^2}{\beta_2^2} B\beta_2\, J_n'(\beta_2 r) + \frac{n}{r} C J_n(\beta_2 r) \right\} \cos n\theta\, e^{i(kz-\omega t)}, \tag{4.72}$$

$$u_\theta = \left\{ -\frac{n}{r}\left[A J_n(\beta_1 r) - \frac{k^2}{\beta_2^2} B\, J_n(\beta_2 r)\right] - \beta_2 C\, J_n'(\beta_2 r) \right\} \sin n\theta\, e^{i(kz-\omega t)}, \tag{4.73}$$

$$u_z = i\,k\left[A J_n(\beta_1 r) + B\, J_n(\beta_2 r)\right] \cos n\theta\, e^{i(kz-\omega t)}. \tag{4.74}$$

The substitution of the last expressions for displacements into geometric relations (2.3) results in the following expressions for deformations:

$$\epsilon_{rr} = \left\{ A\beta_1^2 J_n''(\beta_1 r) - k^2 B J_n''(\beta_2 r) + \frac{n}{r} C\beta_2 J_n'(\beta_2 r) - \frac{n}{r_2} C J_n(\beta_2 r) \right\} \cos n\theta\, e^{i(kz-\omega t)}, \tag{4.75}$$

$$\begin{aligned} \epsilon_{\theta\theta} = \Bigg\{ & \frac{1}{r}\left[A\beta_1 J_n'(\beta_1 r) + \frac{n}{r} C J_n(\beta_2 r)\right] - \frac{n}{r}\left[\frac{n}{r} A J_n(\beta_1 r) + C\beta_2 J_n'(\beta_2 r)\right] \\ & + \frac{k^2}{\beta_2^2} B\left[\frac{n^2}{r^2} J_n(\beta_2 r) - \frac{1}{r}\beta_2\, J_n'(\beta_2 r)\right] \Bigg\} \cos n\theta\, e^{i(kz-\omega t)}, \end{aligned} \tag{4.76}$$

$$\epsilon_{zz} = -k^2\left[A J_n(\beta_1 r) + B\, J_n(\beta_2 r)\right] \cos n\theta\, e^{i(kz-\omega t)}, \tag{4.77}$$

$$\begin{aligned} \epsilon_{r\theta} = \frac{1}{2}\Bigg\{ & \frac{2n}{r} A\left[\frac{1}{r} J_n(\beta_1 r) - \beta_1 J_n'(\beta_1 r)\right] + \frac{k^2}{\beta_2^2} B\left[-\frac{2n}{r^2} J_n(\beta_2 r) + \frac{2n}{r}\beta_2\, J_n'(\beta_2 r)\right] \\ & - C\left[\beta_2^2 J_n''(\beta_2 r) - \frac{1}{r}\beta_2 J_n'(\beta_2 r) + \frac{n^2}{r^2} C J_n(\beta_2 r)\right] \Bigg\} \sin n\theta\, e^{i(kz-\omega t)}, \end{aligned} \tag{4.78}$$

$$\epsilon_{rz} = \frac{i\,k}{2}\left\{ A2\beta_1 J_n'(\beta_1 r) + \left(1 - \frac{k^2}{\beta_2^2}\right) B\beta_2 J_n'(\beta_2 r) + \frac{n}{r} C J_n(\beta_2 r) \right\} \cos n\theta\, e^{i(kz-\omega t)}, \tag{4.79}$$

$$\epsilon_{\theta z} = -\frac{i\,k}{2}\left\{ \frac{2n}{r} A J_n(\beta_1 r) + \left(\frac{n}{r} - \frac{k^2}{\beta_2^2}\right) B J_n(\beta_2 r) + C\beta_2 J_n'(\beta_2 r) \right\} \sin n\theta\, e^{i(kz-\omega t)}. \tag{4.80}$$

The stresses are obtained by substituting the last expressions into Hooke's law (2.2):

$$\begin{aligned} \sigma_{rr} = \Bigg\{ & -\lambda A(\beta_1^2 + k^2) J_n(\beta_1 r) + 2\mu\Bigg[A\beta_1^2 J_n''(\beta_1 r) - k^2 B J_n''(\beta_2 r) \\ & + \frac{n}{r} C\beta_2 J_n'(\beta_2 r) - \frac{n}{r^2} C J_n(\beta_2 r)\Bigg] \Bigg\} \cos n\theta\, e^{i(kz-\omega t)}, \end{aligned} \tag{4.81}$$

$$\begin{aligned} \sigma_{r\theta} = \mu\Bigg\{ & A\left[\frac{2n}{r^2} J_n(\beta_1 r) - \frac{2n}{r}\beta_1 J_n'(\beta_1 r)\right] + \frac{k^2}{\beta_2^2} B\left[-\frac{2n}{r^2} J_n(\beta_2 r) + \frac{2n}{r}\beta_2\, J_n'(\beta_2 r)\right] \\ & - C\left[\beta_2^2 J_n''(\beta_2 r) - \frac{1}{r}\beta_2 J_n'(\beta_2 r) + \frac{n^2}{r^2} J_n(\beta_2 r)\right] \Bigg\} \sin n\theta\, e^{i(kz-\omega t)}, \end{aligned} \tag{4.82}$$

$$\sigma_{rz} = \mu i\, k\left\{ A2\beta_1 J_n'(\beta_1 r) + \left(1 - \frac{k^2}{\beta_2^2}\right) B\beta_2 J_n'(\beta_2 r) + \frac{n}{r} C J_n(\beta_2 r) \right\} \cos n\theta\, e^{i(kz-\omega t)}, \tag{4.83}$$

which can be modified as following:

$$\sigma_{rr} = \Bigg\{ -\lambda A(\beta_1^2 + k^2) J_n(\beta_1 r) + 2\mu \Bigg[-A\left(\frac{\beta_1}{r} J_n'(\beta_1 r) + \left(\beta_1^2 - \frac{n^2}{r^2}\right) J_n(\beta_1 r)\right) - k^2 B\left(\frac{\beta_2}{r} J_n'(\beta_2 r) + \left(\beta_2^2 - \frac{n^2}{r^2}\right) J_n(\beta_2 r)\right) + + \frac{n}{r} C\left(\beta_2 J_n'(\beta_2 r) - \frac{1}{r} J_n(\beta_2 r)\right)\Bigg]\Bigg\} \cos n\theta \, e^{i(kz-\omega t)}, \tag{4.84}$$

$$\sigma_{r\theta} = \mu\Bigg\{ A\left[\frac{2n}{r^2} J_n(\beta_1 r) - \frac{2n}{r}\beta_1 J_n'(\beta_1 r)\right] + \frac{k^2}{\beta_2^2} B\left[-\frac{2n}{r^2} J_n(\beta_2 r) + \frac{2n}{r}\beta_2 J_n'(\beta_2 r)\right] + C\left[\frac{2}{r}\beta_2 J_n'(\beta_2 r) + \left(\beta_2^2 - \frac{2n^2}{r^2}\right) J_n(\beta_2 r)\right]\Bigg\} \cos n\theta \, e^{i(kz-\omega t)}, \tag{4.85}$$

$$\sigma_{rz} = \mu i\, k\Bigg\{ A2\beta_1 J_n'(\beta_1 r) + \left(1 - \frac{k^2}{\beta_2^2}\right) B\beta_2 J_n'(\beta_2 r) + \frac{n}{r} C J_n(\beta_2 r)\Bigg\} \cos n\theta \, e^{i(kz-\omega t)}. \tag{4.86}$$

The results obtained for the components of the stress tensor again display advantage of using Buchwald's potentials. Analyzing equations (4.36)-(4.38) and (4.84)- (4.86), it can be noticed that displacement representation (2.10) produces expressions containing $n+1$ - order Bessel functions such as $J_{n+1}(\beta_1 r)$ and $J_{n+1}(\beta_2 r)$ and it's derivatives $J_{n+1}'(\beta_1 r)$ and $J_{n+1}'(\beta_2 r)$, whereas Buchwald's representation yields much simpler expressions containing only n-order Bessel functions $J_n(\beta_1 r)$ and $J_n(\beta_2 r)$ and it's derivatives $J_n'(\beta_1 r)$ and $J_n'(\beta_2 r)$. It shows that Buchwald's potentials produce simpler expressions, where computation is less laborious.

4.3.3 Sinclair's Method

At the end of our discussion on representation of displacement vector through scalar potentials we should add that there are some other forms of displacement decomposition available, such as one presented by Morse and Feshbach [38]

$$\boldsymbol{u} = \boldsymbol{\nabla}\varphi + \boldsymbol{\nabla} \times (\chi \boldsymbol{e_z}) + a\boldsymbol{\nabla} \times \boldsymbol{\nabla} \times (\psi \boldsymbol{e_z}), \tag{4.87}$$

where a is the radius of the cylinder which is constant with dimensions of length. In component form in cylindrical coordinates it has form

$$u_r = \frac{\partial \varphi}{\partial r} + \frac{1}{r}\frac{\partial \chi}{\partial \theta} + a\frac{\partial^2 \psi}{\partial r \partial z}, \tag{4.88a}$$

$$u_\theta = \frac{1}{r}\frac{\partial \varphi}{\partial \theta} - \frac{\partial \chi}{\partial r} + a\frac{\partial^2 \psi}{\partial \theta \partial z}, \tag{4.88b}$$

$$u_z = \frac{\partial \varphi}{\partial z} - a\left(\frac{\partial^2}{\partial r^2} + \frac{1}{r}\frac{\partial}{\partial r} + \frac{1}{r^2}\frac{\partial^2}{\partial \theta^2}\right)\psi. \tag{4.88c}$$

This approach was applied by Honarvar and Sinclair [46] in the analysis of a wave scattering problem for a transversely isotropic material. The displacement decomposition (4.87) results in the 5th order PDEs, lengthy and cumbersome coupled equations for φ and ψ, whereas Buchwald's representation yields much simplier equations, in the form of compact second order PDEs [48]. Ahmad and Rahman [47], [48] showed that the above mentioned two representations lead to identical characteristic equations and the same final result.

It can be concluded that Buchwald's representation (4.47) is of great importance among considered above three displacement representations (2.10), (4.47) and (4.87). Buchwald's potential yields simplier expressions, and it is less laborious. Therefore it is proposed to use Buchwald's representation in the study of wave propagation in isotropic and transversely isotropic elastic materials [45].

4.4 Frequency Equation for Waves in a Rod

The frequency equation is obtained from the boundary conditions. If the surface is free of traction, the boundary conditions at $r = a$ are given by equation (4.4).

4.4.1 Frequency Equation Derived Using Helmholtz representation

Having substituted the resulting displacements (4.39) into Hooke's law and evaluated the result at $r = a$ the frequency equation was derived as the following vanishing determinant [15]

$$|a_{ij}| = 0, \quad (i, j = 1, 2, 3), \tag{4.89}$$

where

$$a_{11} = \left\{ \frac{\lambda(\beta_1^2 + k^2)(\beta_1 a)^2}{2\mu\beta_1^2} + (\beta_1 a)^2 - n^2 \right\} J_n(\beta_1 a) + \beta_1 a J_n'(\beta_1 a),$$

$$a_{12} = \left\{ n^2 - (\beta_2 a)^2 \right\} J_n(\beta_2 a) - \beta_2 a J_n'(\beta_2 a),$$

$$a_{13} = 2n\left\{ \beta_2 a J_n'(\beta_2 a) - J_n(\beta_2 a) \right\},$$

$$a_{21} = n\left\{ \beta_1 a J_n'(\beta_1 a) - J_n(\beta_1 a) \right\},$$

$$a_{22} = n\left\{ \beta_2 a J_n'(\beta_2 a) - J_n(\beta_2 a) \right\},$$

$$a_{23} = -\left\{ 2n^2 - (\beta_2 a)^2 \right\} J_n(\beta_2 a) + 2\beta_2 a J_n'(\beta_2 a),$$

$$a_{31} = -\beta_1 a J_n'(\beta_1 a),$$

$$a_{32} = -\frac{(\beta_2^2 - k^2)}{2k^2} \beta_2 a J_n'(\beta_2 a),$$

$$a_{23} = n J_n(\beta_2 a).$$

Equation (4.89) is a general characterestic equation for the various types of waves in rods. The frequency equations for torsional, longitudinal, and flexural modes will be developed. The general frequency equation (4.89) yields torsional and longitudinal frequency equations for $n = 0$ and flexural frequency equation for $n = 1$. When investigating the propagation of torsional and longitudial waves one or two displacement components vanish whereas all displacement components remain for flexural modes.

n=0 case:

The general frequency equation (4.89) for the case $n = 0$ yields axi-symmetric modes since there is no dependence on θ, i.e., $\sin n\theta \equiv 0, \quad \cos n\theta \equiv 1$. When $n = 0$ determinant (4.89) has the form:

$$\begin{vmatrix} a_{11} & a_{12} & 0 \\ 0 & 0 & a_{23} \\ a_{31} & a_{32} & 0 \end{vmatrix} = 0, \tag{4.90}$$

which can be split into two factors [15]

$$\begin{vmatrix} a_{11} & a_{12} \\ a_{31} & a_{32} \end{vmatrix} a_{23} = 0, \tag{4.91}$$

where

$$a_{11} = \left\{ \frac{\lambda(\beta_1^2 + k^2)(\beta_1 a)^2}{2\mu\beta_1^2} + (\beta_1 a)^2 \right\} J_0(\beta_1 a) + \beta_1 a J_0'(\beta_1 a),$$

$$a_{12} = -(\beta_2 a)^2 J_0(\beta_2 a) - \beta_2 a J_0'(\beta_2 a),$$

$$a_{31} = -\beta_1 a J_0'(\beta_1 a), \qquad a_{32} = -\frac{\beta_2^2 - k^2}{2k^2}\beta_2 a J_0'(\beta_2 a), \qquad a_{23} = -a_{12},$$

and we note that $J_o'(x) = -J_1(x)$. The axi-symmetric modes can be classified as torsional and axial-radial. For torsional modes the θ component of displacement is the only nonvanishing one whereas for axial-radial modes the component θ vanishes.

Torsional Modes. The axially symmetric modes described by the upper set of functions in (4.39) are the torsional modes. In this case $u_r = u_z = 0$ and $u_\theta \neq 0$. The equation (4.91) factors into two equations. The one corresponding to torsional waves is

$$a_{23} = 0 \quad \Rightarrow \quad \beta_2 a J_0(\beta_2 a) = 2J_1(\beta_2 a) \tag{4.92}$$

Equation (4.92) is the frequency equation for torsional waves, which produces the following dispersion relation for torsional modes

$$(\beta_{2_\nu} a)^2 = (\omega a/c_2)^2 - (\xi a)^2, \tag{4.93}$$

where $\beta_{2_\nu} a$ are the roots of the equation (4.92), the first three of them are [15]

$$\beta_{2_1} a = 5.136, \quad \beta_{2_2} a = 8.417, \quad \beta_{2_3} a = 11.62. \tag{4.94}$$

Let us now consider $\beta_2 = 0$ which is also a solution of the frequency equation (4.92). For $\beta_2 = 0$ the governing equations for $\Psi_z(r)$ yields a solution $\Psi_z = A + B\,ln\,r$, which does not give an acceptable displacement since at $r = 0$ Ψ_z, tends to infinity. But if we take $u_r = u_z = 0$, $u_\theta = u_\theta(r, z)$ and seek the solution of the form $u_\theta = U(r)exp[i(kz - \omega t)]$, then there will be the only non-trivial equation:

$$\frac{d^2U}{dr^2} + \frac{1}{r}\frac{dU}{dr} + \left\{ \beta_2^2 - \frac{1}{r} \right\} U = 0, \tag{4.95}$$

which yields the following solution

$$U = \frac{A}{r} + Br. \tag{4.96}$$

Because of singularity at $r = 0$, in (4.96) $A = 0$ which results in the following displacement field:

$$u_\theta = Br\, exp[i(kz - \omega t)] \tag{4.97}$$

where $k = \omega/c_2$. The mode $\beta_2 = 0$ is independent of frequency and propagates nondispersively with speed $c_2 = \sqrt{\mu/\rho}$.

Axial-Radial Modes of Rod. The axially symmetric modes described by the lower set of trigonometric functions in (4.39) are referred to as axial-radial modes. In this case for $n = 0$, $u_\theta \equiv 0$, $u_r \neq 0$ and $u_z \neq 0$ and equations (2.17a) - (2.17c) will reduce to the form:

$$u_r = \frac{\partial \varphi}{\partial r} - \frac{\partial \psi_\theta}{\partial z}, \quad u_z = \frac{\partial \varphi}{\partial z} + \frac{1}{r}\frac{\partial(\psi_\theta r)}{\partial r}. \tag{4.98}$$

Then solutions for φ and ψ_θ given by (2.17a) and (2.17c) will have the form:

$$\varphi = AJ_n(\beta_1 r)\, e^{i(kz-\omega t)}, \quad \psi_\theta = -CJ_{n+1}(\beta_2 r)\, e^{i(kz-\omega t)}. \tag{4.99}$$

Insertion of solutions (4.99) into the boundary conditions (4.4) leads to a frequency equation which is given by equation (4.91). Expanding cofactor matrix in (4.91), we obtain

$$\begin{aligned}\Delta_1 &= \begin{vmatrix} a_{11} & a_{12} \\ a_{31} & a_{32} \end{vmatrix} \\ &= \begin{vmatrix} \left[\frac{\lambda}{2\mu}((\beta_1)^2 + (k)^2) + (\beta_1)^2\right] a^2 J_0(\beta_1 a) - \beta_1 a J_1(\beta_1 a) & -(\beta_2 a)^2 J_0(\beta_2 a) + \beta_2 a J_1(\beta_2 a) \\ \beta_1 a J_1(\beta_1 a) & \frac{(\beta_2)^2 - (k)^2}{2(k)^2}\beta_2 a J_1(\beta_2 a) \end{vmatrix} = 0.\end{aligned} \tag{4.100}$$

Substitution of the solutions (4.99) into (4.98) yields a displacement field for axial-radial modes[15]:

$$u_r = C\left\{ -\frac{A}{C}\beta_1 J_1(\beta_1 r) + ikJ_1(\beta_2 r)\right\} e^{i(kz-\omega t)}, \tag{4.101}$$

$$u_z = C\left\{ \frac{A}{C} ikJ_0(\beta_1 r) - \beta_2 J_0(\beta_2 r)\right\} e^{i(kz-\omega t)}, \tag{4.102}$$

where

$$\frac{A}{C} = -\left(\frac{\beta_2}{\beta_1}\right)^2 \left(\frac{\beta_2^2 - k^2}{2k^2}\right) \cdot \frac{J_1(\beta_2 a)}{J_1(\beta_1 a)}. \tag{4.103}$$

Equation (4.103) is obtained from the boundary conditions.

Let us divide the second column of the cofactor Δ_1 by $\beta_2 a$ and then add two resulting rows, thus we obtain

$$\begin{aligned}\Delta_1' &= \begin{vmatrix} a_{11}' & a_{12}' \\ a_{31}' & a_{32}' \end{vmatrix} \\ &= \begin{vmatrix} \left[\frac{\lambda}{2\mu}((\beta_1)^2+(k)^2)+(\beta_1)^2\right]a^2 J_0(\beta_1 a) & -\beta_2 a J_0(\beta_2 a)+\frac{(\beta_2)^2+(k)^2}{2(k)^2}J_1(\beta_2 a) \\ \beta_1 a J_1(\beta_1 a) & \frac{\beta_2^2-k^2}{2k^2}J_1(\beta_2 a) \end{vmatrix} = 0.\end{aligned} \tag{4.104}$$

From (4.8) and (4.13) we have

$$\frac{\beta_1^2+k^2}{\beta_2^2+k^2} = \frac{\omega^2}{c_1^2}\frac{c_2^2}{\omega^2} = \frac{\mu}{\lambda+2\mu}, \tag{4.105}$$

from which we find that

$$\frac{\lambda}{\mu} = -2 + \frac{\beta_2^2+k^2}{\beta_1^2+k^2}. \tag{4.106}$$

Incorporating (4.106) the a_{11}' element of cofactor can be modified as

$$a_{11}' = \left[\frac{\lambda}{2\mu}((\beta_1 a)^2+(ka)^2)+(\beta_1 a)^2\right]J_0(\beta_1 a) = \frac{(\beta_2 a)^2-(ka)^2}{2}J_0(\beta_1 a). \tag{4.107}$$

Substituting (4.107) into (4.104) and expanding the resulting determinant yields

$$\begin{aligned}\frac{(\beta_2 a)^2-(ka)^2)}{2}\frac{(\beta_2 a)^2-(ka)^2)}{2(ka)^2}J_0(\beta_1 a)J_1(\beta_2 a)+\beta_1\beta_2 a^2 J_1(\beta_1 a)J_0(\beta_2 a) \\ -(\beta_1 a)\frac{(\beta_2 a)^2+(ka)^2}{2(ka)^2}J_1(\beta_1 a)J_1(\beta_2 a) = 0,\end{aligned} \tag{4.108}$$

which further can be modified multiplying by $(k/a)^2$, thus

$$\boxed{\frac{2\beta_1}{a}(\beta_2^2+k^2)J_1(\beta_1 a)J_1(\beta_2 a)-(\beta_2^2-k^2)^2 J_0(\beta_1 a)J_1(\beta_2 a)-4k^2\beta_1\beta_2 J_1(\beta_1 a)J_0(\beta_2 a)=0.} \tag{4.109}$$

Equation (4.109) is the dispersion relation for nontorsional axisymmetric waves and referred to as *the Pochhammer-Chree frequency equation.*

n=1 case:

The family of modes with $n = 1$ are known as flexural and they correspond to the lowest order family of flexural modes. For $n = 1$ (4.89) will reduce to the following:

$$|a_{ij}| = 0, \tag{4.110}$$

where

$$\begin{aligned}
a_{11} &= \left\{ \frac{\lambda(\beta_1^2 + k^2)(\beta_1 a)^2}{2\mu\beta_1^2} + (\beta_1 a)^2 - 1 \right\} J_1(\beta_1 a) + \beta_1 a J_1'(\beta_1 a), \\
a_{12} &= \big\{1 - (\beta_2 a)^2\big\} J_1 \beta_2 a) - \beta_2 a J_1'(\beta_2 a), \\
a_{13} &= 2\big\{\beta_2 a J_1'\,(\beta_2 a) - J_1(\beta_2 a)\big\}, \\
a_{21} &= \big\{\beta_1 a J_1'\,(\beta_1 a) - J_1(\beta_1 a)\big\}, \\
a_{22} &= \big\{\beta_2 a J_1'\,(\beta_2 a) - J_1(\beta_2 a)\big\}, \\
a_{23} &= -\big\{2 - (\beta_2 a)^2\big\} J_1(\beta_2 a) + 2\beta_2 a J_1'\,(\beta_2 a), \\
a_{31} &= -\beta_1 a J_1'\,(\beta_1 a), \\
a_{32} &= -\frac{(\beta_2^2 - k^2)}{2k^2} \beta_2 a J_1'\,(\beta_2 a), \\
a_{33} &= J_1(\beta_2 a).
\end{aligned}$$

Expansion of the determinant in (4.110) results in the following frequency equation [9]

$$\boxed{J_1(\overline{\alpha}) J_1^2(\overline{\beta}) \big(f_1\, F_{\beta_2}^2 + f_2\, F_{\beta_1}\, F_{\beta_2} + f_3\, F_{\beta_2} + f_4\, F_{\beta_1} + f_5\big) = 0,} \tag{4.111}$$

where

$$\begin{aligned}
&f_1 = 2\big(\overline{\beta}^{\,2} - \overline{k}^{\,2}\big)^{\,2}, \quad f_2 = 2\overline{\beta}^{\,2}\big(5\overline{k}^{\,2} + \overline{\beta}^{\,2}\big), \\
&f_3 = \overline{\beta}^{\,6} - 10\overline{\beta}^{\,4} - 2\overline{\beta}^{\,4}\overline{k}^{\,2} + 2\overline{\beta}^{\,2}\overline{k}^{\,2} + \overline{\beta}^{\,2}\overline{k}^{\,4} - 4\overline{k}^{\,4}, \\
&f_4 = 2\overline{\beta}^{\,2}(2\overline{\beta}^{\,2}\overline{k}^{\,2} - \overline{\beta}^{\,2} - 9\overline{k}^{\,2}), \quad f_5 = \overline{\beta}^{\,2}\big(-\overline{\beta}^{\,4} + 8\overline{\beta}^{\,2} - 2\overline{\beta}^{\,2}\overline{k}^{\,2} + 8\overline{k}^{\,2} - \overline{k}^{\,4}\big), \\
&\overline{\alpha} = \beta_1 a, \quad \overline{\beta} = \beta_2 a, \quad \overline{k} = k\,a, \quad \Omega = \omega a/c_2, \quad F_x = x\frac{J_0(x)}{J_1(x)}.
\end{aligned}$$

The equation (4.111) is know as *the Pochhammer frequency equation for flexural modes in a rod*. It can be noticed that the frequency equation for flexural modes is much more complicated than the ones for axi-symmetric modes.

4.4.2 Frequency Equation Derived Using Buchwald's Potentials

Let us now derive dispersion relations using the Buchwald approach. Evaluating stresses (4.84) -(4.86) at $r = a$ and substituting into the boundary conditions (4.4), we obtain the following determinant of coefficients which vanishes:

$$|b_{ij}| = 0, \quad (i, j = 1, 2, 3) \tag{4.112}$$

where

$$\begin{aligned}
b_{11} &= \frac{\lambda}{2\mu}\big[(\beta_1 a)^2 J_n''(\beta_1 a) + (\beta_1 a) J_n'(\beta_1 a) - (n^2 + (ka)^2) J_n(\beta_1 a)\big] + (\beta_1 a)^2 J_n''(\beta_1 a) \\
&= \bigg[- \frac{\lambda}{2\mu}\big((\beta_1\, a)^2 + (ka)^2\big) - ((\beta_1\, a)^2 - n^2)\bigg] J_n(\beta_1 a) - (\beta_1 a) J_n'(\beta_1 a); \\
b_{12} &= \frac{(k\, a)^2}{(\beta_2 a)^2}\bigg[(\beta_2 a) J_n'(\beta_2 a) + ((\beta_2\, a)^2 - n^2) J_n(\beta_2 a)\bigg]; \\
b_{13} &= - n\big[J_n(\beta_2 a) - (\beta_2 a) J_n'(\beta_2 a)\big]; \\
b_{21} &= 2n\big[J_n(\beta_1 a) - (\beta_1 a) J_n'(\beta_1 a)\big]; \\
b_{22} &= -\frac{2n(k\, a)^2}{(\beta_2 a)^2}\bigg[J_n(\beta_2 a) - (\beta_2 a) J_n'(\beta_2 a)\bigg]; \\
b_{23} &= -(\beta_2 a)^2 J_n''(\beta_2 a) + (\beta_2 a) J_n'(\beta_2 a) - n^2 J_n(\beta_2 a) \\
&= 2\,(\beta_2 a) J_n'(\beta_2 a) + [(\beta_2 a)^2 - 2n^2] J_n(\beta_2 a); \\
b_{31} &= 2(\beta_1 a) J_n'(\beta_1 a); \quad b_{32} = \bigg[1 - \frac{(k\, a)^2}{(\beta_2 a)^2}\bigg](\beta_2\, a) J_n'(\beta_2 a); \quad b_{33} = n J_n(\beta_2 a).
\end{aligned} \tag{4.113}$$

Equations (4.112)- (4.113) agree with ones obtained by Ahmad [47] for transversal isotropic material, with $q_1 = 1, \quad q_2 = -\frac{k^2}{\beta_2^2}$. Let us analyze these relations in more detail.

n=0 case:

As it was mentioned above when $n = 0$ equation (4.113) yields the frequency equation for axisymmetric waves. Thus, when $n = 0$ the determinant in (4.113) reduces to the form:

$$\begin{vmatrix} b_{11} & b_{12} & 0 \\ 0 & 0 & b_{23} \\ b_{31} & b_{32} & 0 \end{vmatrix} = 0, \tag{4.114}$$

which factors into

$$\begin{vmatrix} b_{11} & b_{12} \\ b_{31} & b_{32} \end{vmatrix} b_{23} = 0, \tag{4.115}$$

where

$$\begin{aligned} b_{11} &= -\frac{\lambda}{2\mu}\Big((\beta_1 a)^2 + (a\,k)^2 - (\beta_1 a)^2\Big)J_0(\beta_1 a) - (\beta_1 a)J_0'(\beta_1 a); \\ b_{12} &= \frac{(a\,k)^2}{(\beta_2 a)^2}\Big[(\beta_2 a)J_0'(\beta_2 a) + (\beta_2 a)^2 J_0(\beta_2 a)\Big]; \quad b_{13} = b_{21} = b_{22} = b_{33} = 0; \\ b_{23} &= 2\,(\beta_2 a)J_0'(\beta_2 a) + (\beta_2 a)^2 J_0(\beta_2 a); \\ b_{31} &= 2(\beta_1 a)J_0'(\beta_1 a); \quad b_{32} = \left[1 - \frac{(a\,k)^2}{(\beta_2 a)^2}\right](\beta_2\, a)J_0'(\beta_2 a). \end{aligned} \tag{4.116}$$

As was mentioned earlier (4.115) factors into two equations. For torsional waves we have:

$$b_{23} = 0 \quad \Rightarrow \beta_2 a J_0(\beta_2 a) = 2J_1(\beta_2 a), \tag{4.117}$$

which is the same as (4.92).

To derive the frequency equation for extentional waves we need to require that cofactor in (4.115) vanishes

$$\begin{vmatrix} b_{11} & b_{12} \\ b_{31} & b_{32} \end{vmatrix} = 0. \tag{4.118}$$

Multiplying the second column of cofactor in (4.118) by $\beta_2 a$ and dividing the second row by 2, and then adding the resulting two rows, we obtain

$$\begin{vmatrix} -\frac{\lambda}{2\mu}\Big((\beta_1 a)^2 + (a\,k)^2 + (\beta_1 a)^2\Big)J_0(\beta_1 a) & (a\,k)^2(\beta_2 a)^2 J_0(\beta_2 a) - \frac{(\beta_2 a)^2 + (a\,k)^2}{2}J_1(\beta_2 a) \\ (\beta_1 a)J_1(\beta_1 a) & -\frac{(\beta_2 a)^2 - (a\,k)^2}{2}J_1(\beta_2 a) \end{vmatrix} = 0. \tag{4.119}$$

Utilizing equations (4.105)-(4.106), we have

$$\begin{vmatrix} -\frac{(\beta_2 a)^2 - (a\,k)^2}{2}J_0(\beta_1 a) & (a\,k)^2(\beta_2 a)^2 J_0(\beta_2 a) - \frac{(\beta_2 a)^2 + (a\,k)^2}{2}J_1(\beta_2 a) \\ (\beta_1 a)J_1(\beta_1 a) & -\frac{(\beta_2 a)^2 - (a\,k)^2}{2}J_1(\beta_2 a) \end{vmatrix} = 0. \tag{4.120}$$

Expansion of last determinant yields,

$$\begin{aligned} \frac{\big((\beta_2 a)^2 - (a\,k)^2\big)^2}{4}J_0(\beta_1 a)J_1(\beta_2 a) + (\beta_1 a)(\beta_2 a)(a\,k)^2 J_0(\beta_2 a)J_1(\beta_1 a) \\ -(\beta_1 a)\frac{(\beta_2 a)^2 + (a\,k)^2}{2}J_1(\beta_1 a)J_1(\beta_2 a) = 0 \end{aligned} \tag{4.121}$$

or dividing by a^4, we obtain the frequency equation for axial-radial modes

$$\big(\beta_2^2 - k^2\big)^2 J_0(\beta_1 a) J_1(\beta_2 a) + 4\beta_1\beta_2 k^2 J_0(\beta_2 a) J_1(\beta_1 a) - \frac{2\beta_1}{a}(\beta_2^2 + k^2) J_1(\beta_1 a) J_1(\beta_2 a) = 0, \tag{4.122}$$

which agrees with the Pochhammer-Chree frequency equations (4.109).

n=1 case:

When $n = 1$ we obtain the lowest-order family of flexural modes. In this case the determinant in (4.112) has the form:

$$\begin{vmatrix} b_{11} & b_{12} & b_{13} \\ b_{21} & b_{22} & b_{23} \\ b_{31} & b_{32} & b_{33} \end{vmatrix} = 0, \tag{4.123}$$

where

$$\begin{aligned}
b_{11} &= \Big[-\frac{\lambda}{2\mu}\big((\beta_2 a)^2 + (a\,k)^2\big) - (\beta_2 a)^2 + 1 \Big] J_1(\beta_1 a) - \beta_1 a J_1'(\beta_1 a); \\
b_{12} &= \frac{k^2}{\beta_2^2}\Big[\beta_2 a J_1'(\beta_2 a) + \big((\beta_2 a)^2 - 1\big) J_1(\beta_2 a) \Big]; \\
b_{13} &= (\beta_2 a) J_1'(\beta_2 a) - J_1(\beta_2 a); \\
b_{21} &= 2\big[J_1(\beta_1 a) - (\beta_1 a) J_1'(\beta_1 a) \big]; \\
b_{22} &= -\frac{2k^2}{\beta_2^2}\big[J_1(\beta_2 a) - \beta_2 a J_1'(\beta_2 a) \big]; \\
b_{23} &= 2\beta_2 a J_1'(\beta_2 a) + ((\beta_2 a)^2 - 2) J_1(\beta_2 a); \\
b_{31} &= 2\beta_1 a J_1'(\beta_1 a); \quad b_{32} = \Big[1 - \frac{k^2}{\beta_2^2} \Big] \beta_2\, a J_1'(\beta_2 a); \quad b_{33} = J_1(\beta_2 a).
\end{aligned} \tag{4.124}$$

4.5 Analysis of Numerical Results

4.5.1 Axisymmetric Waves in Rods

Let us now consider the dispersion relations for axisymmetric modes in more detail. The lowest branch of the axial-radial modes extends to zero, which is a longitudinal mode whose propagation velocity in the low frequency limit is governed by Young's modulus [30].

Let us introduce non-dimensional frequency Ω and wavenumber ξ:

$$\Omega = \frac{\omega a}{c_2}, \qquad \xi = ka, \tag{4.125}$$

and let

$$x^2 = (\beta_2 a)^2 = \Omega^2 - \xi^2, \quad y^2 = (\beta_1 a)^2 = \kappa^{-2}\Omega^2 - \xi^2, \quad \kappa^2 = \frac{2(1-\nu)}{1-2\nu}. \tag{4.126}$$

Using equtions (4.125) and (4.126) the frequency equation (4.122) in non-dimensional parameters can be written as:

$$(\Omega^2 - 2\xi^2)^2 J_0(y)J_1(x) + 4xy\xi^2 J_0(x)J_1(y) - 2y\Omega^2 J_1(y)J_1(x) = 0. \tag{4.127}$$

To find cutoff frequencies of the axisymmetric mode we set $\xi = 0$ in (4.127), then

$$xJ_1(x)\left[(\Omega^3 J_0(y)/2 - \Omega^2\kappa^{-1}J_1(y)\right] = \Omega^3 J_1(\Omega)\left[(\Omega J_0(\kappa^{-1}\Omega)/2 - \kappa^{-1}J_1(\kappa^{-1}\Omega)\right] = 0. \tag{4.128}$$

The equation (4.128) factors into two seperate equations, yielding two sets of cutoff frequencies which were calculated on Matlab uzing "fzero" routine.

The first factor of (4.128) yields the following equation:

$$J_1(\Omega) = 0, \tag{4.129}$$

it does not depend on Poisson's ratio ν, some of cutoff frequencies are:

$$0, 3.8317, 7.0156, 10.1735, 13.3237, 16.4706, 19.6159.... \tag{4.130}$$

The modes associated with these cutoff frequencies are referred to as axial-shear modes.

The second factor of (4.128) depends on Poisson's ratio ν and results in the following equation:

$$(\Omega J_0(\kappa^{-1}\Omega)/2 - \kappa^{-1}J_1(\kappa^{-1}\Omega) = 0. \tag{4.131}$$

The numerical evaluation of roots of equation (4.131) leads to the following cutoff frequencies for $\nu = 0.3317$:

$$0, 4.3119, 10.8139, 17.1273.... \tag{4.132}$$

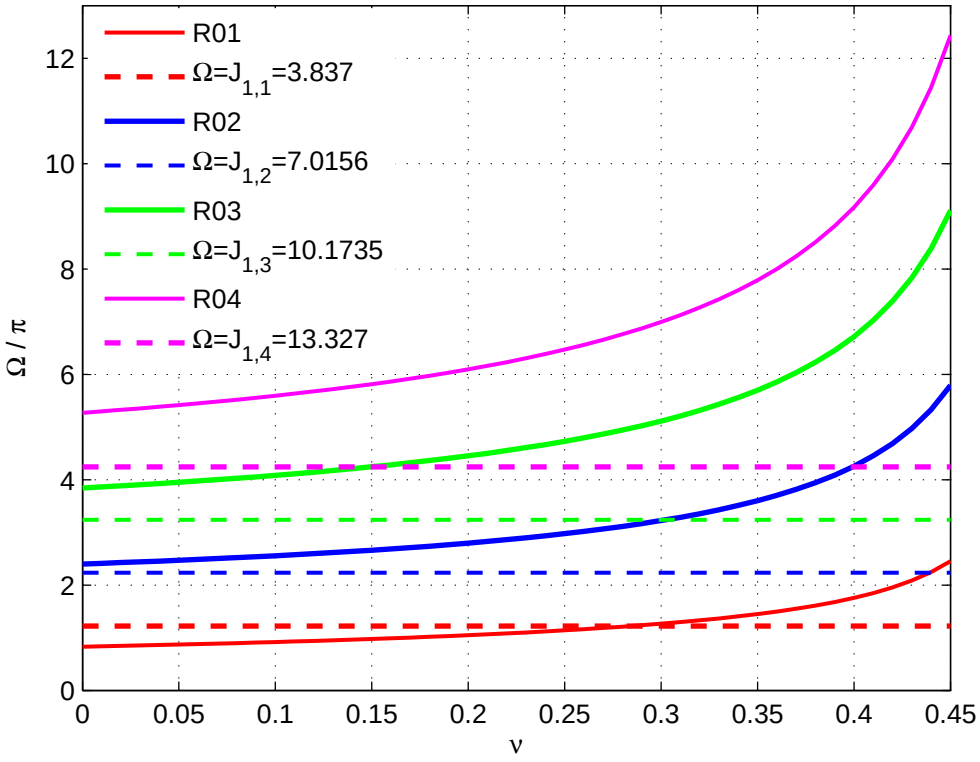

Figure 4.2: Plot of frequency Ω vs Poisson's ratio ν

which agree with results given by Zemanek [44]. The modes associated with these cutoff frequencies are called radial-shear modes. Some numerical results for axisymmetric modes in a rod are given in Figures 4.2-4.3. The material of the rod is elastic, isotropic and homogeneous. Calculations are performed on Matlab using "fzero" routine. Codes are attached in Appendix 2.

In Figure 4.2 for $n = 0$ the cutoffs of axial-shear and radial-shear axisymmetric modes in rod versus Poisson's ratio ν are shown, after the results of Thurston [30]. Here the dashed horizontal lines correspond to axial-shear modes which are zeros of $J_1(\Omega)$, they do not depend on Poisson's ratio; the continuous lines correspond to radial-shear modes. For $\nu = 0$, the first higher mode is radial and the second is axial-shear. The lowest radial cutoff and the first axial-shear cutoff are equal at $\nu = 0.2833$ becomes equal to As $\nu \to 0.5$ the values of frequency Ω at cutoffs of radial modes all tend to infinity whereas the axial-shear cutoffs do

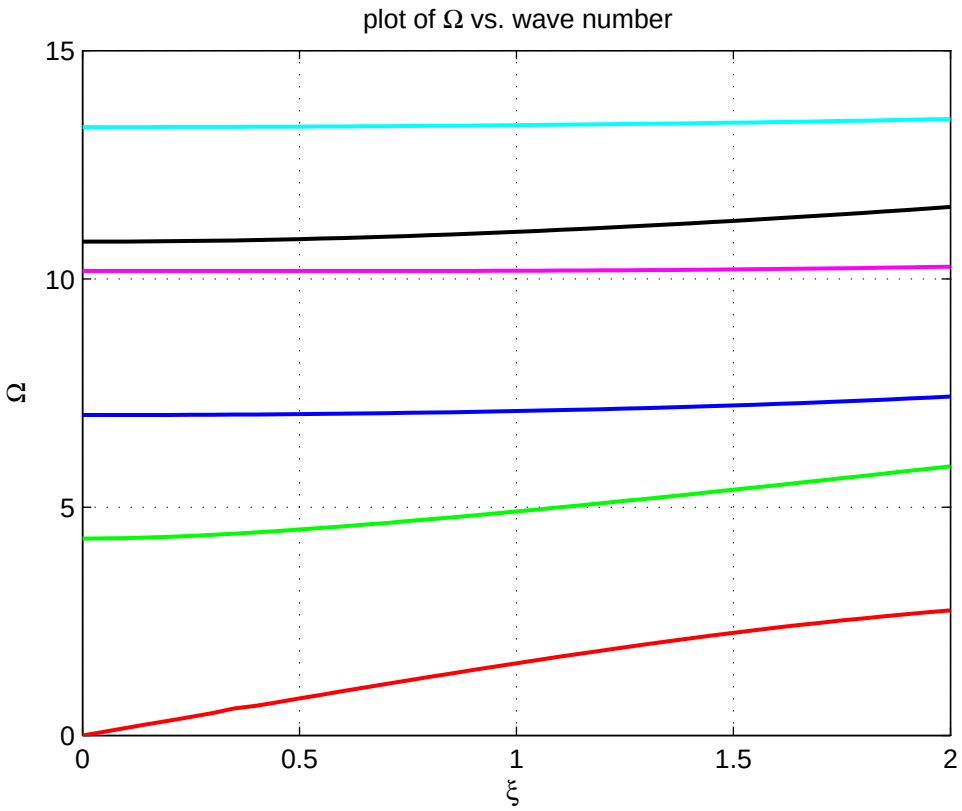

Figure 4.3: Plot of frequency Ω vs wave number ξ

not fluctuate.

The real branches of the frequency spectrum for longitudinal waves in a rod are obtained from the frequency equation (4.127). The roots of equation (4.127) are evaluated on Matlab using 'fzero'. The dispersion relations in the rod for real-valued wavenumbers and $\nu = 0.3317$ are given in Figures 4.3. Here the relative position of nondimentional frequency depends on wave number. The cutoff frequencies (4.130) and (4.132) are used as starting points of each dispersion curve. The graphs shown in Figure 4.3 agree with Zemanek's results [44].

4.5.2 Antisymmetric Waves in Rods

Equation (4.112) becomes the frequency equation for antisymmetric modes for $n \geq 1$. The lowest flexural mode corresponds to $n = 1$ case and refered to as the ordinary flexural mode of propagation.

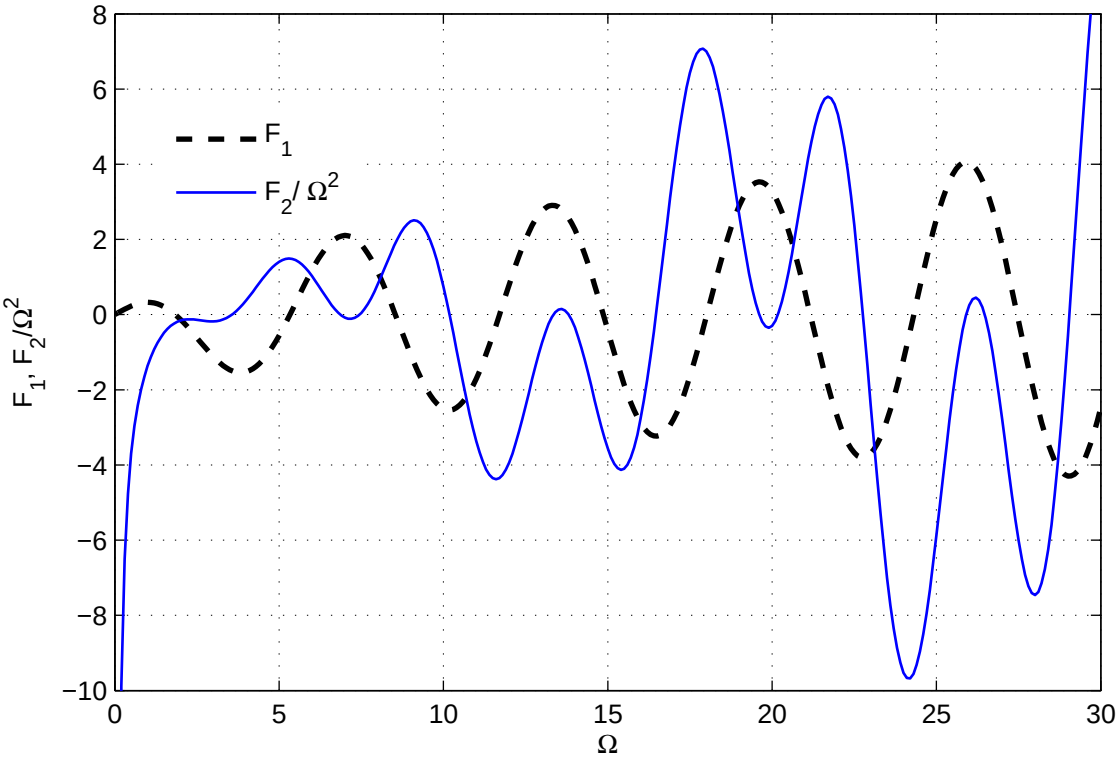

Figure 4.4: Plot of F_1 and F_2/Ω^2 functions versus frequency Ω for $\nu = 0.3317$, $n = 1$

The solutions of frequency equations in plate and rods shows that there is an infinite number of symmetric and antisymmetric modes. Each mode maintains its transverse pattern, though it attenuates and propagating through waveguide, it shifts in phase. These modes are similar to the resonant modes of a drumhead. Low-order modes of drumhead have only a few transverse variations and high-order modes have many forms.

As we saw in previous sections, each mode in a waveguide has a cutoff frequency, also known as its critical frequency, or cuton frequency. The cutoff frequencies correspond to standing waves of one dimensional resonance through the thickness - as expected for zero horizontal wavenumber. This provides a method to estimate thickness from one side only by measuring the frequencies at which resonances occur. Below the cutoff frequency a traveling wave in a given mode cannot be maintained in a waveguide and the mode will not propagate but when excited it will attenuate. At frequencies above the cutoff frequencies the modes

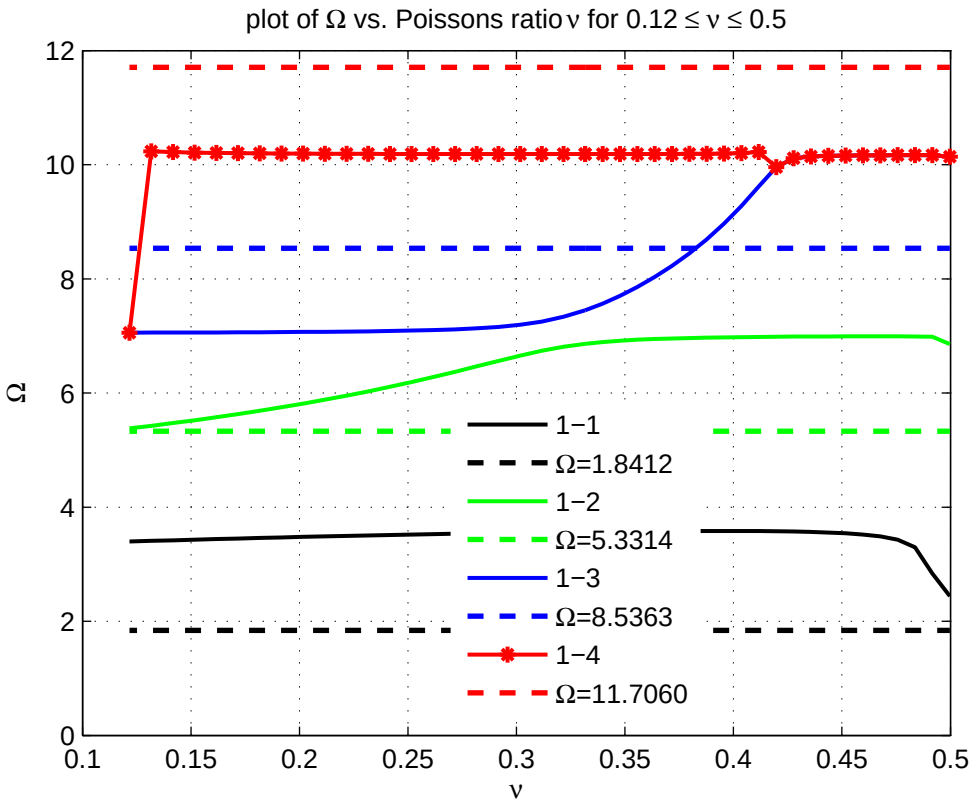

Figure 4.5: Plot of cutoff frequency Ω vs Poisson's ratio ν for $0.12 \leq \nu \leq 0.5$, $n = 1$

propagate through a waveguide to regions far removed from excitation with a finite phase velocity and small attenuation. The critical frequency is the frequency at which the attenuation of the waveguide mode changes rapidly as a function of frequency.

Introducing the non-dimentional frequency Ω and wave number ξ by (4.125) and allowing $\xi \to 0$ enables one to find the cutoff frequencies of the axisymmetric modes. Thus setting $\xi = 0$ in the frequency equation (4.112) leads to the following equation:

$$\begin{aligned}
&\big[\Omega J_{n-1}(\Omega) - nJ_n(\Omega)\big] \cdot \Big\{ 2n^2 \cdot \big[(1+n)J_n(\kappa^{-1}\Omega) - \kappa^{-1}\Omega J_{n-1}(\kappa^{-1}\Omega)\big] \\
&\times \big[\Omega J_{n-1}(\Omega) - (n+1)J_n(\Omega)\big] - \left[\left(n^2 + n - \frac{\Omega}{2}\right) J_n(\kappa^{-1}\Omega) - \kappa^{-1}\Omega J_{n-1}(\kappa^{-1}\Omega)\right] \\
&\times \big[2(\Omega J_{n-1}(\Omega) - nJ_n(\Omega)) + (\Omega^2 - 2n^2)J_n(\Omega)\big] \Big\} = 0. \qquad (4.133)
\end{aligned}$$

Modifying equation (4.133) it can be factorized into two separate equations:

$$F_1 = 0 \qquad (4.134)$$

and

$$F_2 = 0, \tag{4.135}$$

where

$$F_1 = \Omega J_{n-1}(\Omega) - nJ_n(\Omega) \tag{4.136}$$

and

$$\begin{aligned} F_2 =& \big[\kappa^{-1}\Omega J_{n-1}(\kappa^{-1}\Omega) - (n+1)J_n(\kappa^{-1}\Omega)\big] \cdot \big[2(n^2-1)\big[nJ_n(\Omega) - \Omega J_{n-1}(\Omega)\big] + \Omega^2 J_n(\Omega)\big] \\ &-\left(n^2 - 1 - \frac{\Omega^2}{2}\right) J_n(\kappa^{-1}\Omega) \times \big[2\Omega J_{n-1}(\Omega) + (\Omega^2 - 2n^2 - 2n)J_n(\Omega)\big]. \end{aligned} \tag{4.137}$$

Equations (4.134) and (4.135) agree with ones given by Zemanek [44]. Equation (4.134) and (4.137) yield two independent sets of the cutoff frequencies. The first equation (4.134) yields the cutoff frequencies of axial-shear modes which are independent of Poisson's ratio. The roots of the second equation (4.137) depend on Poisson's ratio.

When $n = 0$ equation (4.134) becomes equation (4.129) which specifies the cutoff frequencies for axil-shear modes, equation (4.135) becomes the product of equations (4.131) specifying the cutoff frequencies for radial-shear modes and (4.92) with $\xi = 0$ specifying the cutoff frequencies for torsional modes of propagation.

The plots of functions F_1 and F_2/Ω^2 versus frequency Ω for $\nu = 0.3317$ are shown in Figure 4.4 for $n = 1$. Equation (4.134) yields the following cutoff frequencies:

$$0,\ 1.8412,\ 5.3314,\ 8.5363,\ 11.7060,\ 14.8636,\ 18.0155,\ 21.1644,\ 24.3113,\ 27.4571,\ 30.6019, \ldots \tag{4.138}$$

The cutoff frequencies defined from equation (4.135) for $\nu = 0.3317$ are:

$$\begin{aligned} &3.5669,\ 6.8623,\ 7.4497,\ 10.1851,\ 13.3477,\ 13.8099,\ 16.4672, \\ &19.6082,\ 20.1783,\ 22.7616,\ 25.9074,\ 26.4708,\ 29.0460, \ldots \end{aligned} \tag{4.139}$$

The roots of the frequency equation corresponding to real propagation constants are depicted in Figures 4.5-4.6. Here the dashed horizontal lines correspond to axial-shear modes which are zeros of equation (4.134), they do not depend ν. The cutoff frequencies (4.138) and (4.139) are the starting points for each branch of dispersion curves in Figure 4.5. These cutoffs

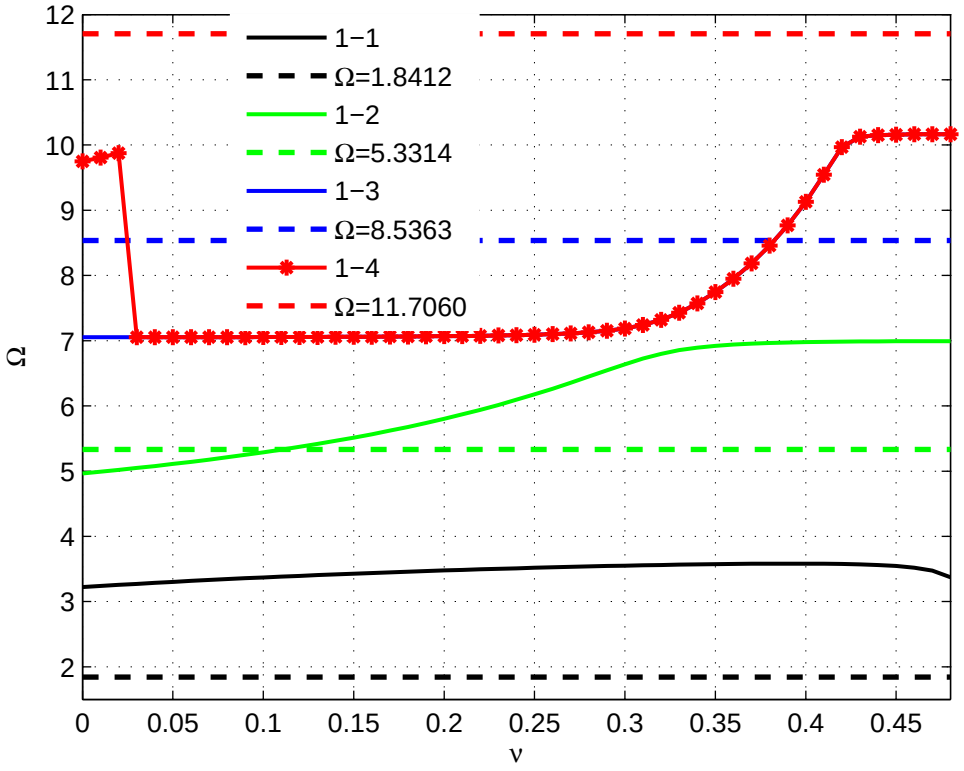

Figure 4.6: Plot of cutoff frequency Ω vs Poisson's ratio ν for $0 \leq \nu \leq 0.45$, $n = 1$

agree with Zemanek's results [44]. The dependence of the cutoff frequencies on Poisson's ratio is depicted for $0.12 \leq \nu \leq 0.5$ in Figure 4.5. Obtained results are stable for $0.14 \leq \nu \leq 0.5$; for $0.12 \leq \nu < 0.14$ the cutoffs started at $\Omega = 7.4497\,(\nu = 0.14)$ jump to the next branch. It is noticed that the cutoff frequencies of some branches intersect or come close to each other. For instance, at $\nu \approx 0.42$ the cutoff starting at branch $\Omega = 7.4497$ intersects with one starting at $\Omega = 10.1851$; as ν increases the cutoff starting at branch $\Omega \approx 5.5\,(\nu = 0.14)$ tends to $\Omega = 7.4497$ - the starting point of the next branch.

In Figure 4.6 for $n = 1$ the cutoffs of antisymmetric modes in rod versus Poisson's ratio ν is shown. To construct a plot of Ω versus ν for small range of Poisson's ratio ν, the cutoff frequencies of equation (4.135) are calculated for $\nu = 0$:

$$0, \quad 3.2215, \quad 4.9656, \quad 7.0524, \quad 9.7483\ldots \tag{4.140}$$

which are taken as starting point in Figure 4.6. An unstable operation of root finder 'fzero'

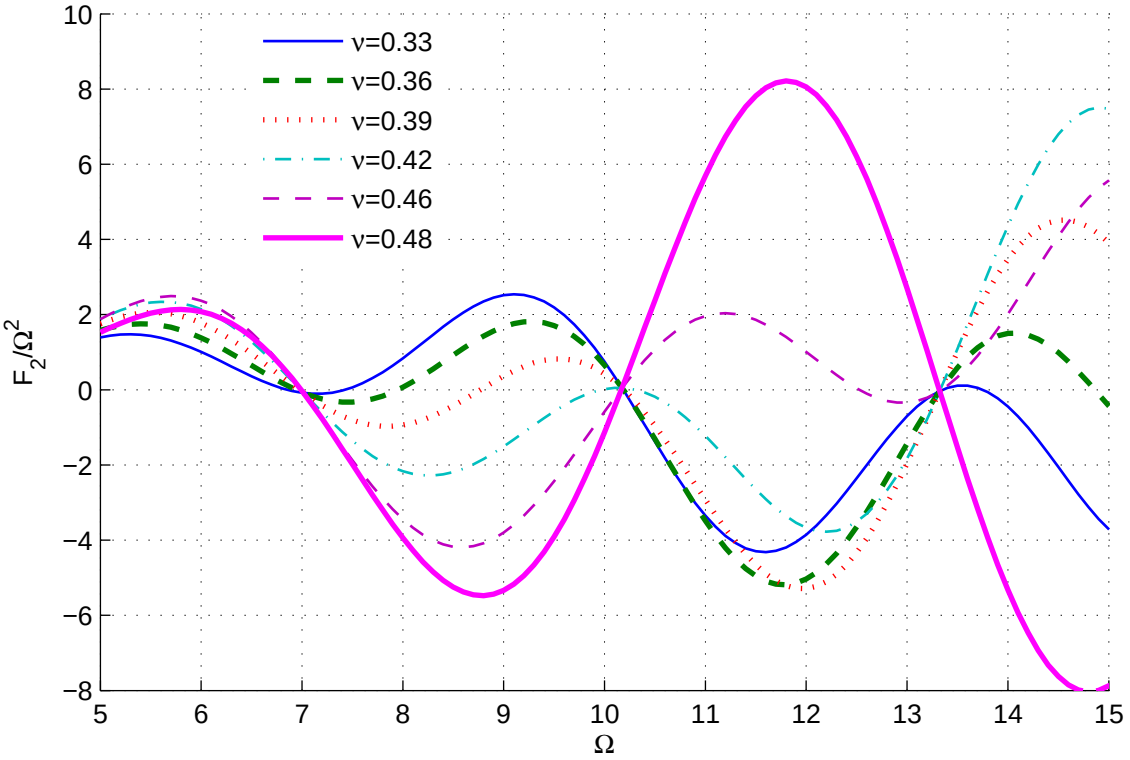

Figure 4.7: Plot of function F_2/Ω^2 vs frequency Ω, $n = 1$

is detected, it jumps from one root to another. The cutoffs starting $\Omega = 4.9656$ tend to starting point of branch starting at $\Omega = 7.0524$ which itself tends to starting point of the next branch $\Omega = 9.7483$. Besides the cutoffs of the branch starting at $\Omega = 9.7483$ drop at $\nu \leq 0.12$ abruptly down to the previous branch starting at $\Omega = 7.0524$. It contradicts the plots given on Figures 4.5 where the branch starting at $\Omega = 9.7483$ does not change much with the increase of ν.

To understand better an intricate behavior of roots of equation (4.135), the dependence of F_2/Ω^2 function on frequency Ω was evaluated for $n = 1$ at fixed values of Poisson's ratio ν. The plot of F_2/Ω^2 versus Ω is depicted in Figure 4.7 for $\nu = 0.33, 0.36, 0.42, 0.45, 0.48$ and in Figure 4.7 for $\nu = 0, 0.02, 0.04, 0.06, 0.08, 0.1, 0.12$. The F_2/Ω^2 function behaves extraordinarily at some cutoff branches. Let us consider first Figure 4.7. There are two roots: $\Omega = 6.86$ and $\Omega = 7.425$ for $\nu = 0.33$. As ν increases, the first root $\Omega = 6.86$ remains

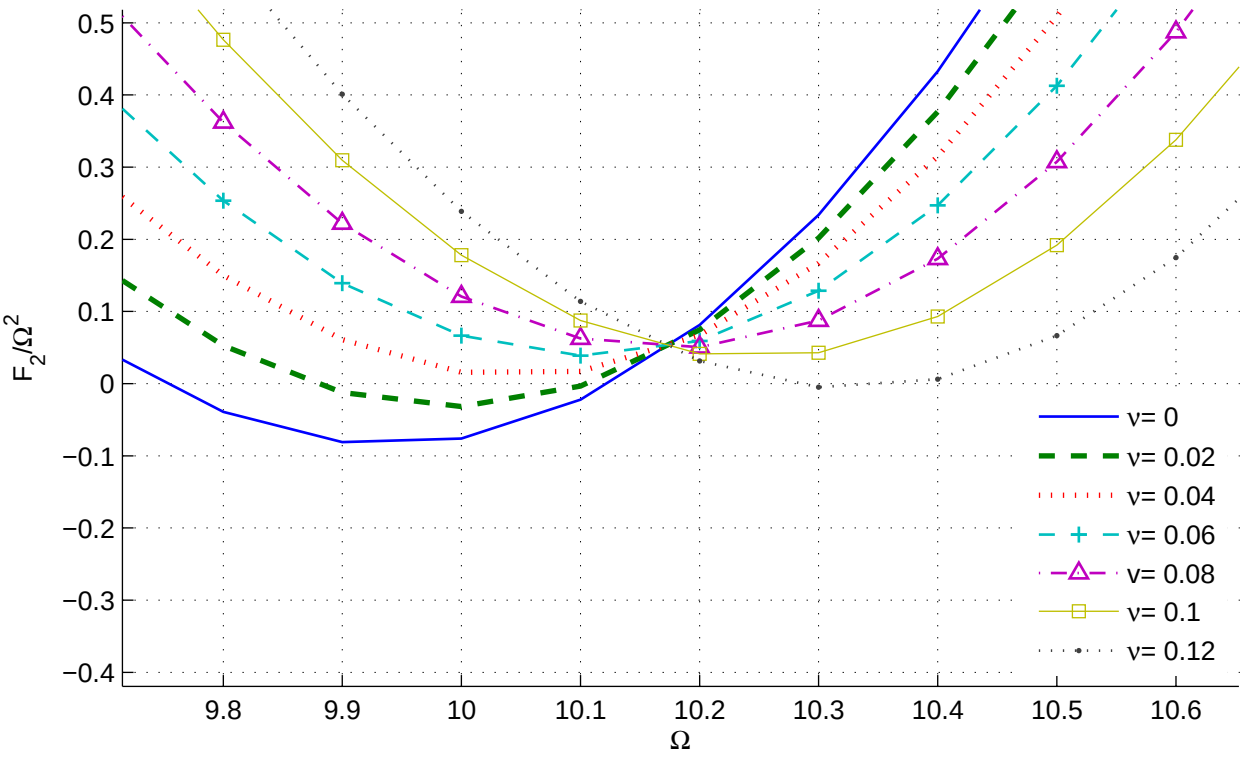

Figure 4.8: Plot of function F_2/Ω^2 vs frequency Ω, $n = 1$

the same for $\nu = 0.48$, the second root $\Omega = 7.425$ shifts to the right and for $\nu = 0.48$ it is $\Omega = 10.1851$, it approaches the next branch. The 'fzero' root finder can not distinguish between the two branches. This explains why the two cutoff branches shown in Figure 4.5 coincide with each other for $\nu \geq 0.42$.

Now let us examine Figure 4.8 in more detail. We can observe that the F_2/Ω^2 function has either two or one root depending on values of Poisson's ratio for interval $\Omega \in [9.7, 10.4]$. Thus F_2/Ω^2 function has two zeros for $\nu = 0; 0.02; 0.12$ and one zero for $\nu = 0.03; 0.04; 0.06; 0.08; 0.1; 0.11$. As ν increases from 0 to 0.1 it shifts up and then again goes down for $\nu = 0.12$. Therefore the cutoff branch started at $\Omega = 9.7483$ and $0.03 < \nu \leq 0.12$ suddenly jump and coincides with the previous branch as shown in Figure 4.5 - 4.6. This results in unstable behavior of the cutoff frequencies as function of ν. As the consequence of this behavior, it is only possible to find dispersion relations in the rod for

certain values of Poisson's ratio ν, e.g. for $0.12 \leq \nu \leq 0.42$. The results given in [44], [3], [16], [15] are within this range of ν.

Chapter 5

Application, Coclusion and Future Work

5.1 Application to Elastic Waves in Waveguides

Propagation characteristics of ultrasonic elastic guided waves are directly related to the microstructure and the mechanical properties of the medium. Because of this feature ultrasonic waves are widely used in the field of characterizations and non-destructive testing of structures to detect defects in waveguides [49], [50], [49], [51].

Ultrasonic non-destructive evaluation can provide a rapid and accurate measurement in a wide range of industries. The ability to inspect large structure from a single probe position makes inspection by ultrasonic waves an appealing solution for many industrial applications (aircraft parts, rails, pipes, stay cables and so on). But there are some difficulties in applying this technique.The multimodal and dispersive nature of the waveguide which can lower the quality of ultrasonic wave test in connection with test sensitivity and the distance of propagation [51]. Thus, prior to performing tests one should be able to calculate and understand the propagated field in a waveguide. Therefore some models of wave propagation in waveguides have been developed by Mindlin [3], Zemanek [44], Puckett et al [52]. These models identify dispersion curves and associated mode shape. For cylindrical shapes this can be done using analogous solutions of dispersion relations shown in Chapter 4 and for plates using results given in Chapter 3 of the thesis. Puckett et al. [52] studied wave propagation of multiple modes in a finite cylinder with excitation using a normal expansion model.

Application of ultrasonic Lamb waves for rapid inspection of metallic and composite structures have been described in a number of studies [49]. A good review of guided Lamb waves for identification of defects in composites is given by Zu et al. [53]. The damage is

Figure 5.1: Application of non-destructive testing using ultrasonic waves

traditionally identified by analyzing the modifications in the received Lamb waves signals. The results presented in Chapter 3 are applicable here. Another possible technique to analyze Lamb wave propagation is the dual signal processing approach [49], by measuring signals at different positions.

Consider a long pipe (pod) used in oil (petroleum) transportation which can be modeled as an infinitely long rod. Sending signals in the pipe gives the ability to extract material properties of the pipe using the solution of dispersion relations obtained in Chapter 4. The picture given in Figure 4.9 is taken from

`http://en.wikipedia.org/wiki/File:Ultrasonic_pipeline_test.JPG#filelinks`

Figure 4.9 shows how technician uses ultrasonic phased array instrument to detect damages on a pipeline weld at a construction site. An ultrasound transducer is connected to a diagnostic machine, scanner, which consists of a frame with magnetic wheels. The scanner holds the probe in contact with the pipe by a spring. The wet area is water or an ultrasonic couplant (such as oil). The couplant allows the sound to pass into the pipe wall. Application of non-destructive inspection techniques, using mechanical guided waves, have potential to monitor

these structures. It gives ability to inspect long lengths of wave guide from a single position.

In recent years methods based on guided ultrasonic waves gained increasing attention for the non-destructive evaluation and the health monitoring of multi-wire strands used in civil structures as prestressing tendons and stay cables [54]. These structures suffer from aging and degradation due to corrosion and fatigue of structural steel members. The classical way to study wave propagation in strand wires (the lowest number of strands is 7) is to use an infinite cylinder. Kwun et al. [55], Laguerre et al. [54], Lanza di Scalea et al. [56] have conducted experimental studies for both cylindrical bar and seven wire strand to find similarities between behaviors of both structures that could be modeled from solutions of Pochhammer-Chree frequency equations for the bare waveguide case.

Conventional non-distractive evaluation requires a coupling medium to permit the ultrasound transmission into the structure investigated. The coupling issues in exciting and detecting elastic Lamb waves are removed in non- contact Laser Based Ultrasonic Systems. Laser Based Ultrasonic (LBU) technique is efficient to study wave propagation in plates due to its large bandwidth and the potential for fast scanning [57], [58], [59]. Lamb waves are used in the ultrasonic characterization of plates to extract mechanical properties of plates. Some symmetric and antisymmetric Lamb modes display atypical characteristics at the minimum frequency, where the group velocity of the mode is zero while the phase velocity remains non-zero, for instance, a backward wave propagation, a resonance peak. Such Lamb modes are called Zero Group Velocity (ZGV) modes. Dispersion curves for some low symmetric and antisymmetric Lamb modes are depicted in Fig. 3.8 and Fig. 3.9, where the first symmetric mode and the second antisymmetric mode have negative slope. Since at minimum frequencies of ZGV modes the energy is gathered under the source, a resonant behavior of these modes is expected. Using LBU technique, ZGV resonances were observed for the first symmetric and the second antisymmetric Lamb mode by Prada et al. in [57], [58] for isotropic plate, and in [59] for anisotropic plate.

5.2 Conclusion

Research has been performed to study elastic wave propogation in rods and plates. A new approach has been proposed in Chapter §3 to study the low frequency behavior of the Rayleigh-Lamb frequency equations. The approach is built on new series expansion of the roots of the Rayleigh-Lamb equations using iteration combined with symbolic algebra on Maple. The non-dimensional frequency is expanded into a series for the wavenumber for symmetric modes in Section §3.3 and for antisymmetric modes in Section §3.4. A numerical evaluation of the series coefficients has been performed by solving of sequence of linear equations. The dispersion relations for frequency, phase speed and group speed for the lowest mode, $n = 1$, have been analyzed in Sections §3.4 and §3.5. The frequency and phase speed dependence on wave number showed a good agreement of series expansion method with exact theory and gives quite accurate results for $0 \leq \xi \leq 0.6$. For $0 \leq \xi \leq 0.6$ keeping 10 terms in series expansion gives more precise result.

The advantage of the proposed series expansion method is that there is no need to evaluate the root the Rayleigh-Lamb frequency equations; it is straightfoward and uses less effort to compute. For low frequency processes the series expansion method gives accurate results. The roots of the Rayleigh-Lamb frequency equations can only be obtained using numerical method which is not exact solution. The disadvantage of the series expansion method is that it works only for low frequencies. For high frequencies series expansion produces high phase speed and frequency. In addition, the obtained frequency expansion is divergent. It is suggested to use some other methods to analyze the Rayleigh-Lamb frequency equations for high frequency spectrum, some approaches are shown in the following section.

Different displacement potential representations have been presented and contrasted. The frequency equations have been derived for symmetric and antisymmetric modes in a rod using two displacement potentials, namely the Helmholtz decomposition for vector fields and Buchwald's vector potentials. A new approach to derive the frequency equations for rods using Buchwald's potential representation is proposed. It has been observed that Buchwald's potentials produce a simpler solution, involving lower order Bessel functions.

The frequency equation are derived and analyzed in Section §4.4 in more detail for the case $n = 0$, corresponds to symmetric modes, and the $n = 1$ case corresponding to propagation antisymmetric modes in a rod. It has been shown that Buchwald's potential and Helmholtz decomposition produce the same frequency equation for $n = 0$ case. The development of the frequency equations for rods has shown that Buchwald's approach is less laborious and time saving.

Numerical results are given in Section §4.5 where the dispersion relations and the cutoff frequencies for axial-shear, radial-shear and flexural modes in the rod are discussed. The obtained results for symmetric modes agreed with ones published earlier. The evaluation of the dependence of cutoff frequencies on Poisson's ratio ν revealed some unexpected interesting behavior of cutoffs for antisymmetric modes. Some branch cuts abruptly jump and coincide with previous or next branch for some values of Poisson's ratio. It has been explained in Section §4.5, looking at the dependence of the F_2/Ω^2 function on frequency Ω at some fixed values of Poisson's ratio. At some branches for some values of frequency Ω the F_2/Ω^2 function has either one, two or no roots depending on a value of Poisson's ratio ν.

5.3 Suggestions for Further Work

While the results in Chapter 3 are restricted to high wave length, $\xi << 1$, they could be extended to finite values of ξ. In order to analyze the Rayleigh-Lamb frequency equations for higher wave number, one could use the Pade approximant method combined with obtained series expansion to expand the radius of convergence. The Padé approximant, developed by Henri Padé, is the "best" approximation of a function by a rational function of given order. The approximant's power series agrees with the power series of the function it is approximating and it may still work where the Taylor series does not converge, like in our case. Another approach is to use the effective equations of refined engineering theories [23] with specified boundary conditions. The refined equations are unclear sometimes, the specified boundary condition should correspond to an order of PDE and a number of independent variables.

The series expansion method was shown above for the lowest family of symmetric and antisymmetric modes when $m = 0$. This method will also work for all modes (m=0,1,2,3) using the following expansion:

$$\Omega^2 = \Omega_m^2 + \sum_{n=1}^{\infty} \xi^{2n} W_n, \tag{5.1}$$

by starting for each mode with the corresponding cutoff frequency Ω_m.

In addition, the proposed series expansion method can be extended to study the roots of the frequency equation for symmetric and antisymmetric waves in a rod.

Buchwald's potentials [37] are the most effective to use in cylindrical coordinates. In the more general case, considering a radially inhomogeneous solid, Shuvalov and Norris' approach [33] based on Stroh framework is the most efficient, where the impedance matrix was also derived using Buchwald's potentials.

D. Appendix. Sample Maple and Matlab Codes

D..1 Appendix 1. Maple Codes

a) Codes for Section 3.3. Symmetric Modes

```
OM2 := Sum(U[n]*xi^(2*n), n = 1 .. 10); k2 := (2*(1-nu))/(1-2*nu);
x2 := OM2-xi^2; y2 := OM2/k2-xi^2; f1 := sin(sqrt(x2))*cos(sqrt(y2))/sqrt(x2);
f2 := sin(sqrt(y2))*cos(sqrt(x2))/sqrt(y2); S11 := (xi^2-x2)^2*f1+4*y2*xi^2*f2;
S := taylor(S11, xi = 0, 20); S0 := simplify(coeftayl(S, xi = 0, 4));
eq := solve({S0}, [U[1]])[2];
for i from 2 by 2 to 10 do S0 := simplify(coeftayl(S, xi = 0, 4+i));
eqt := op(solve({subs(eq, S0)}, [U[(1/2)*i+1]]));
eq := [op(eq), op(eqt)]: end do
for k from 1 by 1 to 6 do V[k] := subs(eq, U[k]); B[k] := simplify(V[k]*C[k]):
C[k] := factorial(2*k-1)*(1-nu)^(2*k-1)
       /((-1)^(2*k-1)*2^k*factorial(k-1)*nu^2); end do
-----------------------------------------------------------------
OUTPUT:

eq := [U[1] = -2/(nu-1), U[2] = (2/3)*nu^2/(nu-1)^3,
U[3] = -(2/45)*nu^2*(7*nu^2+10*nu-6)/(nu-1)^5,
U[4] = (2/945)*nu^2*(62*nu^4+294*nu^3-27*nu^2-168*nu+51)/(nu-1)^7,
U[5] = -(2/14175)*nu^2*(381*nu^6+3852*nu^5+3750*nu^4-5374*nu^3
       -554*nu^2+1524*nu-310)/(nu-1)^9,
U[6] = (2/467775)*nu^2*(5110*nu^8+89650*nu^7+238567*nu^6-107448*nu^5
       -253549*nu^4+145530*nu^3+23919*nu^2-27104*nu+4146)/(nu-1)^11]
V[1] := -2/(nu-1), C[1] := -(1/2)*(1-nu)/nu^2, B[1] := -1/nu^2,
V[2] := (2/3)*nu^2/(nu-1)^3, C[2] := -(3/2)*(1-nu)^3/nu^2, B[2] := 1,
V[3] := -(2/45)*nu^2*(7*nu^2+10*nu-6)/(nu-1)^5
C[3] := -(15/2)*(1-nu)^5/nu^2, B[3] := -(7/3)*nu^2-(10/3)*nu+2
```

```
V[4] := (2/945)*nu^2*(62*nu^4+294*nu^3-27*nu^2-168*nu+51)/(nu-1)^7
C[4] := -(105/2)*(1-nu)^7/nu^2,
B[4] := (62/9)*nu^4+(98/3)*nu^3-3*nu^2-(56/3)*nu+17/3
V[5] := -(2/14175)*nu^2*(381*nu^6+3852*nu^5+3750*nu^4-5374*nu^3
         -554*nu^2+1524*nu-310)/(nu-1)^9; C[5] := -(945/2)*(1-nu)^9/nu^2
B[5] := -(127/5)*nu^6-(1284/5)*nu^5-250*nu^4+(5374/15)*nu^3+(554/15)
        *nu^2-(508/5)*nu+62/,   C[6] := -(10395/2)*(1-nu)^11/nu^2
V[6] := (2/467775)*nu^2*(5110*nu^8+89650*nu^7+238567*nu^6-107448*nu^5
       -253549*nu^4+145530*nu^3+23919*nu^2-27104*nu+4146)/(nu-1)^11
B[6] := (1022/9)*nu^8+(17930/9)*nu^7+(238567/45)*nu^6-(35816/15)*nu^5
       -(253549/45)*nu^4+3234*nu^3+(7973/15)*nu^2-(27104/45)*nu+1382/15
```

b) Codes for Section 3.4. Antisymmetric Modes

```
OM2 := Sum(U[n]*xi^(2*n), n = 2 .. 16);
x2 := OM2-xi^2; k2 := (2*(1-nu))/(1-2*nu);
y2 := OM2/k2-xi^2; f1 := sin(sqrt(x2))*cos(sqrt(y2))/sqrt(x2);
f2 := sin(sqrt(y2))*cos(sqrt(x2))/sqrt(y2);
B := (xi^2-x2)^2*f2+4*x2*xi^2*f1; S := taylor(B, xi = 0, 28);
S0 := simplify(coeftayl(S, xi = 0, 8)); eq := solve({S0}, [U[2]])[2];
S1 := simplify(coeftayl(S, xi = 0, 6));
for i from 2 by 2 to 16 do S0 := simplify(coeftayl(S, xi = 0, 8+i));
eqt := op(solve({subs(eq, S0)}, [U[(1/2)*i+2]]));
eq := [op(eq), op(eqt)] end do
for k from 2 to 10 do W[k] := subs(eq, U[k]);
CL[k] := simplify(factorial(2*k)*(1-nu)^(k-1)/((-1)^k*2^(k+5)));
DL[k] := factor(W[k]*CL[k]); DT[k] := taylor(DL[k], nu = 1, 10) end do
------------------------------------------------------------------------
OUTPUT:
```

```
eq := [U[2] = -2/(3*(nu-1)), U[3] = (2/45)*(7*nu-17)/(nu-1)^2,
U[4] = -(2/945)*(62*nu^2-418*nu+489)/(nu-1)^3,
U[5] = (2/14175)*(381*nu^3-4995*nu^2+14613*nu-11189)/(nu-1)^4,
U[6] = -(2/467775)*(5110*nu^4-110090*nu^3+584257*nu^2-1059940*nu+602410)
       /(nu-1)^5,
U[7] = (2/638512875)*(2828954*nu^5-90572134*nu^4+754982390*nu^3-2386810276
      *nu^2+3109098177*nu-1404361931)/(nu-1)^6,
U[8] = -(2/1915538625)*(3440220*nu^6-153108900*nu^5+1840593186*nu^4
       -8868547040*nu^3+19607784669*nu^2-19849038802*nu+7437643415)
       /(nu-1)^7,
U[9] = (2/488462349375)*(355554717*nu^7-20978379363*nu^6+343393156317
       *nu^5-2332360918791*nu^4+7695401450679*nu^3-12978692736341*nu^2
       +10724754208055*nu-3433209020623)/(nu-1)^8,
U[10] = -(2/194896477400625)*(57496915570*nu^8-4341050683790*nu^7
       +92811983812139*nu^6-843435286359132*nu^5+3856675179582919*nu^4
       -9557544387771638*nu^3+12977929665725313*nu^2
    -9051135401463140*nu+2528890541707756)/(nu-1)^9]
W[2]  := -2/(3*(nu-1)), CL[2]:= -(3/16)*nu+3/16, DL[2]:= 1/8,DT[2]:= 1/8,
W[3]  := (2/45)*(7*nu-17)/(nu-1)^2,    CL[3] := -(45/16)*(nu-1)^2,
DL[3]:= -(7/8)*nu+17/8, DT[3]:= 5/4-7/8*(nu-1), CL[4]:= -(315/4)*(nu-1)^3,
W[4]:=-(2/945)*(62*nu^2-418*nu+489)/(nu-1)^3, CL[4] := -(315/4)*(nu-1)^3,
DL[4]:= (31/3)*nu^2-(209/3)*nu+163/2, DT[4]:= 133/6-49*(nu-1)+(31/3)*(nu-1)^2
W[5]:= (2/14175)*(381*nu^3-4995*nu^2+14613*nu-11189)/(nu-1)^4,
CL[5] := -(14175/4)*(nu-1)^4
DL[5] := -(381/2)*nu^3+(4995/2)*nu^2-(14613/2)*nu+11189/2
DT[5] := 595-2883*(nu-1)+1926*(nu-1)^2-(381/2)*(nu-1)^3
W[6]  := -(2/467775)*(5110*nu^4-110090*nu^3+584257*nu^2-1059940*nu
          +602410)/(nu-1)^5,    CL[6] := -(467775/2)*(nu-1)^5
DL[6] := 5110*nu^4-110090*nu^3+584257*nu^2-1059940*nu+602410
```

```
DT[6] := 21747-201256*(nu-1)+284647*(nu-1)^2-89650*(nu-1)^3
         +5110*(nu-1)^4
W[7]  := (2/638512875)*(2828954*nu^5-90572134*nu^4+754982390*nu^3
        -2386810276*nu^2+3109098177*nu-1404361931)/(nu-1)^6,
CL[7] := -(42567525/2)*(nu-1)^6
DL[7] := -(2828954/15)*nu^5+(90572134/15)*nu^4-(150996478/3)*nu^3
         +(2386810276/15)*nu^2-(1036366059/5)*nu+1404361931/15
DT[7] := 988988-252281029/15*(nu-1)+(127401274/3)*(nu-1)^2-(140327798/5)
         *(nu-1)^3+(25475788/5)*(nu-1)^4-(2828954/15)*(nu-1)^5
W[8]  := -(2/1915538625)*(3440220*nu^6-153108900*nu^5+1840593186*nu^4
         -8868547040*nu^3+19607784669*nu^2-19849038802*nu
         +7437643415)/(nu-1)^7,    CL[8] := -2554051500*(nu-1)^7
DL[8] := 9173920*nu^6-408290400*nu^5+4908248496*nu^4-(70948376320/3)
         *nu^3+52287425784*nu^2-(158792310416/3)*nu+59501147320/3
DT[8] := 150133984/3-4973128160/3*(nu-1)+6843245240*(nu-1)^2-(23747671168/3)
        *(nu-1)^3+3004405296*(nu-1)^4-353246880*(nu-1)^5+9173920 (nu-1)^6
W[9] = (2/488462349375)*(355554717*nu^7-20978379363*nu^6+343393156317*nu^5
       -2332360918791*nu^4+7695401450679*nu^3-12978692736341*nu^2
       +10724754208055*nu-3433209020623)/(nu-1)^8,
CL[9] := -390769879500*(nu-1)^8
DL[9] := -(2844437736/5)*nu^7+(167827034904/5)*nu^6-(2747145250536/5)*nu^5
         +(18658887350328/5)*nu^4-(61563211605432/5)*nu^3+(103829541890728/5)
         *nu^2-17159606732888*nu+27465672164984/5
DT[9] := 2138696560-941710405376/5*(nu-1)+(6079451002144/5)*(nu-1)^2
        -2228425866432*(nu-1)^3+(7341011300448/5)*(nu-1)^4-(1799916233568/5)
        *(nu-1)^5+(147915970752/5)*(nu-1)^6-(2844437736/5)*(nu-1)^7
W[10] = -(2/194896477400625)*(57496915570*nu^8-4341050683790*nu^7+*nu^6
       -843435286359132*nu^5+3856675179582919*nu^4-9557544387771638*nu^3
       +12977929665725313*nu^2-9051135401463140*nu+2528890541707756)/(nu-1)^9
```

```
CL[10] := -74246277105000*(nu-1)^9
DL[10] := (919950649120/21)*nu^8-(69456810940640/21)*nu^7+(1484991740994224
          /21)*nu^6-(4498321527248704/7)*nu^5+(61706802873326704/21)*nu^4
          -(152920710204346208/21)*nu^3+(69215624883868336/7)*nu^2
          -(144818166423410240/21)*nu+40462248667324096/21
DT[10] := -208590934864/3-71863824869824/3*(nu-1)+(716851023485824/3)*(nu-1)^2
          -(1960397265026816/3)*(nu-1)^3+14140264242025504/21 (nu-1)^4
          -5992089929183488/21 (nu-1)^5+1024552682585104/21 (nu-1)^6
          -20699068582560/7 (nu-1)^7+919950649120/21 (nu-1)^8
```

D..2 Appendix 2. Matlab Codes

a)Codes for Section 2.5

```
%Beam_Tim_R_EB1.m: Plot of Phase velocity  \Omega / \xi versus wave number
nu=0.29; k1 = 10*(1+nu)/(12+11*nu); k2=3; a=2*(1+nu)/k2; a1=1/k2+a/k1;
a2=4*a/(k1*k2);  sp = 6; sv = 0:0.01:sp;
for J=1:length(sv)
    s2=sv(J).^2; s4=sv(J).^4; s6=sv(J).^6; s8=sv(J).^8; s10=sv(J).^10;
    s12=sv(J).^12;    xv1(J)=a*s4;     xv2(J)=a*s4./(1+s2/k2);
    xv3(J)=(k1*k2+(k1+2*(1+nu))*s2)/2-sqrt(((k1*k2+(k1+2*(1+nu))*s2)/2)...\
    .^2-2*(1+nu)*k1*s4);
end
OMEGA1=sqrt(xv1)./sv; OMEGA2=sqrt(xv2)./sv; OMEGA3=sqrt(xv3)./sv;
plot(sv,OMEGA1,'b--','LineWidth',1.5); hold on;
plot(sv,OMEGA2,'g-','LineWidth',1.5);plot(sv,OMEGA3,'r-.','LineWidth',1.5);
hold off; grid on; xlabel('\xi');  ylabel('\Omega / \xi ');
title('Plot of \Omega/ \xi vs. wave number \xi')
legend('Euler-Bernoulli','Rayleigh','Timoshenko')
```

b)Codes for Section 3.4

```
% ANTISYM_Omega2
%Plot of Frequency \Omega vs. wave number \xi
%\nu- Poisson's ratio, sv- \xi vector(wave number),  \OMEGA  -frequency
nu=0.25; sv=linspace(0,1); W(1)= zeros(1,length(nu)); W(2)= -2./(3.*(nu-1));
W(3)= (2./45).*(7.*nu-17)./(nu-1).^2;
W(4)= -(2./945).*(62.*nu.^2-418.*nu+489)./(nu-1).^3;
W(5)= (2./14175).*(381.*nu.^3-4995.*nu.^2+14613.*nu-11189)./(nu-1).^4;
W(6)= -(2./467775).*(5110.*nu.^4-110090.*nu.^3+584257.*nu.^2.../
     -1059940.*nu+602410)./(nu-1).^5;
W(7)= (2./638512875)*(2828954.*nu.^5-90572134.*nu.^4+754982390.../
      .*nu.^3-2386810276.*nu.^2+3109098177.*nu-1404361931)./(nu-1).^6;
W(8)= -(2/1915538625).*(3440220.*nu.^6-153108900.*nu.^5+1840593186.../
      .*nu.^4-8868547040.*nu.^3+19607784669.*nu.^2-19849038802.../
      .*nu+7437643415)./(nu-1).^7;
W(9)= 2./488462349375.*(355554717.*nu.^7-20978379363.*nu.^6+ .../
      343393156317.*nu.^5-2332360918791.*nu.^4+ 7695401450679.../
      .*nu.^3-12978692736341.*nu.^2+10724754208055.*nu.../
      -3433209020623)./(nu-1).^8
W(10,:)=-(2/194896477400625)*(57496915570*nu.^8-4341050683790.../
      *nu.^7+92811983812139*nu.^6-843435286359132*nu.^5.../
      +3856675179582919*nu.^4-9557544387771638*nu.^3.../
      +12977929665725313*nu.^2-9051135401463140*nu+.../
       2528890541707756)./(nu-1).^9;   O=zeros(1,length(sv));
for n=1:1
    O=O+W(n)*sv.^(2*n)
end
OMEGA1=sqrt(O); O=zeros(1,length(sv));
for n=1:2
    O=O+W(n)*sv.^(2*n)
```

```
end
OMEGA2=sqrt(O); O=zeros(1,length(sv));
for n=1:3
    O=O+W(n)*sv.^(2*n)
end
OMEGA3=sqrt(O); O=zeros(1,length(sv));
for n=1:4
    O=O+W(n)*sv.^(2*n)
end
OMEGA4=sqrt(O); O=zeros(1,length(sv));
for n=1:5
    O=O+W(n)*sv.^(2*n)
end
OMEGA5=sqrt(O); O=zeros(1,length(sv));
for n=1:6
    O=O+W(n)*sv.^(2*n)
end
OMEGA6=sqrt(O); O=zeros(1,length(sv));
for n=1:7
    O=O+W(n)*sv.^(2*n)
end
OMEGA7=sqrt(O); O=zeros(1,length(sv));
for n=1:8
    O=O+W(n)*sv.^(2*n)
end
OMEGA8=sqrt(O); O=zeros(1,length(sv));
for n=1:9
    O=O+W(n)*sv.^(2*n)
end
```

```
OMEGA9=sqrt(O); O=zeros(1,length(sv));
for n=1:10
    O=O+W(n)*sv.^(2*n)
end
OMEGA10=sqrt(O); hold on
plot(sv,OMEGA1,'r-.','LineWidth',2.5); plot(sv,OMEGA2,'b-','LineWidth',2);
plot(sv,OMEGA3,'m--','LineWidth',2);  plot(sv,OMEGA4,'g-','LineWidth',2);
plot(sv,OMEGA5,'r-','LineWidth',2.5); plot(sv,OMEGA6,'k:','LineWidth',2.5)
plot(sv,OMEGA7,'c-.','LineWidth',2.5); plot(sv,OMEGA8,'k-','LineWidth',1.5)
plot(sv,OMEGA9,'b--','LineWidth',2); plot(sv,OMEGA10,'m:','LineWidth',2.5);
hold off; grid on; xlabel('\xi '); ylabel('\Omega' )
legend('1','2','3','4','5','6','7','8','9','10'); AXIS([0 1 0 2.5])
```

c) Codes for Section 3.5

```
% RL_find_roots11.m
% Program plots dispersion relations for plate using R.L. roots
% ISYM=1 corresponds to symmetric modes
% ISYM=2 corresponds to antisymmetric modes
clear; clf; ISYM=2; nu=0.25; k2 = 2*(1-nu)/(1-2*nu) ;
numroots=8; sp = 5; sv = 0.01:0.01:sp; a0=(.2)^2;
for N=1:numroots
    a0=N^2-.99;
for J=1:length(sv)
    s2=sv(J)^2;
    if N==1
        Dfun= @(a) 1;
    else
        Dfun= @(a) prod( (a-xv(J,1:N-1) ) );
    end
```

```
    if ISYM==1
       xv(J,N)=fzero(@(a) RL_sym1(a,s2,k2)/Dfun(a), a0);
    else
       xv(J,N)=fzero(@(a) RL_antisym1(a,s2,k2)/Dfun(a), a0);
    end
    a0=xv(J,N);
end
end
OMEGA=sqrt(xv); plot(sv,OMEGA, 'LineWidth',1.5); grid on
xlabel('\xi '); ylabel('\Omega'); title('plot of \Omega vs. wave number')
%%%%%%%%%%%%%%%%%%%%%%%%%%%%%%%%%%%%%%%%%%%%%%%%%%%%%%%%%%%%%%%%%%%%%%%%%%%
% RL_sym1.m
function f = RL_sym1(a,s2,k2)
x = sqrt(a-s2); y = sqrt(a./k2-s2);
f = ( sin(x)./x.*cos(y).*(a-2*s2).^2+cos(x).*sin(y).* 4.*s2.*y)./a;
end
%%%%%%%%%%%%%%%%%%%%%%%%%%%%%%%%%%%%%%%%%%%%%%%%%%%%%%%%%%%%%%%%%%%%%%%%%%%
% RL_antisym1.m
function f = RL_antisym1(a,s2,k2)
x = sqrt(a-s2); y = sqrt(a./k2-s2);
f = ( sin(x).* cos(y).* 4.* s2.*x + cos(x).*sin(y)./y .*(a-2*s2).^2 )./a;
end
%%%%%%%%%%%%%%%%%%%%%%%%%%%%%%%%%%%%%%%%%%%%%%%%%%%%%%%%%%%%%%%%%%%%%%%%%%%
```

d) Codes for Section 4.5. Symmetric Modes

```
% Rod_nu_01.m
% Plot of frequency \Omega versus Poisson's ratio
clear; clf; nu = 0:0.01:0.45; tic
a0=2.6038;
```

```
for J=1:length(nu)
    k=sqrt(2*(1-nu(J))./(1-2*nu(J)));    k2 = k.*k;
    xv(J)=fzero(@(a) Rod511_sym(a,k), a0);    a0=xv(J);
end
a0=3.837
for M=1:length(nu)
    k=sqrt(2*(1-nu(J))./(1-2*nu(J)));    k2 = k.*k;
    xw(M)=fzero(@(a) Rod6_sym(a), a0);    a0=xw(M);
end
OMEGA1=xv/pi; OMEGA2=xw/pi;
plot(nu,OMEGA1,'r-','LineWidth',1.5); hold on
plot(nu,OMEGA2,'r--','LineWidth',2);legend('R01','\Omega=J_{1,1}=3.837')
a0=7.5398;
for J=1:length(nu)
    k=sqrt(2*(1-nu(J))./(1-2*nu(J)));    k2 = k.*k;
    xv(J)=fzero(@(a) Rod511_sym(a,k), a0);     a0=xv(J);
 end
a0=7.0156
for M=1:length(nu)
    k=sqrt(2*(1-nu(J))./(1-2*nu(J)));    k2 = k.*k;
    xw(M)=fzero(@(a) Rod6_sym(a), a0);    a0=xw(M);
end
OMEGA3=xv/pi; OMEGA4=xw/pi; plot(nu,OMEGA3,'b-','LineWidth',2);
plot(nu,OMEGA4,'b--','LineWidth',1.5);
legend('R02','\Omega=J_{1,2}=7.0156')
a0=12.0722;
for J=1:length(nu)
    k=sqrt(2*(1-nu(J))./(1-2*nu(J)));    k2 = k.*k;
    xv(J)=fzero(@(a) Rod511_sym(a,k), a0);     a0=xv(J);
```

```
end
a0=10.1735;
for M=1:length(nu)
    k=sqrt(2*(1-nu(J))./(1-2*nu(J)));    k2 = k.*k;
    xw(M)=fzero(@(a) Rod6_sym(a), a0);    a0=xw(M);
end
OMEGA5=xv/pi; OMEGA6=xw/pi; plot(nu,OMEGA5,'g-','LineWidth',2)
plot(nu,OMEGA6,'g--','LineWidth',1.5)
legend('R03','\Omega=J_{1,3}=10.1735')
a0=16.5548;
for J=1:length(nu)
    k=sqrt(2*(1-nu(J))./(1-2*nu(J)));    k2 = k.*k;
    xv(J)=fzero(@(a) Rod511_sym(a,k), a0);    a0=xv(J);
end
a0=13.3237;
for M=1:length(nu)
    k=sqrt(2*(1-nu(J))./(1-2*nu(J)));    k2 = k.*k;
    xw(M)=fzero(@(a) Rod6_sym(a), a0);    a0=xw(M);
end
OMEGA7=xv/pi; OMEGA8=xw/pi; plot(nu,OMEGA7,'m-','LineWidth',1.5)
plot(nu,OMEGA8,'m--','LineWidth',2)
legend('R01','\Omega=J_{1,1}=3.837','R02','\Omega=J_{1,2}=7.0156','R03',.../
'\Omega=J_{1,3}=10.1735','R04','\Omega=J_{1,4}=13.327')
hold off; grid on; xlabel('\nu'); ylabel('\Omega / \pi')
AXIS([0 0.45 0 13]);toc
%%%%%%%%%%%%%%%%%%%%%%%%%%%%%%%%%%%%%%%%%%%%%%%%%%%%%%%%%%%%%%%%%%%%%%%%%%%%
% Rod6_sym.m
function ff = Rod6_sym(a)
%axial shear modes
```

```
ff=besselj(1,a);
end
%%%%%%%%%%%%%%%%%%%%%%%%%%%%%%%%%%%%%%%%%%%%%%%%%%%%%%%%%%%%%%%%%%%%%%%%%%%%%%%%
% Rod511_sym.m
function f3 = Rod511_sym(a,k)
%s2=0  cut off frequencies, radial shear modes
x = a; y = a./k; Jy0 = besselj(0,y); Jy1 = besselj(1,y);
f3= x.*Jy0-2*Jy1./k;
end
%%%%%%%%%%%%%%%%%%%%%%%%%%%%%%%%%%%%%%%%%%%%%%%%%%%%%%%%%%%%%%%%%%%%%%%%%%%%%%%%
```

References

[1] J.W.S. Rayleigh. *Theory of Sound. Vol. 1.* Dover, New York, 1945.

[2] W.J. Weaver, S.P. Timoshenko, and D.P. Young. *Vibration Problems in Engineering.* Wiley-Interscience, 1990.

[3] R. Mindlin. Influence of rotary inertia and shear onfflexural vibrations of isotropic elastic plates. *J. Appl. Mech.*, 18:31–38, 1951.

[4] W. Flugge. *Axially Symmetric Motions of a Two-layer Timoshenko Type Cylindrical Shells.* Springer-Verlag, Berlin, 1973.

[5] P.M. Naghdi. *The Theory of Shells and Plates: Encyclopedia of Physics.* Springer, Verlag, 1972.

[6] S. Markus. *The Mechanics of Vibrations of Cylindrical Shells.* Elsevier, Amsterdam, 1988.

[7] G. Hermann and I. Mirsky. Three dimensional and shell theory analysis of axially symmetric motions of cylinders. *J. Appl. Mech. ASME*, 23(4):563–568, 1956.

[8] H. Lamb. On waves in an elastic plate. *Proc. R. Soc. A*, 93:114, 1917.

[9] L. Pochhammer. Uber die fortpflanzungsgeschwindigkeiten kleiner schwingungen in einem unbegrenzten isotropen kreiscylinder. *J. Fur. reine and angewandte Math. (Crelle)*, 81:324–336, 1876.

[10] C. Chree. The equations of an isotropic elastic solid in polar and cylindrical coordinates, their solutions and applications. *Trans. Camb. Phil. Soc. Math. Phys. Sci.*, 14:250, 1889.

[11] A.N. Holden. Longitudinal modes of elastic waves in isotropic cylinders and slabs. *Bell. Sys. tech. J.*, 30:956–969, 1951.

[12] M.A. Onoe, H.D. McNiven, and R.D. Mindlin. Dispersion of axially symmetric waves in elastic rods. *J. Appl. Mech. ASME*, 29:729–734, 1962.

[13] R.D. Mindlin. *"Waves and Vibrations in Isotropic Elastic Plates", in: Structural Mechanics.* Pergamon Press, New York, 1960.

[14] D.C. Gazis. Three-dimensional investigation of the propagation of waves in hollow circular cylinders - i. analytic foundation. ii. numerical results. *J. Acoust. Soc. Am.*, 31 (5):568–578, May 1959.

[15] K.F. Graff. *Wave Motion in Elastic Solids.* Dover, New York, 1991.

[16] J.D. Achenbach. *Wave Propagation in Elastic Solids*. North-Holland Publishing Company - Amsterdam-London, American Elsevier Publisher Company, Inc.-New York, 1973.

[17] G. Jemielita. On kinematical assumptions of refined theories of plates: A survey. *Transactions of the ASME*, 57:1088–1091, 1990.

[18] B.F. Vlasov. On the equations of the theory of bending of plates. *Izv. AN SSSR, OMN*, 12:57–60, 1957.

[19] E. Reissner. Reflections on the theory of elastic plates. *Appl. Mech. Rev.*, 38:1453–1464, 1985.

[20] A.N. Norris. Flexural waves on narrow plates. *J. Acoust. Soc. Am.*, 113:2647–2658, 2003.

[21] Z.P. Jones and Z.S. Whittier. Axially symmetric motions of a two-layer timoshenko type cylindrical shells. *AIAA J.*, 7(2):244–250, 1969.

[22] S.Y Rao. Vibrations of layered shells with transversal shear and rotary inertia effects. *J. Sound. Vib.*, 1:147–170, 1983.

[23] A. Bostrom, G. Johansson, and P. Olsson. On the rational derivation of a hierarchy of dynamics equations for a homogeneous, isotropic, elastic plate. *Int. J. Solids Struct.*, 38:2487–2501, 2001.

[24] G.M. Kulikov. Refined global approximation theory of multilayered plates and shells. *J. Engng. Mech. ASCE*, 127:119–125, 2001.

[25] Kh.Kh. Khudoynazarov. Transversal vibrations of thick and thin cylindrical shells, interacting with deformable medium. In *Proceedings of the 8th Int. Conference on Shell Structures: Theory and Applications, Gdansk-Jurata, Poland, Balkema, London, 343-348.*, 2005.

[26] F.A. Amirkulova. Mathematical vibration modeling of the pre-stressed viscoelastic thick walled cylindrical shell. In *Proceedings of The Bellagio International Workshop on Mathematical Modeling, Simulation, E-Learning and Improved Education in Underserved Institutions, Bellagio Rockefeller Study and Conference Center, Italy, November, 2006. Springer, 298-321*, 2007.

[27] N.J. Stephen. Mindlin plate theory: Best shear coefficient and higher spectra validity. *J. Sound & Vibration*, 202(4):539–553, 1997.

[28] A.N. Guz. Elastic waves in bodies with initial (residual) stressses. *Int. Applied Mechanics*, 38(1):23–59., 2002.

[29] I.A. Guz and J.J. Rushchitsky. Computational simulation of harmonic wave propagation in fibrous micro- and nanocomposites. *Composites Science and Technology*, 67(5):861–866, April, 2007.

[30] R.N. Thurston. Elastic waves in rods and clad rods. *J. Acoust. Soc. Am.*, 64(1):1–37, 1978.

[31] I. Selezov. Hyperbolic models of wave propagation in rods, plates and shells. *Izv.RAN. Mekh.Tverdogo Tela*, 29:64–77, 1994.

[32] N.A. Shulga. *Dynamics and Stability of Materials, Vol. 2 of the 12-Volume Series: Mechanics of Composites*. Naukova Dumka, Kiev, 1993.

[33] A.N. Norris and A.L. Shuvalov. Wave impedence matrices for cylindrically anisotropic radially inhomogeneous elastic solids. *Q. J. Mech. Appl. Math.*, In Press.

[34] S.M. Han, H. Benaroya, and T. Wei. Dynamics of transversely vibrating beams using four engineering theories. *J. Sound. Vib.*, 255(5):935–988, 1999.

[35] W.J. Bottega. *Engineering Vibrations*. CRC Press Taylor and Francis Group, 2006.

[36] G.R. Cowper. The shear coefficient in timoshenko's beam theory. *J. Appl. Mech. ASME*, 33:335 –340, 1966.

[37] V.T. Buchwald. Raylegih waves in transversely isotropic media. *Q. J. Mech. Appl. Math.*, 14:293–317, 1961.

[38] P.M. Morse and H. Feshbach. *Methods of Theoretical Physics*. McGraw-Hill Book Co., New York, 1953.

[39] S.K. Shear and A.B. Focke. The dispersion of supersonic waves in cylindrical rods of polycrystalline silver, nickel and magnesium. *Phys. Rev.*, 57:532–537, 1940.

[40] D. Bancroft. The velocity of longitudinal waves in cylindrical bars. *Phys. Rev.*, 59:588–593, 1941.

[41] W.A. Green. *Dispersion Relations for Elastic Waves in Bars*, chapter 5 , Vol. I. North-Holland Publishing Company - Amsterdam, 1960.

[42] E.A Volterra. A one-dimensional theory of wave propagation in elastic rods based on the 'method of internal constrains'. *Ing.-Arch.*, 23:410, 1955.

[43] R.W. Morse. Dispersion of compressional waves in isotropic rods of rectangular cross section. *J. Acoust. Soc. Am.*, 20:833–838, 1948.

[44] J.J. Zemanek. An experimental and theoretical investigation of elastic wave propagation in a cylinder. *J. Acoust. Soc. Am.*, 51:265–283, 1972.

[45] P. Chadwick. Wave propagation in transversely isotropic heat conducting elastic materials. *Mathematika*, 17:255–274, 1970.

[46] F. Honarvar and A.N. Sinclair. Acoustic wave scattering from transversely isotropic cylinders. *J. Acoust. Soc. Am.*, 100(1):57–63, 1996.

[47] F. Ahmad and A. Rahman. Acoustic scattering by transversely isotropic cylinders. *Int. J. Engng. Sc.*, 38:325–335, 2000.

[48] A. Rahman and F. Ahmad. Representation of the displacement in terms of the scalar functions for use in transversely isotropic materials. *J. Acoust. Soc. Am.*, 104:3675–3676, 1998.

[49] J. Assaad, F.EI. Grondel, S. Youbi, E. Moulin, and C. Delebarre. Dual signal processing approach for lamb wave analysis. In *Ultrasonic Wave Propagation in Non Homogeneous Media*, 2009.

[50] L. Laguerre, A. Grimault, and M. Deschamps. Ultrasonic transient bounded-beam propagation in solid cylinder waveguide embedded in a solid medium. *J. Acoust. Soc. Am.*, 121:1924–1934, 2007.

[51] S. Yaacoubi, L. Laguerre, E. Ducasse, and M. Deschamps. A 3d semi-analitical model to predict the behavior of ultrasonicbbounded beam traveling in cylindrical solid bar embedded in a solid matrix. In *Ultrasonic Wave Propagation in Non Homogeneous Media*, 2009.

[52] A. Puckett and M. Peterson. A semi-analitical model for predicting multiple waveguide propagating axially symmetric modes in cylindrical waveguides. *Ultrasonics*, 43:197–207, 2005.

[53] Z.Q. Zu, L. Ye, and Y. Lu. Guided lamb waves for identification of damage in composite structures: a review. *J. Sound. Vib.*, 295:753–780, 2006.

[54] L. Laguerre, Brissaud M., and J. Aime. Magnetostrictive pulse-echo device for non-destructive evaluation of steel cylindrical materials using waves. *Ultasonics*, 39:503–514, 2002.

[55] H. Kwun, K.A. Bartels, and J.J. Hanley. Effects of tensile loading on the properties of elastic-wave propagation in a strand. *J. Acoust. Soc. Am.*, 103:3370–3375, 1998.

[56] F. Lanza di Scalea, P. Rizzo, and F. Seible. Stress measurement and defect detection in steel strands by guided stress waves. *J. Mater. Civil Eng.*, 15:219–227, 2003.

[57] C. Prada, O. Balogun, and T. Murray. Laser-based ultrasonic generation and detection of zero-group velocity lamb waves in thin plates. *Appl. Phys. Lett.*, 87:194109, 2005.

[58] C. Prada, D. Clorennec, and D. Royer. Power law decay of zero group velocity lamb modes. *Wave Motion*, 45(6):723–728, 2008.

[59] C. Prada, D. Clorennec, T. Murray, and D.Modes Royer. Influence of teh asisotropy on zero-group velocity lamb. *J. Acoust. Soc. Am.*, 126(2):620–625, 2009.

Vita

Feruza Abdukadirovna Amirkulova

2010	Teaching assistant, Department of Mechanical and Aerospace Engineering, Rutgers University
2000	Ph.D. in Technics, Academy of Science of Uzbekistan
1990-1995	B.Sc. AND M.Sc. in Mathematics from Samarkand State University
1990	Graduated from high school 52, Samarkand City, Uzbekistan.